FACULDADE DE ENGENHARIA DA UNIVERSIDADE DO PORTO

Printed parts in PLA by FFF: a degradation analysis of the exposure to citric acid and water

Ana Sofia Brochado Oliveira



Mestrado em Engenharia Mecânica

Supervisor: Prof. Dr. Fernando Jorge Lino Alves

Second Supervisor: Dr. Leonardo Santana

September 9, 2024

© Ana Oliveira, 2024

Printed parts in PLA by FFF: a degradation analysis of the exposure to citric acid and water

Ana Sofia Brochado Oliveira

Mestrado em Engenharia Mecânica

September 9, 2024

Resumo

O processo de Fabrico de Filamentos Fundidos (FFF) destaca-se como um dos processos mais populares de fabrico aditivo (AM), dada a sua simplicidade e custo acessível. No entanto, as peças produzidas por FFF muitas vezes não apresentam a mesma confiabilidade das fabricadas por métodos tradicionais. Além disso, o FFF nem sempre cumpre o potencial de ser mais sustentável, pois desde que o seu uso se tornou mais acessível ao público em geral, permitiu que estes usassem as suas impressoras pessoais para construirem vários objetos do dia-a-dia, originando um consumo de plástico por vezes desnecessário. Muitos desses elementos são expostos a humidade, ácidos presentes nos alimentos, sujidade, entre outros mecanismos que podem levar à degradação precoce das peças impressas. Por isso, torna-se crucial investigar e documentar as propriedades tecnológicas das peças impressas por FFF, tais como as propriedades mecânicas, massa, estrutura molecular, entre outras, especialmente em condições de exposição a substâncias que podemos encontrar no nosso dia-a-dia, como o ácido cítrico e a água. Compreender como estes materiais reagem à degradação é essencial para avaliar a sua durabilidade e sustentabilidade.

Este trabalho apresenta um estudo sobre a degradação de amostras de Ácido Polilático (PLA) impressas por FFF expostas a ácido cítrico e água. Foram avaliadas diversas propriedades, incluindo massa, dimensões, estrutura molecular e resposta mecânica à flexão. Para uma comparação mais precisa dos resultados, as amostras foram impressas com duas densidades de preenchimento distintas: 2% e 100%. Foram impressas 112 amostras, divididas igualmente entre as duas densidades de preenchimento. As amostras foram organizadas em grupos de 7 amostras cada, totalizando 8 grupos para cada densidade de preenchimento. No grupo com 100% de densidade de preenchimento, foi incluído 1 grupo de amostras controle, 3 grupos de amostras expostas a água a três temperaturas diferentes (ambiente, 60°C e 90°C). Outros 4 grupos de amostras foram submersas em ácido cítrico, 2 grupos foram imersos em uma solução de ácido cítrico com concentração de 1.4418% e outros 2 grupos em uma solução de 2.8647%, ambos a duas temperaturas diferentes (ambiente e 90°C) para cada concentração de ácido cítrico. As mesmas condições foram aplicadas aos grupos com 2% de densidade de preenchimento.

Os resultados do estudo mostraram que, o estudo da massa e das dimensões não levou a resultados significativos nas várias amostras de PLA estudadas, independentemente do valor de percentagem de preenchimento, meio líquido usado ou temperatura de exposição. A maior diferença encontrada foi no espetro de FTIR obtido após exposição das amostras com 2% de densidade de preenchimento ao ácido cítrico, à temperatura ambiente, onde se verificou o aparecimento de uma nova zona no mesmo. Ao nível das propriedades mecânicas, verificou-se um aumento tanto da Resistência Máxima à Flexão (MFS) como do Módulo de Flexão (FM) nas amostras com 2% de densidade de preenchimento. Nas amostras com 100% de densidade de preenchimento verificou-se uma diminuição da MFS e um aumento da FM. O trabalho realizado nesta tese demonstra que a exposição do PLA a temperaturas superiores à sua temperatura de transição vítrea induz a degradação e a fratura das amostras, tornando impossível a realização de certos testes ou a obtenção de conclusões específicas sobre os grupos de amostras submetidos a essas condições.

Além disso, as amostras com 100% de densidade de preenchimento fornecem resultados mais fiáveis e permitem conclusões mais definitivas.

Palavras-Chave: FFF, PLA, Ácido Cítrico, Água, Estudo de Degradação.

Abstract

The Fused Filament Fabrication (FFF) process stands out as one of the most popular additive manufacturing (AM) processes due to its simplicity and affordable cost. However, parts produced by FFF often do not exhibit the same reliability as those manufactured by traditional methods. Additionally, FFF does not always fulfill its potential for sustainability, as its accessibility to the general public has allowed individuals to use personal 3D printers to create various everyday objects, sometimes leading to unnecessary plastic consumption. Many of these objects are exposed to humidity, acids found in food, dirt, and other mechanisms that can result in the premature degradation of printed parts. Therefore, it is crucial to investigate and document the technological properties of parts printed by FFF, such as mechanical properties, mass, molecular structure, and others, particularly under exposure to substances commonly found in daily life, like citric acid and water. Understanding how these materials react to degradation is essential for assessing their durability and sustainability.

This study presents an analysis of the degradation of Polylactic Acid (PLA) samples printed by FFF exposed to citric acid and water. Various properties were evaluated, including mass, dimensions, molecular structure, and mechanical flexural response. For a more precise comparison of the results, the samples were printed with two different infill densities: 2% and 100%. A total of 112 samples were printed, evenly divided between the two infill densities. The samples were organized into groups of 7 each, totaling 8 groups for each infill density. For the 100% infill density group, 1 control group was included, and 3 groups were exposed to water at three different temperatures (room temperature, 60°C, and 90°C). Another 4 groups were submerged in citric acid, with 2 groups immersed in a citric acid solution with a concentration of 1.4418% and the other 2 in a 2.8647% solution, each at two different temperatures (room temperature and 90°C) for each citric acid concentration. The same conditions were applied to the groups with 2% infill density.

The study results showed that the analysis of mass and dimensions did not yield significant results across the various PLA samples, regardless of infill percentage, liquid medium used, or exposure temperature. The most notable difference was found in the FTIR spectrum obtained after exposing the 2% infill density samples to citric acid at room temperature, where a new zone appeared in the spectrum. In terms of mechanical properties, both the Maximum Flexural Strength (MFS) and Flexural Modulus (FM) increased in the 2% infill density samples. In the 100% infill density samples, a decrease in MFS and an increase in FM were observed. The work conducted in this thesis demonstrates that exposure of PLA to temperatures above its glass transition temperature induces degradation and fracturing of the samples, making it impossible to perform certain tests or draw specific conclusions about the groups of samples subjected to these conditions. Additionally, the 100% infill density samples provided more reliable results and allowed for more definitive conclusions.

Keywords: FFF, PLA, Citric Acid, Water, Degradation Study.

Acknowledgments

Completing this dissertation has been a challenging but rewarding journey, and it would not have been possible without the support, guidance, and encouragement of several incredible individuals.

First, I would like to express my deepest gratitude to my supervisor, Prof. Dr. Fernando Jorge Lino Alves, and my co-supervisor, Dr. Leonardo Santana. Your expertise, guidance, and insightful feedback have been invaluable in shaping this work. Thank you for your patience, encouragement, and for always pushing me to strive for excellence.

To my family, thank you for being my foundation throughout this journey. Your love, encouragement and belief in me have been unwavering, giving me the strength and motivation to continue.

To my husband, who has been my rock throughout this journey, thank you for your endless patience, understanding, and encouragement. Your belief in me, even when I doubted myself, has been a constant source of strength. I am forever grateful to have you by my side.

A heartfelt acknowledgment goes to my four-legged babies: Luna, Açúcar, Leia, and Milu. Your playful energy, comforting presence, and unconditional love have been a source of joy and companionship through the highs and lows of this process. You have been with me through long nights and early mornings, reminding me to take breaks and offering much-needed moments of happiness.

To engineer Beatriz Graça, for her invaluable assistance and expertise in the FTIR analysis, which played a crucial role in this work.

I would also like to express my gratitude to INEGI, Laboratório Associado de Energia, Transportes e Aeronáutica, for their invaluable resources during this research.

Thank you all for being an essential part of this journey.

Ana Sofia Oliveira

"...But I am finally in a place where anxiety isn´t my norm. For those struggling to remember that, know that it is possible"

Stefania Rossi

Contents

1 Introduction **1**
- 1.1 Contextualization . . . 1
- 1.2 Objectives . . . 2
  - 1.2.1 Main Objective . . . 2
  - 1.2.2 Specific Objectives . . . 2

2 State of the Art **3**
- 2.1 Polymeric Materials . . . 3
  - 2.1.1 Thermoplastics: semi-crystalline and amorphous . . . 5
  - 2.1.2 Transition Temperatures . . . 6
  - 2.1.3 Mechanical Properties . . . 9
  - 2.1.4 Water absorption mechanisms . . . 12
  - 2.1.5 Degradation Mechanisms in polymeric materials . . . 15
- 2.2 Food Acids . . . 17
  - 2.2.1 Types . . . 17
  - 2.2.2 Scale of measurement and classification . . . 18
  - 2.2.3 Effects of Food Acids on Polymeric Materials . . . 18
- 2.3 Polylactic acid (PLA) . . . 20
  - 2.3.1 Mechanical and Thermal Properties . . . 20
  - 2.3.2 Barrier Properties . . . 21
  - 2.3.3 Behavior in water . . . 22
  - 2.3.4 Behavior in Food Acids . . . 23
  - 2.3.5 Resistance to degradation . . . 24
- 2.4 Extrusion Based Additive Manufacturing . . . 24
  - 2.4.1 Fused Filament Fabrication (FFF) . . . 25
  - 2.4.2 Process Parameters . . . 26
  - 2.4.3 Materials . . . 28
  - 2.4.4 Water diffusion in printed parts . . . 29
  - 2.4.5 Degradation mechanism on printed parts . . . 30

3 Materials and Methods **31**
- 3.1 Materials . . . 32
- 3.2 3D Printing System . . . 32
  - 3.2.1 3D Printer . . . 32
  - 3.2.2 Software . . . 33
  - 3.2.3 Equipment calibration and printing parameters . . . 34
- 3.3 Case Study . . . 36
  - 3.3.1 Degradation of 3D-printed parts . . . 36

3.3.2 After Printing Study . . . 44
3.3.3 Water Study . . . 44
3.3.4 Citric Acid Study . . . 44

4 Analysis and comparison of the results **46**
4.1 Filament Characterization Results . . . 46
4.1.1 FTIR . . . 46
4.1.2 Mass Measurements . . . 48
4.1.3 Dimensional Measurements . . . 48
4.1.4 Flexural Tests . . . 48
4.2 Degradation Study . . . 49
4.2.1 Filling Percentage: 2% . . . 49
4.2.2 Filling Percentage: 100% . . . 64

5 Conclusions and Future Work **80**
5.1 Conclusions . . . 80
5.2 Future Work . . . 82

References **83**

Appendices **87**

Appendix A Literature Study of Degradation Mechanisms **88**

Appendix B Calibration Cubes Measurements **94**

Appendix C FILKEMP PLA-N Filament Technical Sheet **96**

Appendix D Diffusion Coefficient Calculation Sheets **99**

List of Figures

2.1 Inside the history of polymers [3]. . . . 5
2.2 Schematic of a semi-crystalline polymer [4]. . . . 6
2.3 Melting and softening behavior of semicrystalline and amorphous materials [9]. . . 8
2.4 Temperature dependent behavior of polymers [13]. . . . 10
2.5 Mechanical behavior of polymers [16]. . . . 12
2.6 Schematic of a typical Fickian absorption curve [18]. . . . 14
2.7 Diagram of hydrogen bonding [21]. . . . 15
2.8 Overall degradation understanding for polymers and biopolymers [23]. . . . 16
2.9 (a) Overall hydrolytic degradation of PLA and transformations, (b) PLA hydrolysis via acid and base catalysis [23]. . . . 17
2.10 pH Scale [26]. . . . 18
2.11 PLA life cycle starting with corn and sugar-beet [29]. . . . 20
2.12 Barrier properties of PLA in comparison to other common polymers [31]. . . . 22
2.13 CT scan of a cross-section of a 3D printed sample (top) and injection molded sample (bottom) [32]. . . . 23
2.14 Chemical structure of PLA with its functional groups [34]. . . . 23
2.15 Schematic Diagram of the Fused Filament Fabrication (FFF) process [38]. . . . 25
2.16 Layer thickness visual effects – (a) 0.1mm; (b) 0.05mm [5]. . . . 26
2.17 Graphical definition of raster angle [5]. . . . 26
2.18 Variation of infill density [5]. . . . 27
2.19 Infill patterns commonly used [5]. . . . 27
2.20 Various build orientations at which different test samples can be printed [5]. . . . 28

3.1 Schematic of the experimental procedures. . . . 31
3.2 Filament used FILKEMP PLA-N [40]. . . . 32
3.3 Prusa i3 MK3S Printer [41]. . . . 33
3.4 PrusaSlicer Software. . . . 33
3.5 Calibration Cubes. . . . 35
3.6 Representation of the printed samples with a 2% infill density (dimensions in [mm]). 37
3.7 Representation of the printed samples with a 100% infill density. . . . 37
3.8 Identification code nomenclature. . . . 37
3.9 STARWAX Citric Acid. . . . 38
3.10 Cary 630 FTIR [41]. . . . 39
3.11 Digital Scale House HLD300. . . . 40
3.12 Digital micrometer used. . . . 41
3.13 Digital caliper used. . . . 41
3.14 Measuring points. . . . 41
3.15 Bending Test Machine in LPDS [5]. . . . 42

3.16 (a) Oven [5]; (b) Samples inside the oven. 43
3.17 Representation of the immersion of the samples inside a plastic bottle and a glass container. 44
3.18 Bottles containing the citric acid solution [2] and the labeled samples. 45

4.1 FTIR analysis curves obtained from group 7 (control group 100%) and group 1 (control group 2%). 46
4.2 Graph of mean mass measurement difference obtained for 2% filling percentage samples. 51
4.3 Group 3 samples after exposure. 52
4.4 Groups: a) 4; b) 11 and c) 12 samples after exposure. 52
4.5 MFS response from the 2% filling percentage samples. 56
4.6 FM response from the 2% filling percentage samples. 57
4.7 FTIR curves before immersion of each sample group with a 2% infill density at RT. 58
4.8 FTIR curves after immersion of each sample group with a 2% infill density at RT. 59
4.9 FTIR curves before immersion of each sample group with a 2% infill density at 60°C. 60
4.10 FTIR curves after immersion of each sample group with a 2% infill density at 60°C. 61
4.11 FTIR curves before immersion of each sample group with a 2% infill density at 90°C. 62
4.12 FTIR curves after immersion of each sample group with a 2% infill density at 90°. 63
4.13 Mean mass evolution of the 100% infill samples before and after submersion. . . 65
4.14 Mass over time for group 8 samples. 66
4.15 Mass over time for group 9 samples. 67
4.16 Group 9 samples after exposure. 67
4.17 Mass average over time for groups: a) 13: b) 15. 68
4.18 MFS response from the 100% filling percentage samples. 72
4.19 FM response from the 100% filling percentage samples. 73
4.20 FTIR curves before immersion of each sample group with a 100% infill density at RT. 74
4.21 FTIR curves after immersion of each sample group with a 100% infill density at RT. 75
4.22 FTIR curves before immersion of each sample group with a 100% infill density at 60°C. 76
4.23 FTIR curves after immersion of each sample group with a 100% infill density at 60°C. 77
4.24 FTIR curves before immersion of each sample group with a 100% infill density at 90°. 78
4.25 FTIR curves after immersion of each sample group with a 100% infill density at 90°. 79

List of Tables

2.1 Glass Transition Temperatures of Common Thermoplastics [5]. 7
2.2 Thermal Properties of Common Thermoplastics [5]. 8
2.3 Functional Groups in Polymers and Their Example Polymers [22]. 15
2.4 PLA mechanical and specific mechanical properties [31]. 21
2.5 PLA Thermal Properties [31]. 21
2.6 Common Pure Filaments Used in FFF and Their Properties (adapted from [38]). . 29

3.1 PLA filament's technical characteristics (C). 32
3.2 Prusa i3 MK3S Technical Parameters [41]. 34
3.3 Printing Parameters [41]. 34
3.4 Average dimensions of calibration cubes. 36
3.5 SLW 53 Oven Specifications 43

4.1 Results of FTIR analysis by regions delimited in the curves. 47
4.2 Relationship between the Wavenumber (cm^{-1}) and the functional group [5]. . . . 47
4.3 Control groups mass measurement. 48
4.4 Dimensions of the control groups samples. 48
4.5 Mechanical tests responses from the control groups. 49
4.6 2% filling percentage conditions mass measurement. 50
4.7 Mean increase for 2% filling percentage samples. 51
4.8 Diffusion Coefficient for each group with 2% infill. 53
4.9 Dimensions of the samples with a 2% infill density before and after exposition. . 54
4.10 Mechanical tests responses from the samples with a 2% filling percentage. 55
4.11 Peaks of FTIR curves and its relative wavenumbers before immersion of each sample group with a 2% infill density at RT. 58
4.12 Peaks of FTIR curves and its relative wavenumbers after immersion of each sample group with a 2% infill density at RT. 59
4.13 Peaks of FTIR curves and its relative wavenumbers before immersion of each sample group with a 2% infill density at 60°C. 60
4.14 Peaks of FTIR curves and its relative wavenumbers after immersion of each sample group with a 2% infill density at 60°C. 61
4.15 Peaks of FTIR curves and its relative wavenumbers before immersion of each sample group with a 2% infill density at 90°C. 62
4.16 Peaks of FTIR curves and its relative wavenumbers after immersion of each sample group with a 2% infill density at 90°C. 63
4.17 100% filling percentage conditions mass measurement. 64
4.18 Mean increase for 100% filling percentage samples. 65
4.19 Diffusion Coefficient for each 100% infill group. 69

4.20 Dimensions of the samples with a 100% infill density before and after exposition. 71
4.21 Mechanical tests responses from the samples with a 100% filling percentage. . . 72
4.22 Peaks of FTIR curves and their relative wavenumbers before immersion of each sample group with a 100% infill density at RT. 74
4.23 Peaks of FTIR curves and their relative wavenumbers after immersion of each sample group with a 100% infill density at RT. 75
4.24 Peaks of FTIR curves and its relative wavenumbers before immersion of each sample group with a 100% infill density at 60°C. 76
4.25 Peaks of FTIR curves and its relative wavenumbers after immersion of each sample group with a 100% infill density at 60°C. 77
4.26 Peaks of FTIR curves and their relative wavenumbers before immersion of each sample group with a 100% infill density at 90°. 78
4.27 Peaks of FTIR curves and their relative wavenumbers before immersion of each sample group with a 100% infill density at 90°. 79

Abbreviations

ABS	Acrylonitrile Butadiene Styrene
AM	Additive Manufacturing
CA	Citric Acid
CAD	Computer-Aided Design
EBAM	Extrusion Based Additive Manufacturing
FDM	Fused Deposition Modeling
FFF	Fused Filament Fabrication
FM	Flexural Modulus
HDPE	High-Density Polyethylene
HIPS	High Impact Polystyrene
LDPE	Low-Density Polyethylene
MFS	Maximum Flexural Strength
PA	Polyamide (Nylon)
PC	Polycarbonate
PEEK	Polyether Ether Ketone
PETG	Polyethylene Terephthalate Glycol
PLA	Polylactic Acid
PP	Polypropylene
PS	Polystyrene
PVA	Polyvinyl Alcohol
RT	Room Temperature
SML	Stratasys Machine Language
TE	Tissue Engineering
TPU	Thermoplastic Polyurethane

Chapter 1

Introduction

1.1 Contextualization

In the domain of Additive Manufacturing (AM), the application of Fused Filament Fabrication (FFF) technology to produce printed parts using Polylactic Acid (PLA) has gained widespread attention. This burgeoning interest is due to not only the versatility and cost-effectiveness of FFF but also stems from the material properties of PLA, making it a popular choice for creating intricate components. However, as these printed parts find their way into various applications, a critical consideration arises—the potential impact of liquid environments on the degradation of PLA-based printed objects.

This study embarks on a comprehensive exploration into the intricate interplay between PLA, FFF technology, and the chemical environment introduced by acids in food and water. While PLA is well-regarded for its mechanical and thermal properties, its susceptibility to degradation under specific conditions poses a noteworthy challenge. The ubiquitous presence of acids in various food items necessitates a comprehensive analysis to understand how these environmental factors may influence the structural integrity and performance of printed parts.

The focus of this study is to conduct a degradation analysis, scrutinizing the effects of acids commonly found in food on PLA-based printed components. As these printed parts become increasingly integrated into everyday objects and consumer products, it becomes imperative to unravel the potential consequences of exposure to acidic environments. This investigation aims to contribute valuable insights to the broader discourse on the durability and suitability of PLA-based printed parts in applications where exposure to food-related acids is inevitable. Through this exploration, we endeavor to deepen our understanding of the complex dynamics between 3D printing materials, manufacturing processes, and real-world environmental conditions, ultimately informing future advancements in the field of additive manufacturing.

1.2 Objectives

1.2.1 Main Objective

The primary objective of this study is to comprehensively assess the impact of exposure to common liquid environments, specifically citric acid, on PLA printed parts, via FFF, by applying structured analytical techniques and mechanical testing. This evaluation entails an analysis of the mechanical properties, mass variations, molecular structure and color of the printed components subjected to varying temperatures.

1.2.2 Specific Objectives

This master's dissertation has the following topics as specific objectives:

Regarding the project,

1. to print test specimens with two different infill densities (2% and 100%), for posterior analysis and comparison of quality after exposure to different degradation environments;
2. to characterize PLA filaments by analyzing their physical and mechanical properties;
3. to study the influence of the liquid environment to which the samples were exposed in the diffusion coefficient of the material;
4. to study the effects of exposure to food acids, focusing on citric acid, on the degradation of PLA printed parts by examining changes in mass and mechanical properties over time;
5. to study the effects of different temperatures (room temperature, 60ºC, and 90ºC) on the degradation of PLA printed parts by examining changes in the mechanical properties;
6. to validate the usability of these printed parts in environments with acidic food media, assessing their performance under various conditions, providing valuable insights for the practical use of PLA in food-related applications;
7. to validate the results by comparing them with the available information in the literature.

As for the student,

1. gain an in-depth understanding of polymer degradation mechanisms;
2. apply structured analysis techniques to solve issues related to FFF 3D printing;
3. develop practical skills in characterizing polymers and parts produced using FFF technology.

Chapter 2

State of the Art

The primary objective of this chapter is to highlight key aspects within the realm of Additive Manufacturing, with a particular emphasis on Fused Filament Fabrication. Additionally, the chapter will delve into significant materials, exploring their crucial properties.

2.1 Polymeric Materials

Polymeric materials became universally present since the beginning of the 20th century, becoming the fastest-growing segment of the United States chemical industry during the rapid industrialization of the post-World War II era. The increasing demand for mass-produced synthetic alternatives to scarce natural resources led to polymeric materials research becoming a priority [1].

The study of polymers has always been an interdisciplinary science where chemists, chemical and mechanical engineers, and materials scientists have worked together to explore the chemical structure and synthesis of polymers, devise methods to scale up production and processing and assess the wide range of mechanical properties present in polymeric materials. Due to these efforts, polymers were found to be an extraordinary class of materials having a broad range of possible applications [1].

Modern vehicles contain increasing amounts of polymers and polymer-based composites replacing traditional materials, such as metals and ceramics, in various applications. For example, in automotive applications, polymers are used in interior components like dashboards, door panels, and seat cushions, which benefit from being lightweight, reducing overall vehicle weight and improving fuel efficiency. In aircraft, polymer composites are used to construct fuselage sections and wings, offering significant weight savings, enhanced fuel efficiency, and superior corrosion resistance compared to traditional metal alloys. These advancements contribute to increased performance, reduced maintenance costs, and lower emissions in the automotive and aerospace industries. Polymers can also be found throughout the entire construction industry in the form of piping, insulation, laminates, and flooring and also heavily influence the consumer industry by being integral components in products such as packaging materials, electronic devices, household goods, and textiles, enhancing durability, flexibility, and design versatility [1].

More examples could be given for many different industries, but suffice it to say the current usage of polymers now surpasses that of metals in terms of volume and mass.

With the rapid and widespread adoption of polymers over time, coupled with their mass production for consumer markets and industrial applications, new challenges have emerged, particularly regarding the growing concern for environmental sustainability [1]. Currently, the majority of modern polymers are derived from petroleum leading to arguments that this heightened dependence on polymers represents a substantial strain on our limited carbon resources. However, the raw materials for polymers account for less than 2% of total petroleum and natural gas consumption worldwide so a total eradication of polymer usage would have little to no impact on the conservation of these resources. In fact, reverting to its traditional counterparts would lead to a higher total energy cost and environmental pollution such as glass vs. plastic water bottles, for example. Another major concern is that polymers do not normally degrade in the environment leading to increasingly large amounts of waste and landfill space consumption. One of the challenges in using them is to develop suitable recycling methods or effective techniques to improve the degradation of disposable items [1].

Thermoplastics are a class of polymers that can be softened through heating and processed through various methods without showing any changes in chemical properties after several cycles, causing them to be suitable for recycling [2]. In this thesis, we will be focusing on thermoplastics and one in particular, polylactic acid or polylactide (PLA).

Figure 2.1 provides an overview of the history of polymers and references PLA from its development to its introduction in biomedical applications after establishing it as a nontoxic, nontissue-reactive, and slowly degrading compound that could be metabolized through the respiratory system [3].

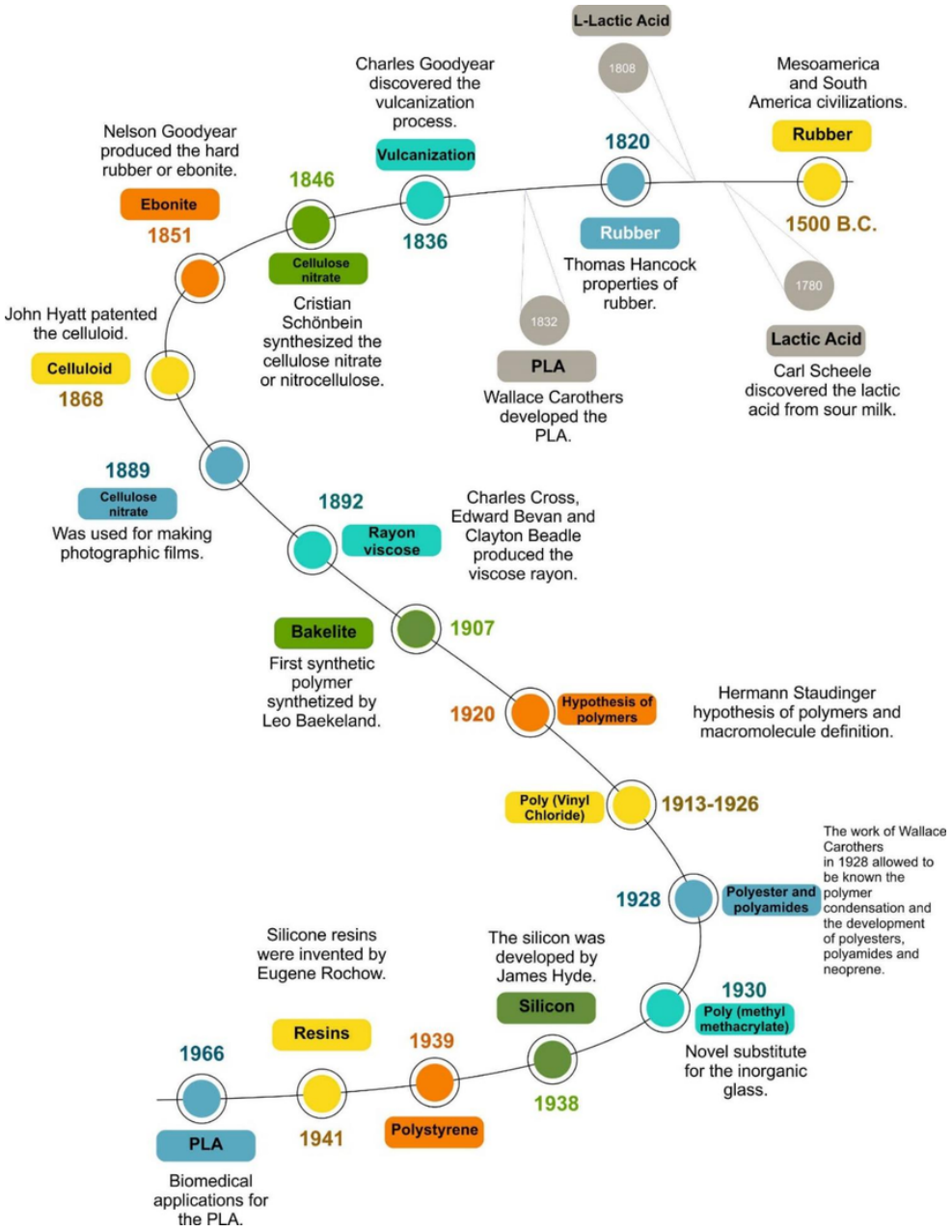


Figure 2.1: Inside the history of polymers [3].

2.1.1 Thermoplastics: semi-crystalline and amorphous

Thermoplastics, and polymers in general, are created by combining smaller molecules, designated as monomers, usually through covalent bonding to form long chains using a process called polymerisation. In a polymer chain, the atoms that compose it are strongly bonded due to the nature of its interatomic linkage, while the forces between chains are weaker [2].

The polymer chains may vary widely depending on the type of monomers that compose it, originating side branches on the chains themselves. The chains can form ordered and repetitive crystalline regions if these branches are scarce and of minimal length, whereas if the polymer

has numerous elongated side branches, ordered regions can't form, resulting in the polymer being amorphous. We can always find amorphous regions amid the crystallites so these polymers are called semi-crystalline and not crystalline only [2] (see Figure 2.2).

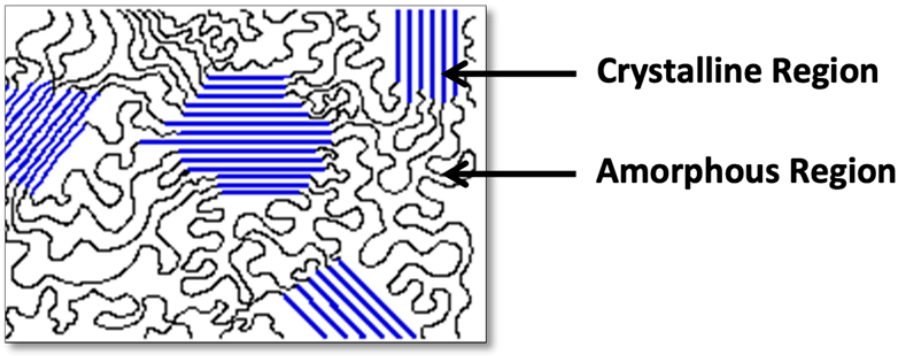


Figure 2.2: Schematic of a semi-crystalline polymer [4].

The degree of crystallinity and the morphology of the crystalline regions play an important role in the physical, mechanical, and thermodynamic properties of semi-crystalline polymers. A high degree of crystallinity means that the polymer is rigid and exhibits a high melting point, and high crystalline melting (T_m) and glass transition (T_g) temperatures. These properties heavily influence the characteristics of polymers as they directly impact the observed mechanical attributes of the material [2].

2.1.2 Transition Temperatures

Polymers can have at least three characterizing temperatures that define their thermal properties [5]:

1. Glass Transition Temperature (T_g)
2. Crystalline Melting Temperature (T_m)
3. Crystallization Temperature (T_c)

2.1.2.1 Glass Transition Temperature (T_g)

The glass transition temperature (T_g) is the average temperature during the process of heating a polymeric material from a low to high temperature where molecular mobility starts to occur. Below that range, the material progresses into a rigid and glass-like state as the molecules settle into a static position [6] as the polymer lacks the amount of energy required to allow chains to displace.

The T_g of polymeric materials can vary widely based on intrinsic factors such as morphology, crystallinity, molecular weight, and density, and extrinsic factors, such as the conditions and

techniques used during its creation and analysis of these properties. These factors determine the transition temperature at which the amorphous phase shifts from its glassy state to a rubbery state [7].

The glass transition temperature is used to determine the application of a material as it directly affects several properties of polymeric materials, including strength, damping, flexibility at low temperatures, and wet grip, among others. As such, high T_g elastomers are favored over low T_g elastomers for applications where high mechanical strength and flexibility are necessary, whereas low T_g elastomers are preferred in situations where low-temperature flexibility, low heat generation, high resilience, and low rolling resistance are required [6].

Table 2.1 indicates the T_g of some common polymers.

Table 2.1: Glass Transition Temperatures of Common Thermoplastics [5].

Polymer	T_g **[°C]**
Polylactic Acid (PLA)	55
Polyethylene Terephthalate Glycol (PETG)	75-85
Acrylonitrile Butadiene Styrene (ABS)	105
Nylon (Polyamide, PA)	40-80

2.1.2.2 Crystalline melting temperature T_m

The crystalline melting temperature, often referred to in the literature as "melting point" or "melt temperature", is the temperature at which semi-crystalline polymer transitions from its crystalline state to a viscous flow state. Unlike low-molecular materials, in polymers this process occurs in a temperature range due to its internal molecular arrangements, causing T_m to be a physical characteristic of difficult calculation [8].

Semi-crystalline thermoplastics commence softening at T_g but they do not demonstrate a fluid behavior until T_m range is reached, which is generally higher than T_g. Between T_g and T_m the material can demonstrate significant stretching when subjected to relatively light loads, known as the "rubbery region" [9], as can be seen in figure 2.3.

2.1.2.3 Crystallization temperature (T_c)

As a polymer cools after being subjected to a melting temperature, above its T_m, it transitions from an amorphous liquid state of the melt to the crystalline state as it reaches a low enough temperature that allows a large number of its polymeric chains at a given position to organize themselves in a regular pattern once again spacially, enabling the formation of a crystalline structure. This process occurs along multiple points forming new crystals eventually traversing the entire polymeric mass leading to the crystallization of the melt [10].

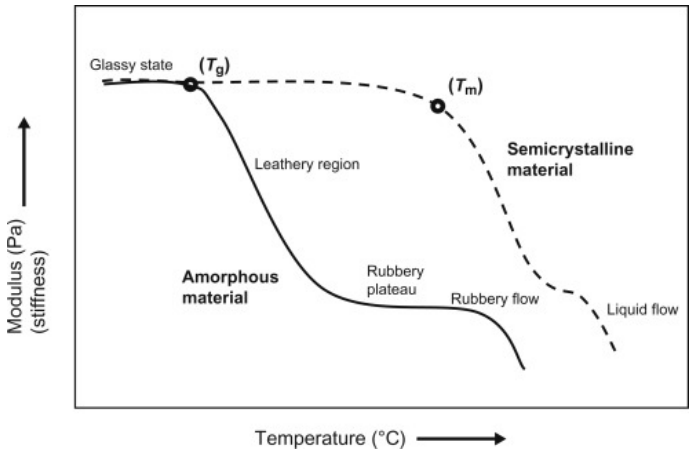


Figure 2.3: Melting and softening behavior of semicrystalline and amorphous materials [9].

This crystallization process takes place during the cooling down of the material in a temperature range between the T_g and T_m of the material, so it is common to define a single intermediary value in this range as the crystallization temperature of the polymer, T_c [10].

In conclusion, the thermal properties of a thermoplastic are crucial for characterizing a polymeric material. Understanding these properties provides valuable insights into the polymer's behavior, structure, and potential applications by helping to predict how the polymer will behave under different thermal conditions, such as heating, cooling, or exposure to varying environmental temperatures or mechanical factors.

Table 2.2 exhibits some thermal properties for commonly used polymers.

Table 2.2: Thermal Properties of Common Thermoplastics [5].

Polymer	T_c [°C]	T_m [°C]	**Thermal Conductivity [W/m·K]**
Polylactic Acid (PLA)	60-80	165	0.33-0.46
Polyethylene (PE)	80-115	110-130	0.33-0.46
Polypropylene (PP)	100-130	160-170	0.22
Polyethylene Terephthalate (PET)	140-180	250-260	0.15-0.24
Polyvinyl Chloride (PVC)	N/A	100-260	0.14-0.17
Polystyrene (PS)	N/A	240-270	0.12-0.17
Polycarbonate (PC)	N/A	220-230	0.19-0.22
Nylon (Polyamide, PA)	160-220	220-265	0.23-0.28
Polyoxymethylene (POM, Acetal)	150-160	175	0.31
Polybutylene Terephthalate (PBT)	170-180	225-230	0.25

2.1.3 Mechanical Properties

As discussed in previous sections, the extensive adoption of polymeric materials in many industries can be attributed to the lower cost of production, easier large-scale production, and unique mechanical properties of different materials making them range from liquids and soft rubbers to hard and rigid solids. These properties can be altered to modify the mechanical behavior of a material to suit a desired need for a given application, which can affect other properties simultaneously. Many structural factors play a crucial role in shaping the mechanical behavior of polymers, such as [11]:

1. **Molecular weight:** refers to the size of the polymer molecules, and is determined by the length of the polymer chains. A high molecular weight normally leads to increased tensile strength and viscosity and can improve the thermal and chemical resistances of the material.

2. **Cross-linking:** the connection of polymer chains through covalent bonds. Increases rigidity, strength, and heat resistance.

3. **Branching:** is the presence of side chains branching off the main chain. Reduces the crystallinity of the material, increasing flexibility and reducing overall density.

4. **Crystallinity:** indicates the degree to which polymer chains are ordered into a crystalline structure. The higher the crystallinity, the higher the polymer's mechanical strength, and stiffness, but reduced impact resistance and transparency.

5. **Crystal morphology:** describes the shape and size of the crystalline regions. Affects the material's optic properties as mechanical performance.

6. **Copolymerization (random, block, and graft):** the process of combining more than one distinct monomer to form a copolymer. These can be distributed randomly, in blocks, or grafted onto another pre-existing chain. This can enhance properties such as toughness, flexibility, and chemical resistance.

7. **Plasticization:** involves adding a plasticizer to a polymer, to increase its flexibility and reduce its brittleness. This leads to a decrease in the glass transition temperature T_g, making the polymer more flexible at low temperatures.

8. **Molecular orientation:** the alignment of the polymer chains in a specific direction. Can enhance tensile strength and modulus in the direction of alignment. However, the inverse can happen in the opposite direction.

9. **Fillers:** materials added to polymers to enhance certain properties. Influence many properties, improving strength, stiffness, impact resistance, reduce shrinkage, and can affect thermal and electrical properties.

10. **Blending:** physically blending two or more polymers. Combines advantageous properties of different polymers, but depends on the compatibility and interaction between the blended polymers.

11. **Phase separation and orientation in blocks, grafts, and blends:** occurs when distinct polymer segments are immiscible and form distinct domains. Common in block or graft copolymers, and blended polymers. Can lead to materials with unique properties due to the existence of distinct phases.

Mechanical behavior involves a material's deformation when subjected to stress. Polymers are not purely elastic materials, meaning their deformation under applied forces is not fully reversible once the stress is removed; while small deformations under low stress may allow the material to return to its original shape (elastic behavior), larger deformations or prolonged loading can cause permanent changes in shape (plastic deformation) or even structural damage, preventing full recovery. [12].

Purely elastic materials return to their original shape and size after removal of the force, as the material releases the energy stored during stress. In viscous materials, on the other hand, as forces are applied the material deforms in proportion to the time subjected to stress until applied forces are removed, not returning to its original form since energy is lost into the system [12].

Polymers exhibit both elastic and viscous behavior. This results in immediate elastic deformation and time-dependent plastic or viscous deformation, known as viscoelasticity. Viscoelastic materials exhibit time and temperature dependence: at lower temperatures, their elastic characteristics become more prominent, resulting in a stiffer and more resilient response to the applied forces. Whereas, at higher temperatures, their viscous behavior becomes more pronounced, leading to a softer, more pliable material that deforms more easily and may not fully recover its original shape after the force is removed (Figure 2.4) [12].

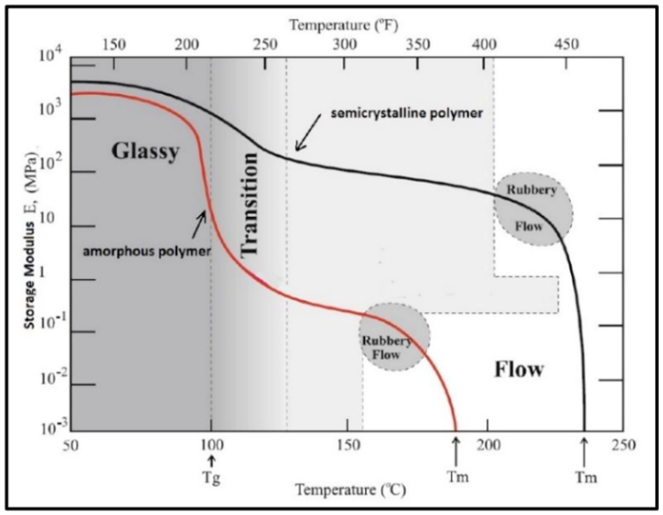


Figure 2.4: Temperature dependent behavior of polymers [13].

Characterizing the mechanical properties of polymers involves a range of tests and analyses to determine how the material behaves under various types of stress (σ) and strain (ε), such as static or dynamic testing, destructive and non-destructive testing, and short or long-term testing, among others. While there is not a single common factor among these tests, there are parameters that are frequently used to describe the stress-strain properties of polymers providing a comprehensive understanding of their mechanical behavior, allowing engineers to select and design materials for specific applications based on their mechanical performance. Below I list some of these properties [14, 15]:

1. **Young's Modulus (E):** also known as the modulus of elasticity, describes the stiffness in the elastic region of the material. Higher modules indicate a stiffer material.
2. **Yield Strength (σ_y):** the yield at which plastic deformation starts. Marks the end of plastic behavior.
3. **Ultimate Tensile Strength (σ_{UTS}):** maximum stress before mechanical failure. Indicates the maximum load-carrying capacity.
4. **Elongation at Break (ε_b):** percent elongation at point of fracture. Measures a material's ductility.
5. **Toughness:** total area under the stress-strain curve up to fracture, representing the energy absorbed. Reflects the ability to absorb energy and resist fracture.
6. **Hardness:** measures the resistance of a polymer surface to indentation.
7. **Creep Resistance:** measures the material's ability to resist deformation under constant stress over time.
8. **Stress Relaxation:** measures the decrease in stress under constant strain over time.
9. **Glass Transition Temperature (T_g):** transition temperature from glassy to rubbery state.
10. **Melting Temperature (T_m):** temperature at which a crystalline polymer melts.

For polymers, three main types of stress-strain behavior generalize how some materials will react to the application of stress forces which categorizes a polymer as brittle, plastic, or elastomer (see Figure 2.5) [16]:

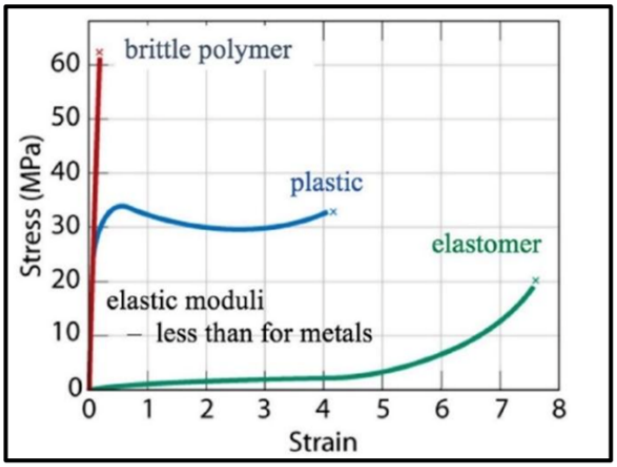


Figure 2.5: Mechanical behavior of polymers [16].

1. **Brittle Polymer**
    - Reaches maximum stress quickly and fractures with low strain;
    - Small plastic deformation; material breaks soon after reaching maximum stress.
2. **Plastic**
    - Initial linear region where material deforms elastically;
    - From yield point (σ_y) it exhibits plastic deformation, withstanding significant strain at constant stress;
    - Curve flattens, indicating that the polymer can stretch without a significant increase in stress.
3. **Elastomer**
    - Large strain capability with much lower initial stress;
    - Curve rises gradually, indicating the material can stretch significantly before breaking;
    - Stress increases at higher strains, indicating non-linear elastic behavior.

2.1.4 Water absorption mechanisms

Water absorption in polymeric materials significantly influences their mechanical properties and overall performance. Polymers, especially hydrophilic ones, can absorb moisture from their surroundings leading to changes in various properties of the material, including mechanical strength, dimensional stability, and thermal behavior [17].

The effect on the mechanical properties of a polymer due to water absorption is influenced by room temperature, where studies have found that properties can be changed in different or

even opposite ways at different low and high temperatures. For instance, at room temperature and higher, water functions as a softening agent by spacing between chains. Conversely, at cryogenic temperatures, wet samples are stiffer than dry ones [17].

Several factors can influence the rate and amount of moisture absorption of polymeric materials the intrinsic properties of the material such as crystallinity, since a less crystalline polymer has a less ordered structure and higher free volume, environmental temperature, relative humidity, exposure time, thickness of the sample, and the moisture absorption mechanisms present. Absorbed moisture can cause the material to become plasticized, impacting its mechanical performance. This results in a lower polymer glass transition temperature, thereby decreasing the maximum permissible operating temperature. Additionally, the softened polymer is prone to swelling and damage caused by internal vapor pressure, which arises from moisture evaporation during phase changes at elevated temperatures. [18].

Three primary moisture absorption mechanisms can be involved in water absorption in polymeric materials depending on the nature of the material itself and environmental conditions: diffusion, capillary action, and hydrogen bonding.

2.1.4.1 Diffusion

Diffusion is the primary mechanism by which water molecules penetrate the polymer matrix, filling voids and free volume. This process is driven by the concentration gradient between the external environment and the polymer interior [19].

Fickian and non-Fickian moisture diffusion

For many polymers, water absorption follows Fick's laws of diffusion, where the rate of absorption is proportional to the concentration gradient. In this case, the water molecules move into the polymer at a rate dependent on the difference in water concentration between the polymer surface and its interior [19].

The Fickian transport of moisture in polymers or polymer composites is characterized by

$$\frac{\partial C}{\partial t} = D\left(\frac{\partial^2 C}{\partial x^2} + \frac{\partial^2 C}{\partial y^2} + \frac{\partial^2 C}{\partial z^2}\right) \tag{2.1}$$

This equation is known as the general diffusion law or Fick's second law of diffusion (Fick's law, for short). C (kg/m^3) is the moisture concentration, $t(s)$ the time, and D (m^2/s) is the diffusion coefficient or diffusivity of the moisture in polymers [18].

The temperature dependence of the diffusion constant is expressed by the Arrhenius equation:

$$D = D_0 \exp\left(-\frac{E_d}{kT}\right) \tag{2.2}$$

where D_0 is a pre-factor, E_d is the activation energy, $k = 1,38x10^{-23} J/K$ is the Boltzmann's constant, and T the absolute temperature. It is important to note that the pre-factor and activation energy constants differ across the glass transition temperature. In other words, to fully describe

the moisture diffusivity as a function of temperature across this range, a material typically requires two distinct sets of constants [18].

Although Fick's diffusion model offers a reasonable approximation of moisture uptake characteristics, it rarely provides a complete description of the uptake data and fails to account for changes in polymers due to relaxation, degradation, or cracking [18].

Non-Fickian diffusion, or anomalous diffusion as it is referred to in literature, occurs when the polymer matrix undergoes significant structural changes upon water intake. This results in a constant or non-linear rate of water penetration, independent of the initial concentration and this is where it deviates from the classical Fick's laws of diffusion [18]. Understanding non-Fickian diffusion is crucial for accurately predicting the long-term performance of polymers in humid environments and for designing materials that can better withstand moisture-induced changes.

The most common technique to analyze moisture uptake by a polymer is periodic weight gain measurements, see Figure 2.6 [18].

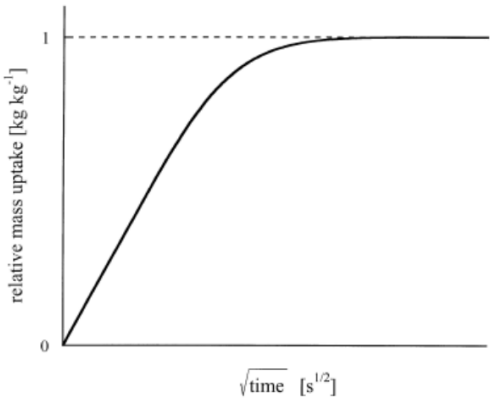


Figure 2.6: Schematic of a typical Fickian absorption curve [18].

2.1.4.2 Capillary Action

Capillary action plays a significant role in the moisture absorption of polymers, especially those with porous structures, microcracks, or voids. This mechanism involves the movement of water into the polymer through small capillaries or channels, driven by surface tension and adhesive forces between water molecules and the polymer surface. While not as universally relevant as diffusion or hydrogen bonding, capillary action can be highly pertinent in certain types of polymers and applications, such as porous polymers, composite materials where the matrix may contain microvoids between fibers, and aged or degraded materials that may have developed micro-cracks due to mechanical stress or environmental exposure over time [20].

2.1.4.3 Hydrogen Bonding

Hydrogen bonding significantly influences the moisture absorption properties of polymers, especially those with hydrophilic characteristics that have an affinity for water and can absorb moisture readily. These polymers typically contain function groups capable of forming hydrogen bonds with water molecules [21].

Hydrogen bonds are an attractive interaction between a hydrogen atom covalently bonded to a highly electronegative atom and another electronegative atom with a lone pair of electrons (see Figure 2.7). The strongest hydrogen bonds are formed with first-row elements such as boron, fluorine, oxygen, and nitrogen [21]. These elements are highly electronegative and possess lone pairs of electrons, making them ideal for hydrogen bond formation.

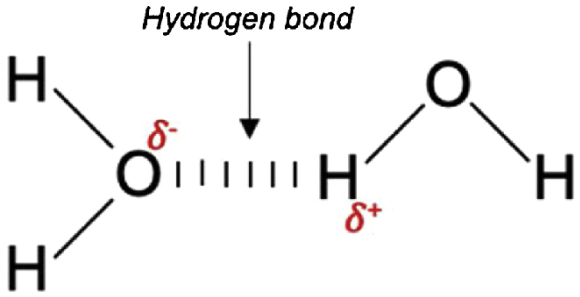


Figure 2.7: Diagram of hydrogen bonding [21].

In Table 2.3 we have a list of the main polymer functional groups, which contain these elements, facilitating the formation of strong hydrogen bonds with water molecules significantly influencing the material's affinity for water [22].

Table 2.3: Functional Groups in Polymers and Their Example Polymers [22].

Functional Group	Formula	Bonding Atoms	Example Polymers
Hydroxyl	-OH	O	Polyvinyl Alcohol (PVA), Cellulose
Amide	-CONH-	O, N	Polyamide (Nylon), Polyacrylamide (PAM)
Carboxyl	-COOH	O	Polyacrylic Acid (PAA)
Ether	-O-	O	Polyethylene Glycol (PEG), PEO
Carbonyl (in Lactam)	-C=O	O	Polyvinylpyrrolidone (PVP)
Amino	-NH2	N	Chitosan, Proteins

2.1.5 Degradation Mechanisms in polymeric materials

The processes that lead to changes in the appearance, mechanical and chemical properties, and overall performance of polymeric materials over time due to environmental conditions are known as degradation mechanisms. Several degradation mechanisms can act on polymeric materials, determined by their structure, mass, degree of crystallinity, processing and manufacturing conditions, and environmental and usage conditions. Polymer degradation can occur due to various

factors and result in significantly distinct changes to the material, influenced by the nature of the material itself. In brief, the degradation in polymeric materials refers to the fragmentation of macromolecules into lower molecular weight chains, which subsequently alters the chemical composition of the polymer and reduces the overall physical performance [23] (see Figure 2.8).

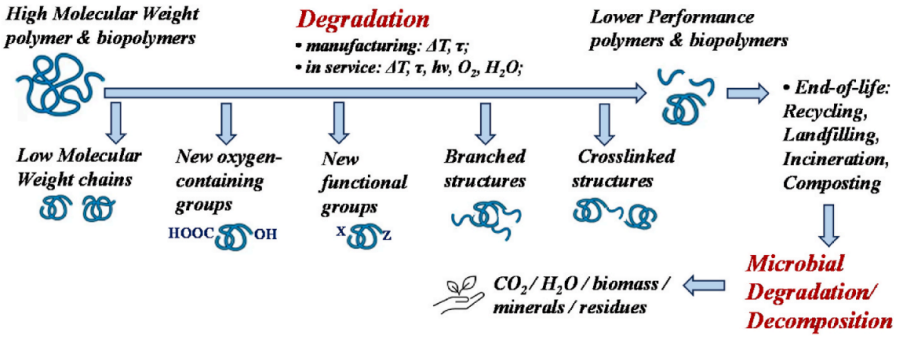


Figure 2.8: Overall degradation understanding for polymers and biopolymers [23].

Polymers are exposed to distinct sources of stress while in service and can be subjected to random material or environmental failures, complicating the description of degradation phenomena. However one can assume that polymer samples mainly undergo thermal, mechanical, photooxidative, hydrolytic and oxidative degradation.

- **Thermal degradation**: The main causes of thermal degradation include temperature variations, starting with the formation and propagation of free radicals, often accelerated by the presence of oxygen. Random scission, depolymerization, and side group elimination are generally the three types of thermal degradation mechanisms [23].

- **Mechanical degradation**: The primary causes of mechanical degradation are shear, tensile and/or compressive forces acting in the solid state which can cause macromolecules to break down leading to a negative impact in performance earlier than expected. Although mechanical factors are not the main contributors for polymer degradation, they can activate or accelerate the process [23].

- **Photodegradation**: The absorption of photon energy by polymers leads to the photodegradation of polymeric materials. This process breaks chemical bonds and chains, generating free radicals and reducing the molecular weight, which leads to a fast degradation of the mechanical properties of a polymer. When it occurs in air, oxygen availability accelerates the degradation rate due to the rapid formation of new oxygen-containing species. PLA's photo-oxidation affects its physical and mechanical properties [23].

- **Hydrolitic degradation**: This degradation mechanism involves the reaction of vulnerable bonds in macromolecules present in the polymer with water molecules existent in the environment, leading to the breaking of these bonds and the formation of chains with lower

molecular weights. Kinetic hydrolytic degradation can be accelerated if the environment temperature is higher than the room temperature. PLA is a bio-based degradable biopolymer, and due to its chemical nature, it is susceptible to hydrolysis. The hydrolysis of PLA initiates with the formation of lactic acid molecules, as shown in Figure 2.9a. This process can occur via acid or basic catalysis, and the products of PLA hydrolysis vary depending on the type of catalysis [23].

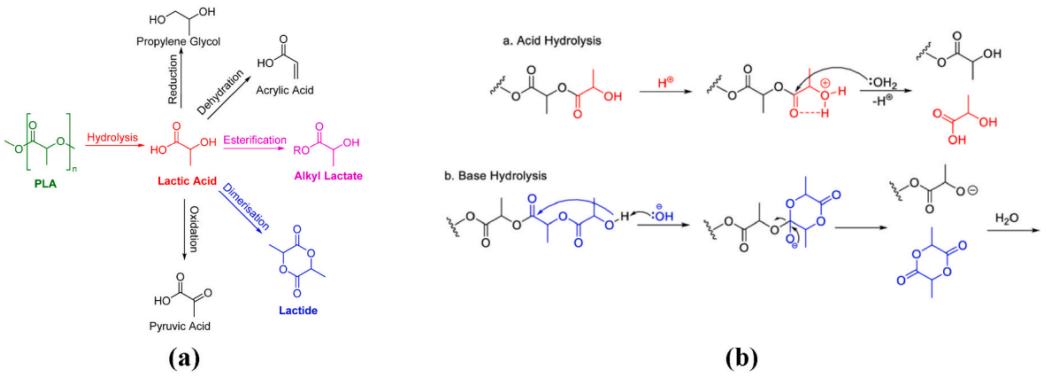


Figure 2.9: (a) Overall hydrolytic degradation of PLA and transformations, (b) PLA hydrolysis via acid and base catalysis [23].

- **Oxidation**: It usually initiates with the formation of radicals upon external stresses due to the presence of chemicals, and then it continues with the formation of oxygen-containing species. The rate at which this phenomenon happens, and the extent of the reaction are determined by the physical and chemical structure of the material [23].

2.2 Food Acids

To enhance the sour taste of foods and beverages, substances known as food acids can be added. These food acids can be divided into organic acids, such as citric acid, and inorganic acids, such as phosphoric acid [24].

2.2.1 Types

The main acids and their derivatives used in the food industry are acetic, adipic, citric, phosphoric, fumaric, lactic, malic, propionic, sorbic, succinic, and tartaric acids [24].

Food acids play various roles, including enhancing flavor, masking undesirable aromas, regulating pH, acting as buffering agents, fermentation agents, preservation agents, curing accelerators and sequestrants of metal ions. They are also used in retail-packaged gelatins, due to their low hygroscopicity, allowing the use of less moisture-resistant packaging, making them less expensive [24].

The solubility and hygroscopicity of food acids are important factors in the choice of which food acid to use. The most soluble food acids are also the most hygroscopic, which means they easily absorb water, which affects handling and shelf life [24].

2.2.2 Scale of measurement and classification

The scale used to measure the acidity or alkalinity of substances, including food acids, is the pH scale. The pH scale ranges from 0 to 14, with 7 considered neutral. Values below 7 indicate acidity, and values above 7 indicate alkalinity [25].

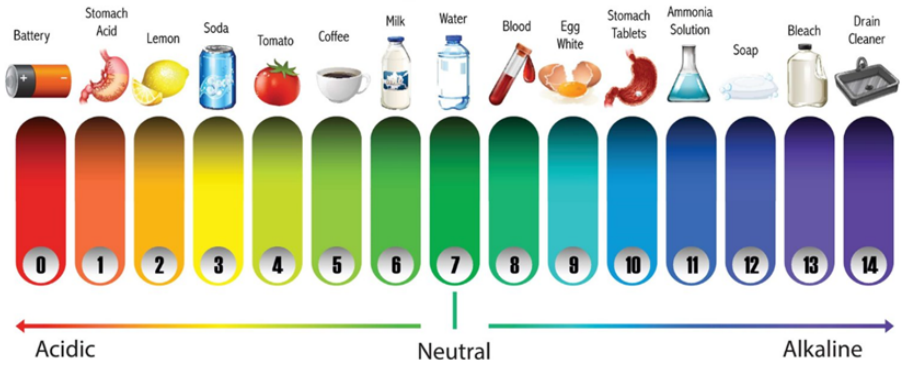


Figure 2.10: pH Scale [26].

The pH of food acids can vary, but they generally fall within the acidic range. Examples include citric acid (found in citric fruits), acetic acid (found in vinegar), and malic acid (found in apples) [25].

2.2.3 Effects of Food Acids on Polymeric Materials

Different polymers respond differently when interacting with food acids. Generally, the interaction between polymers and food acids can lead to changes in physical properties and chemical degradation. For most polymers, food acids accelerate degradation and, consequently, reduce durability.

Table 2.2.3 summarizes the major chemical and physical changes that food acids can cause in various polymeric materials, adapted from [27, 28]:

Type of Change	Polymeric Material	Effect	Description
Chemical Degradation	Polyesters (e.g., PET)	Hydrolysis	Reduction in molecular weight and mechanical strength due to acid-catalyzed hydrolysis
	Polyamides (e.g., Nylon)	Hydrolysis	Chain scission and weakening of material
	Polyolefins (e.g., PE, PP)	Oxidative Degradation	Cracking, discoloration, and loss of mechanical properties
Physical	PVC	Plasticization	Increased flexibility, deformation, and reduced tensile strength
	Cellulose-based Polymers	Plasticization/ Swelling	Swelling, reduced mechanical strength, and altered barrier properties
	Polycarbonates	Stress Cracking	Formation of cracks under mechanical stress
	Nylon, Polyamides	Swelling	Absorption of acids and moisture leading to swelling, reduced mechanical strength, and dimensional instability
	Polystyrene, Polyurethane	Discoloration	Yellowing and aesthetic degradation
	Polyethylene, Polypropylene	Softening/ Embrittlement	Softening and increased susceptibility to cracking under stress
	PVC	Softening	Reduced mechanical strength and increased vulnerability to damage
	Polyesters (e.g., PET)	Surface Degradation	Loss of gloss and smoothness, affecting aesthetic and functional properties
	Nylon	Surface Degradation	Roughened surface, potential to harbor contaminants

2.3 Polylactic acid (PLA)

Polylactic acid, also known as polylactide (PLA), is a thermoplastic which presents relatively high-strength and modulus, made from renewable resources, such as corn starch or sugarcane, allowing the biological cycle to come full circle (Figure 2.11) [29, 30].

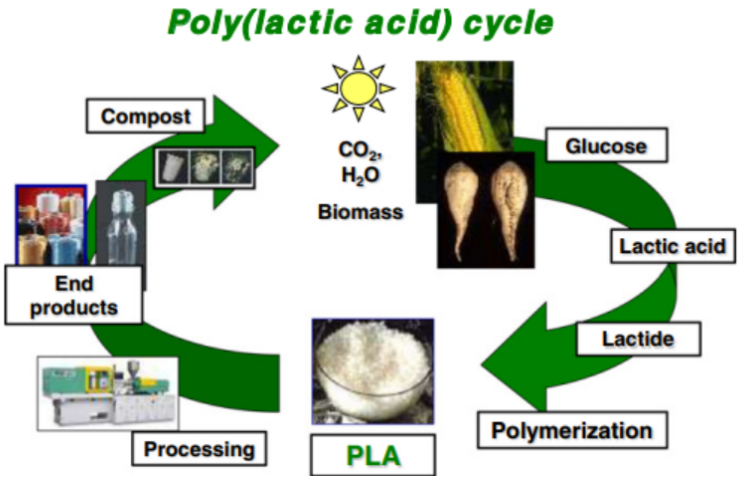


Figure 2.11: PLA life cycle starting with corn and sugar-beet [29].

Recently, new technological advancements have made PLA a great candidate as a substitute for synthetic polymers derived from petrochemicals in packaging and textile industries. However, PLA has certain drawbacks, such as low thermal resistance, and brittleness, and others, and various applications demand distinct end-use characteristics. Consequently, adding micro- and/or nanofillers, reinforcing fibers, and specialized additives to the PLA matrix is thought to be an effective way to achieve desired end-use features and significant property improvements for the material [29].

2.3.1 Mechanical and Thermal Properties

PLA is well-known for its mechanical properties, which exceed those of traditional plastics. Tensile strength (σ, in MPa), tensile modulus (E, in GPa), ultimate strain (ε, in %) and polymer density (ρ, in g/cm^3) are the most studied mechanical properties of PLA. From these properties, the PLA-specific tensile strength and tensile modulus range are given in table 2.4. PLA specific tensile strength (σ^*, in Nm/g) and specific tensile modulus (E^*, in kNm/g), are obtained by dividing PLA tensile strength and modulus, respectively, by its density [31].

Table 2.4: PLA mechanical and specific mechanical properties [31].

Property	**Unit**	**PLA**
ρ	g/cm^3	1.21-1.25
σ	MPa	21-60
E	GPa	0.35-3.5
ε	%	2.5-6
σ^*	Nm/g	16.8-48.0
E^*	kNm/g	0.28-2.80

The mechanical properties of PLA are greatly influenced by its thermal properties (Table 2.5).

Table 2.5: PLA Thermal Properties [31].

Characteristic	Unit	Amount
Solid density	g/cm^3	1.252
Melt density	g/cm^3	1.073
T_g	°C	55
T_m	°C	165
Specific heat (Cp)	K/kg°C	
190 °C		2060
100 °C		1955
55 °C		1590
Thermal conductivity	W/m°C	
190 °C		0.195
109 °C		0.197
48 °C		0.111

The T_g significantly influences the mechanical properties of the material, although its value may decrease at higher room temperatures. T_g is said to potentially act as a threshold temperature for a specific polymer, above which mechanical properties may deteriorate drastically [31]. Above T_m, the entire polymer chain becomes mobile and the mechanical properties are virtually reduced to zero, making this temperature one of the most important parameters when processing these materials [31]. In summary, understanding the thermal properties of PLA is important to optimize the mechanical performance of the polymer in various applications, from synthesis to processing, fabrication, and end-use product development.

2.3.2 Barrier Properties

The barrier properties of PLA pertain to its capacity to resist the transmission of gases, water vapor, and aromatic molecules. We will briefly present below how PLA behaves in these three aspects [31].

- **Gas permeation:** As we can see in Figure 2.12, PLA has moderate barrier properties against gases such as oxygen (O_2) and carbon dioxide (CO_2). PLA showed higher oxygen permeability than PET, meaning PET is more effective at blocking the passage of O_2, making it a better choice for applications where low oxygen permeability is critical, such as food and beverage packaging [31].

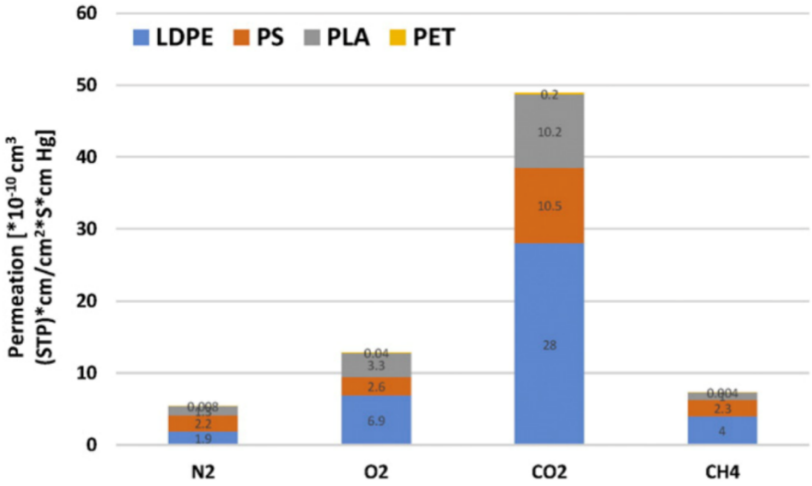


Figure 2.12: Barrier properties of PLA in comparison to other common polymers [31].

- **Moisture Permeation:** PLA has relatively poor moisture barrier properties, which can limit its use in applications requiring high moisture resistance. Regarding water vapor barrier, PET has the best performance, offering significant moisture resistance [31].
- **Aroma permeation:** PLA contributes a unique barrier characteristic by offering a moderate aroma barrier, which helps retain the aroma of products within the packaging [31].

Biopolymers face challenges in achieving barrier properties that are comparable to conventional synthetic polymers, such as PET, while still maintaining biodegradability. Some approaches are available in order to improve the PLA barrier properties. These approaches include applying coatings, performing chemical and physical modifications, and incorporating additives [31].

2.3.3 Behavior in water

PLA has both hydrophilic properties, thanks to the presence of polar oxygen linkages, and hydrophobic traits due to its methyl side groups. Being naturally hydrophilic, PLA undergoes moderate decomposition (hydrolysis) depending on temperature and moisture levels. It remains stable in water within a temperature range of 15°C to 40°C. [32].

When a PLA sample is immersed in water, its mechanical properties degrade. While stiffness can be partially restored upon drying, the material's strength cannot be fully recovered. PLA 3D-printed samples often exhibit a porous structure, as shown in Figure 2.13, which contributes to rapid water absorption [32].

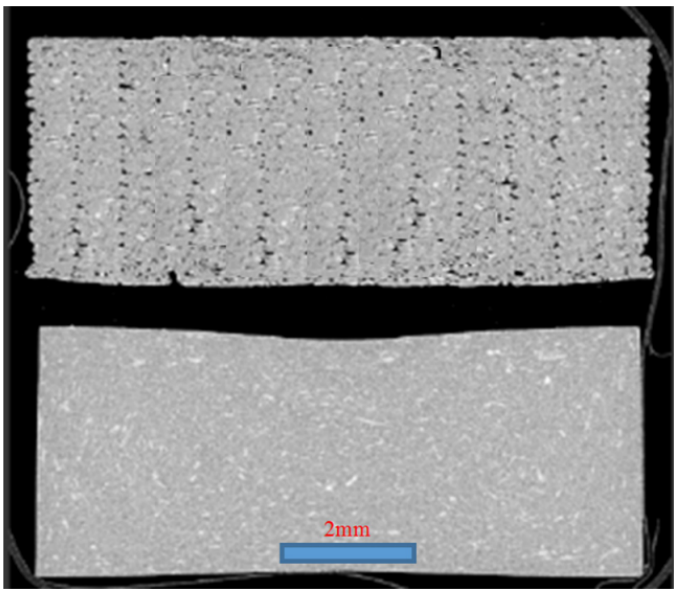


Figure 2.13: CT scan of a cross-section of a 3D printed sample (top) and injection molded sample (bottom) [32].

The tensile properties of PLA — such as tensile strength, tensile strain, and tensile modulus — remain largely unaffected by water storage. However, when PLA is stored in water, hydrolysis occurs, enhancing the mobility of its polymer chains and leading to increased crystallinity. As for its thermal properties (T_g, T_c, and T_m), hydrolysis does not have a significant impact [32].

2.3.4 Behavior in Food Acids

The degradation of PLA in the presence of an acid, such as citric acid, occurs via acid-catalyzed hydrolysis. Studies have shown that the acid-catalyzed hydrolysis of PLA involves the ester groups being attacked by water molecules, with citric acid acting as a catalyst [33]. Figure 2.14 presents the structural formula of PLA, with the functional groups color-coded [34].

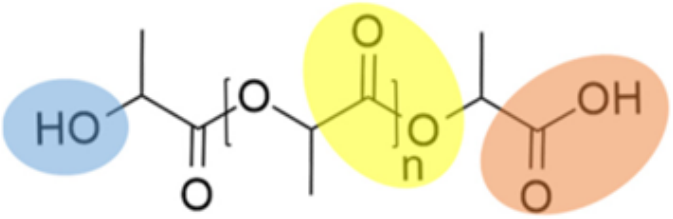


Figure 2.14: Chemical structure of PLA with its functional groups [34].

Where,

- in blue, the hydroxyl group is (-OH);
- in yellow, the ester group (-COO-);
- in orange, the carboxylic acid group (-COOH).

The hydrolysis of these ester bonds results in the breakdown of PLA chains into shorter polymer chains and eventually forming lactic acid monomers. This mechanism is relevant in applications where is critical to control the degradation level, such as in biomedical devices [33, 34].

2.3.5 Resistance to degradation

PLA can degrade through various means, including exposure to water, sunlight, microorganisms, and enzymes. Among these, water-induced degradation, or hydrolysis, is the most common. The natural degradation rate of PLA is influenced by factors such as crystallinity and molecular weight. As depicted in Figure 2.9, the degradation of PLA results in the formation of lactic acids and short oligomers [35, 36].

In the crystalline regions of PLA, the polymer chains are tightly packed and highly ordered, which limits their interaction with water molecules and consequently slows down the hydrolysis process. In contrast, the amorphous regions of PLA, where the polymer chains are randomly arranged and lack a definite structure, are more susceptible to water interaction and thus degrade more quickly [37].

However, under certain conditions—such as high temperatures or the presence of specific enzymes—PLA can degrade more rapidly. While PLA possesses moderate thermal stability, as mentioned in subsection 2.3.1, exposure to temperatures above its glass transition temperature (around 55°C) leads to thermal degradation, which in turn compromises its mechanical properties. In summary, PLA's resistance to degradation is highly dependent on the conditions it is exposed to and the specific applications in which it is used. Understanding these factors is crucial for optimizing PLA's performance and extending its lifespan across various applications.

2.4 Extrusion Based Additive Manufacturing

Extrusion Based Additive Manufacturing (EBAM) is a broad category of additive manufacturing processes that involve the continuous extrusion of material through a nozzle to build up a part layer by layer. This method can use a variety of materials, including plastics, metals, and ceramics, depending on the specific application. The extrusion process allows for the creation of complex shapes and is commonly used for producing prototypes, functional parts, and end-use products [38].

2.4.1 Fused Filament Fabrication (FFF)

Fused Filament Fabrication (FFF) is a widely used additive manufacturing (AM) process. FFF uses thermoplastics in the form of long filaments to create three-dimensional (3D) products from a digital model without any (or with minimal) human intervention. It is considered a low-cost additive manufacturing (AM) process that involves pressurizing and melting the filament in a liquefier before depositing it onto the build platform through a nozzle (Figure 2.15). The chosen filament material is very important as it directly influences the mechanical properties, thermal conductivity, and electrical conductivity of the final part [38].

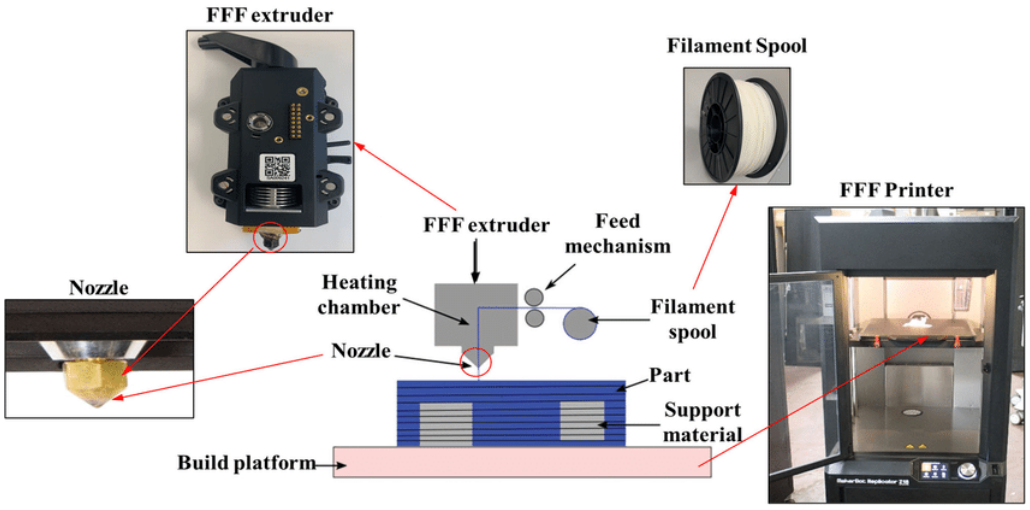


Figure 2.15: Schematic Diagram of the Fused Filament Fabrication (FFF) process [38].

In general, the stages involved in part fabrication using Fused Filament Fabrication (FFF) technology are [38]:

1. **CAD modeling:** Convert the CAD model into a machine-readable format, such as stereolithographic (STL) or additive manufacturing format (AMF);

2. **Slicing:** The 3D model for printing, it is divided into numerous thin layers through a process called slicing. This step converts the model into a series of sequential cross-sections, which the printer uses as a blueprint to build the object layer by layer. At this stage, the process parameters, such as layer height, infill density, and other relevant factors, are established.

3. **Generate G-Code:** Create the G-code, a programming language used to control the movement of the FFF extruder in the XY plane, for each layer.

4. **Upload to printer:** Upload the STL file to the FFF machine software;

5. **Printing:** Depositing each layer, on top of the previous one according to the G-code instructions. This process is repeated until the part is fully fabricated.

Most commercial FFF machines come with software that handles slicing and G-code generation. In such cases, the STL file is uploaded directly into the machine's software for processing [38].

2.4.2 Process Parameters

Important properties such as surface roughness, dimensional accuracy, and mechanical properties are greatly influenced by the Fusion Filament Fabrication (FFF) process parameters, that can be divided into three main categories: **slicing parameters**, **orientation** and **temperature conditions** [38].

2.4.2.1 Slicing parameters

- **Layer thickness/height**: The thickness of each deposited layer in the build platform [5];

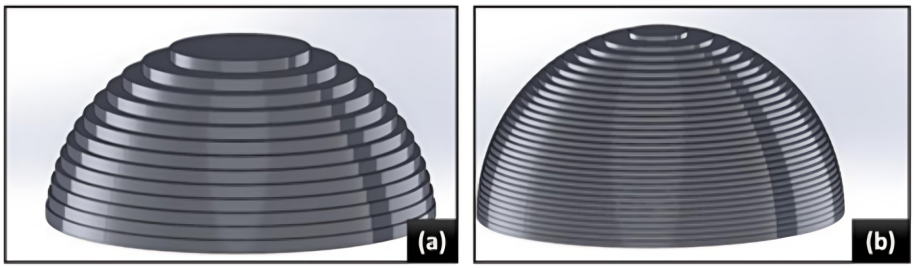


Figure 2.16: Layer thickness visual effects – (a) 0.1mm; (b) 0.05mm [5].

- **Raster width:** depends on the nozzle diameter, and it is defined as the width of the deposition beds [5];
- **Raster orientation/angle**: The direction of a raster relative to the x-axis of the respective build platform [5];

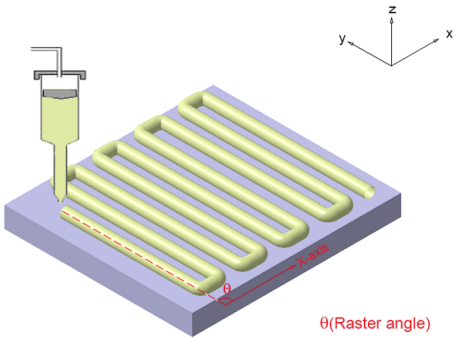


Figure 2.17: Graphical definition of raster angle [5].

- **Flow rate**: The volume of the filament extruded through the nozzle per unit of time [5];

- **Print speed**: Linear speed of the extruder during the print process [5];
- **Infill density**: The percentage of the volume of the internal structure to be filled with filament material [5].

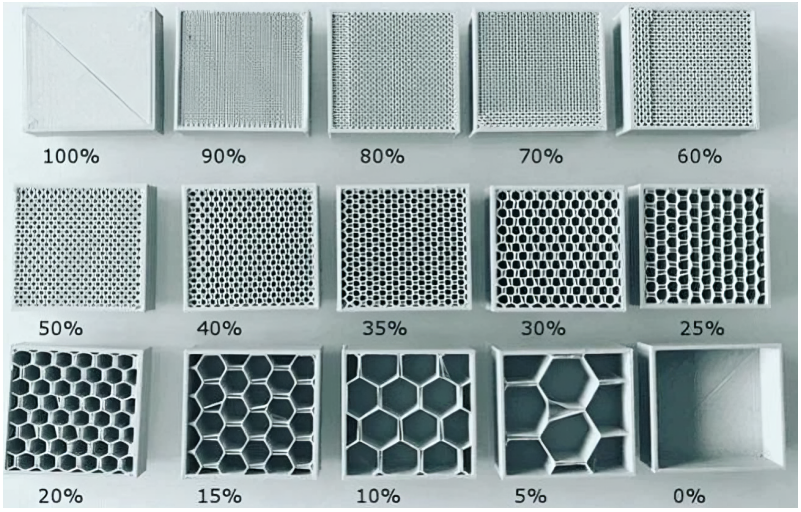


Figure 2.18: Variation of infill density [5].

- **Air gaps**: In a layer, the gap between two adjacent rasters. If overlapped, this value is said to be negative [5];
- **Contour width**: The width of the material bead used for contours [5];
- **Raster width**: Width of deposited beads [5];
- **Infill pattern**: Some common infill patterns are hexagonal, diamond, or linear [5];

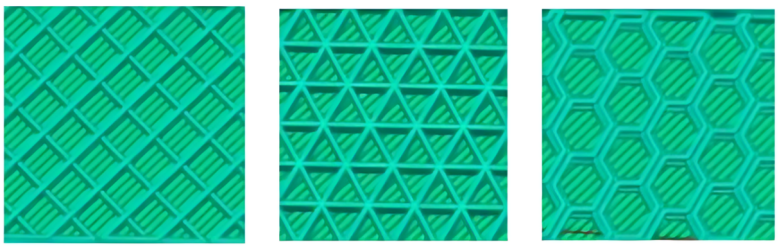


Figure 2.19: Infill patterns commonly used [5].

2.4.2.2 Orientation

In Fused Filament Fabrication (FFF), build orientation refers to how a 3D model is positioned on the build platform relative to the Cartesian coordinate system, which consists of three axes: X (horizontal), Y (depth), and Z (vertical) [5].

The orientation of a part during printing significantly impacts its mechanical properties — such as mechanical strength —, surface finish, print time, and material usage [5].

By carefully selecting the build orientation relative to these axes, operators can optimize the quality and performance of the printed part, taking full advantage of the FFF process's capabilities while mitigating its limitations [5].

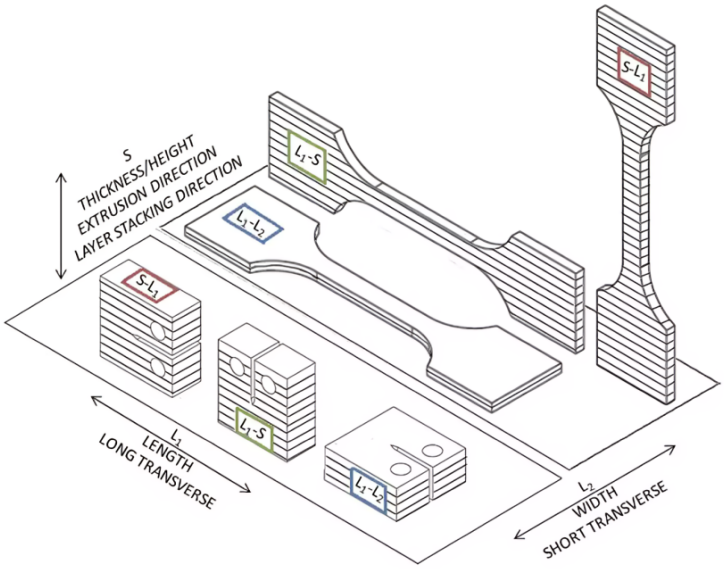


Figure 2.20: Various build orientations at which different test samples can be printed [5].

2.4.2.3 Temperature conditions

- **Extrusion temperature:** The temperature at which the filament is heated in a liquefier during the print process [5].
- **Bed/platform temperature:** The temperature of printing bed or build platform [5].
- **Room temperature:** The surrounding temperature where a FFF machine is located. This temperature may impact moisture content, warping, or cooling rate [5].

2.4.3 Materials

Thermoplastic materials are commonly used as the raw material for this Additive Manufacturing (AM) process, with the choice of filament depending on the specific application and part requirements, as different thermoplastics offer distinct properties [38]. Table 3.1 lists some common pure filaments used in FFF and their properties and applications.

Each of these materials has its own set of advantages and limitations, making the selection highly dependent on the specific requirements of the application, such as strength, flexibility, heat resistance, and ease of printing. Understanding these properties helps in optimizing the performance of the final printed parts in FFF processes[38].

Table 2.6: Common Pure Filaments Used in FFF and Their Properties (adapted from [38]).

Filament	Properties	Applications
PLA	Biodegradable, easy to print, low warping, limited heat resistance	Ideal for general-purpose printing, prototypes, and consumer products where environmental impact is a consideration.
ABS	Tough, impact-resistant, higher temperature tolerance, prone to warping	Suitable for functional prototypes, mechanical parts, and products requiring durability and strength.
PETG	Good chemical resistance, transparent, slightly flexible, strong	Versatile for both mechanical and aesthetic applications, including parts that require a balance of strength and flexibility.
PA	High strength, flexible, wear-resistant	Used for durable parts such as gears, bearings, and functional prototypes that require flexibility and mechanical performance.
TPU	Flexible, elastic, abrasion-resistant	Ideal for applications needing flexibility and durability, like seals, gaskets, and footwear components.

2.4.4 Water diffusion in printed parts

Water diffusion in printed parts by FFF technology is a concern, especially for applications exposed to humid environments or submerged in water. When exposed to moisture, printed polymers can experience material degradation and consequently changes in mechanical properties such as modulus, mechanical strength, and ductility [39].

Polymers absorb moisture as water molecules penetrate the material, a process heavily influenced by both temperature and ambient humidity. On a microscopic scale, factors such as the polymer's polarity, degree of crosslinking, and the presence of hydrophilic groups play a significant role in this moisture diffusion. As moisture permeates the polymer, it leads to an increase in the material's mass [39].

This phenomenon is modeled using Fick's law of diffusion with the temperature-dependent diffusion coefficient, D, being determined by equation 2.3:

$$D_t = \pi \left(\frac{h}{4M_{\text{sat}}} \right)^2 \left(\frac{M_t}{\sqrt{t}} \right)^2 \tag{2.3}$$

where, D is the diffusion coefficient (mm^2/s), h is the specimen thickness (mm), M_t is mass after absorption of time t (grams), t is time (seconds) and M_{sat} is the saturated water content (%), calculated by equation 2.4:

$$M(\%) = \frac{M_t - M_i}{M_i} \times 100 \tag{2.4}$$

where, M_i is the initial mass before immersion (grams), and M_t is the mass after absorption after time t [39].

Understanding water diffusion in FFF printed parts is crucial for ensuring the longevity and performance of polymers in humid or submerged conditions.

2.4.5 Degradation mechanism on printed parts

The degradation mechanisms in printed parts can include thermal, chemical, and mechanical degradation and environmental factors such as UV exposure and moisture absorption. Extensive research has been done on the effects of various types of degradation on AM-printed parts of different materials. Appendix A lists this literature study.

To improve the durability and performance of AM-printed parts it is crucial to understand these mechanisms. Many strategies can help mitigate these degradation effects and improve the longevity of 3D-printed components.

Chapter 3

Materials and Methods

This chapter outlines the methodology used in this master's dissertation, along with the equipment and materials employed. Figure 3.1 provides a schematic representation of the main steps involved in the experimental and research processes.

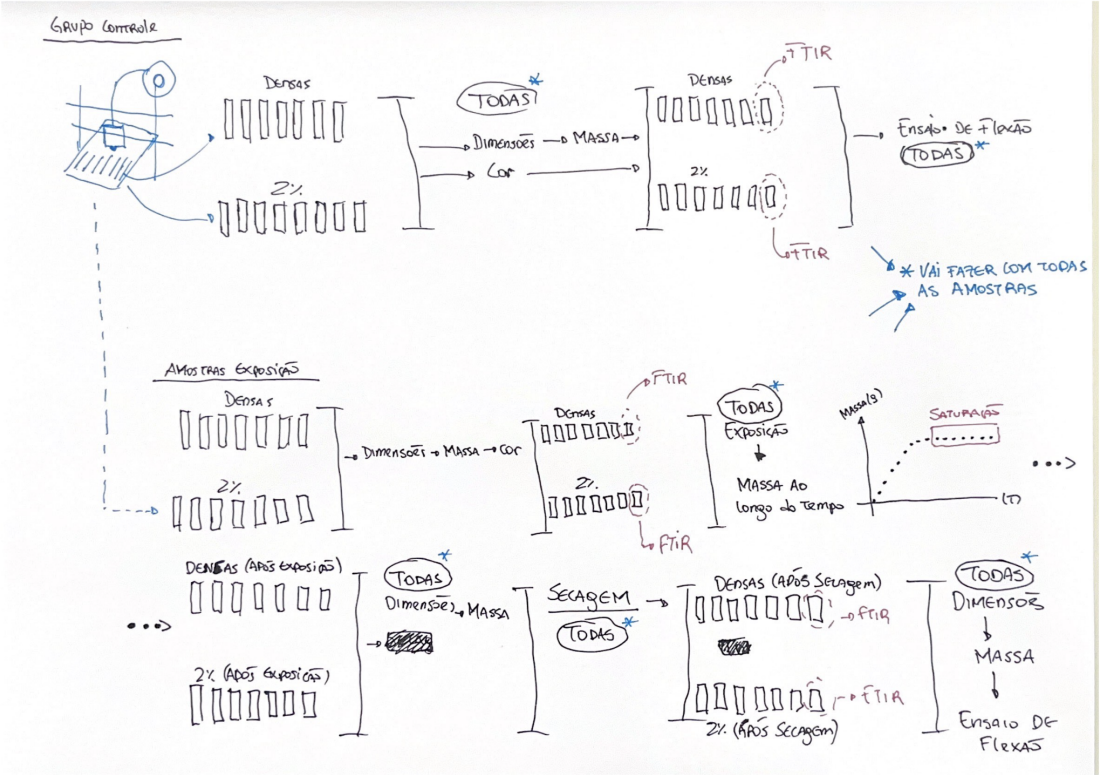


Figure 3.1: Schematic of the experimental procedures.

3.1 Materials

In this thesis, the PLA filament used to print all the samples was transparent PLA from Filkemp^{TM} supplier, see Figure 3.2. From now on, the filament will be mentioned by FILKEMP PLA-N.



Figure 3.2: Filament used FILKEMP PLA-N [40].

The technical specifications of the filament are presented in table 3.1:

Table 3.1: PLA filament's technical characteristics (C).

Properties/Parameters	**FILKEMP PLA-N**
Filament diameter (mm)	1.75 ± 0.05
Melt Flow Index (g/10min)	13 ± 2
Glass transition temperature (°C)	66.5
Melt temperature (°C)	172 ± 5
Printing temperature (°C)	200 - 215
Printing bed temperature (°C)	60
Flexural modulus (MPa)	2120 ± 480

3.2 3D Printing System

3.2.1 3D Printer

In this research the 3D printer utilized for printing all the mentioned parts was the Prusa i3 MK3S, see Figure 3.3.

As shown in Figure 3.3 above, the printer was placed inside an acrylic enclosure. This way it was possible to provide a physical barrier against temperature fluctuations from the external environment, which could potentially influence the printing quality of the samples for the study. Table 3.2 presents the technical specifications of the printer.

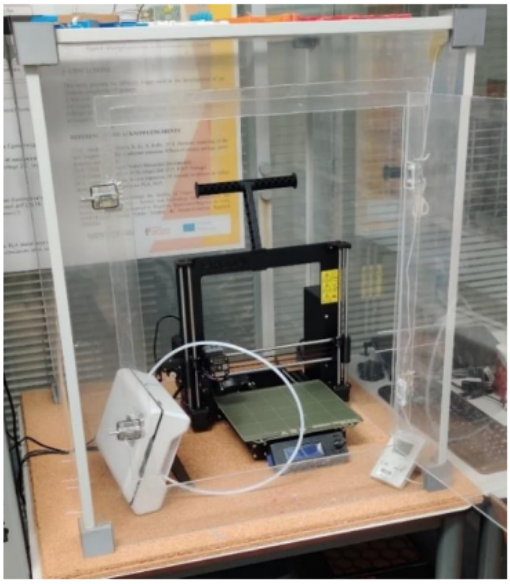


Figure 3.3: Prusa i3 MK3S Printer [41].

3.2.2 Software

To produce the calibration cubes, typically 20x20x20 mm models used to test and fine-tune the 3D printer's accuracy, print quality, and performance—and the flexural test specimens used in this thesis, it was necessary to generate the required files (G-codes). This involved using slicer software that was capable of importing STL files and adjusting printing parameters. The PrusaSlicer (version 2.5.0) software was used for this project (Figure 3.4).

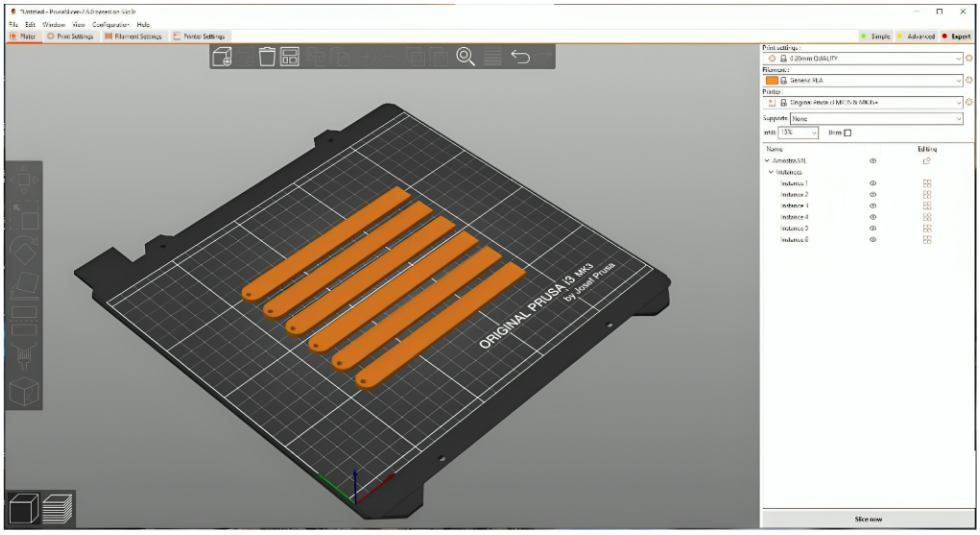


Figure 3.4: PrusaSlicer Software.

Table 3.2: Prusa i3 MK3S Technical Parameters [41].

Parameter	**Technical Data Values**
Build Volume	25×21×21 [mm]
Layer Height	0.05 – 0.35 [mm]
Nozzle	0.4 [mm]
Filament Diameter	1.75 [mm]
Supported Materials	Wide range of thermoplastics, including PLA, PETG, ASA, ABS, PC (Polycarbonate), CPE, PVA/BVOH, PVB, HIPS, PP (Polypropylene), Carbon filled, Woodfill and other filled materials
Max Travel Speed	200+ [mm/s]
Max Nozzle Temperature	300°C
Max Heatbed Temperature	120°C
Extruder	Direct Drive, Bondtech gears
Print Surface	Removable magnetic steel sheets with different surface finishes, heated with cold corners compensation
Printer Dimensions	7 [Kg], 50×55×40 [cm]
Power Consumption	PLA settings: 80 [W]

3.2.3 Equipment calibration and printing parameters

Prior to printing the flexural samples, it was necessary to validate the printing parameters intended to use across this research. The parameters adopted in this work were those specified by [42], [5] and [41], for PLA parts, as detailed in Table 3.3.

Table 3.3: Printing Parameters [41].

Parameters	**Values**
Number of Perimeters	3
Seam	Aligned
Perimeter Printing Speed	20 [mm/s]
Fill Printing Speed	40 [mm/s]
Overlapping Adjacent Lines	27%
Extrusion Temperature (1st layer/following)	215° / 210°C
Bed Temperature	60°C
Extrusion Multiplier	1
Fill Type	Aligned Rectilinear
Fill Angle	0°
Layer Height	0.2 [mm]
Retraction Length	1 [mm]
Retraction Speed	30 [mm/s]

To assess the appropriateness of his configuration for printing ASTM D790 [43] flexural samples, five cubes of 20 mm per side, illustrated in Figure 3.5, were 3D printed and subjected to

evaluation through two distinct analyses: qualitative (visual inspection) and quantitative (mass and dimension measurements).

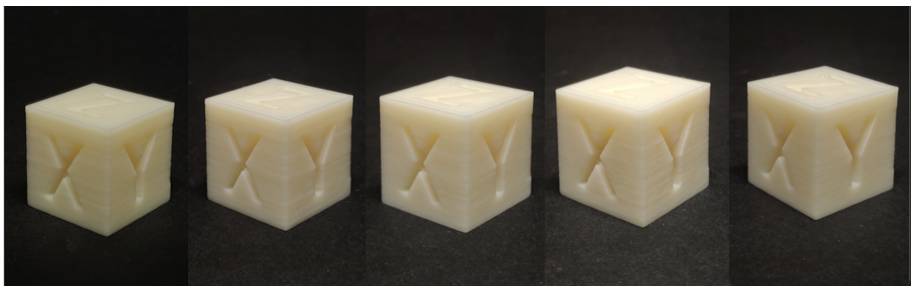


Figure 3.5: Calibration Cubes.

When it comes to FFF printing methods there are several factors that can affect the print quality such as [5]:

1. **Over/under extrusion** - **over extrusion** occurs when excess material is deposited, resulting in filament buildup, while **under extrusion** leads to insufficient flow, creating gaps and weak layers in the print;

2. **Material warping** is the deformation of a printed part caused by uneven cooling, leading to curled or distorted shapes that affect dimensional accuracy and adhesion to the build plate;

3. **Elephant's foot** is a defect where the lower layers of a print are wider than intended, often due to excessive heat causing them to spread before solidifying;

4. **Layer delamination** occurs when layer adhesion is insufficient, causing visible separations or cracks that compromise the print's structural integrity;

5. **Infill and perimeters detachment** occurs when the inner filling structure separates from the outer walls, leading to a weak and hollow print that may lose its intended shape;

6. **Oozing** is the unwanted extrusion of filament from the nozzle during non-printing movements, resulting in strings or blobs on the print surface that can affect its finish;

7. **Surface bubbles** are air pockets trapped within print layers, often caused by moisture in the filament or rapid cooling, leading to a rough texture and weakened structure;

8. **Corner distortion** refers to the warping of corners in a print, often due to uneven cooling or poor adhesion, resulting in dimensional inaccuracies;

9. **Material overheating** occurs when filament is exposed to excessive heat during printing, degrading its properties and causing discoloration or brittleness;

10. **Deposition of degraded material** occurs when improperly stored or overheated filament is extruded, leading to prints with weak mechanical properties and poor surface quality.

Each of the five printed cubes was visually inspected. No defects were detected, indicating a successful quality analysis. As a result, the process could proceed to the quantitative analysis. As mentioned before, for the quantitative analysis two distinct analyses were performed: mass and dimension measurements. The mass of the five calibration cubes was measured using a digital scale, House HLD300 with a resolution of $\pm 0.05g$.

Finally, a dimensional analysis was conducted by measuring each axis (X, Y, and Z) of each cube. Each axis was measured three times to ensure consistent values, after which the average and coefficient of variation (CV) [%] were calculated. A ZHJAN caliper with a resolution of 0.01 mm and an accuracy of ±0.02 mm was used for the measurements. Detailed specifications of the instrument are provided in Section 3.3.

The dimensional measurements obtained for the five calibration cubes are shown in Table 3.4 as follows:

Table 3.4: Average dimensions of calibration cubes.

Cube direction	**Average dimensions [mm]**	**CV (%)**
x	20.02 ± 0.02	0.06
y	20.01 ± 0.02	0.07
z	20.07 ± 0.02	0.19

These results validate that all the parameters established for the calibration procedure were met. Consequently, the printing parameters set by Castro [42], shown in Table 3.3, remained unchanged and were ready to be applied for the prints of the ASTM D790 flexural samples.

3.3 Case Study

3.3.1 Degradation of 3D-printed parts

To carry out this study, flexural samples were designed following a modified ASTM D790 [43]. The samples were modified in a small way to facilitate identification: a hole was added to allow a wire to pass through, helping to label each sample. This change was made using 3D design software.

However, when it was time for the exhibition and considering that the samples needed to be measured regularly, this identification method was deemed impractical. Instead, a permanent marker was used to label the group and sample number directly on each piece.

The samples were printed with infill densities of 2% and 100% to assess the extreme ends of the density spectrum. The choice of 2% as the minimum infill density was made to ensure structural integrity during both the printing process and subsequent handling of the samples. The samples were oriented as depicted in Figure 3.4, positioned flat along one of the two widest faces. This orientation was selected to enhance stability during printing and to achieve improved print quality.

To better distinguish between the samples with 2% and 100% infill density, two different designs were created, as shown in figures 3.6 e 3.7. These distinct designs allowed for a clear visual differentiation between the samples, ensuring that the varying infill densities could be easily identified during analysis and testing.

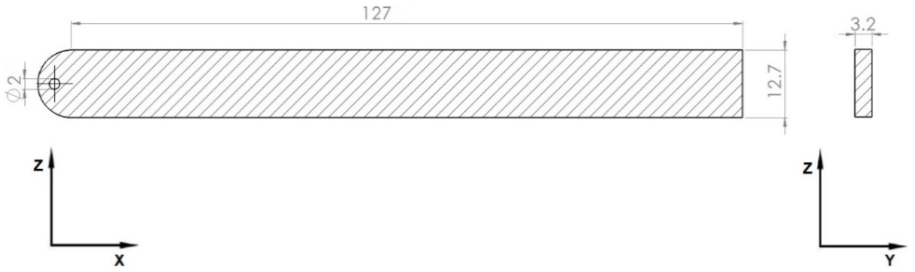


Figure 3.6: Representation of the printed samples with a 2% infill density (dimensions in [mm]).

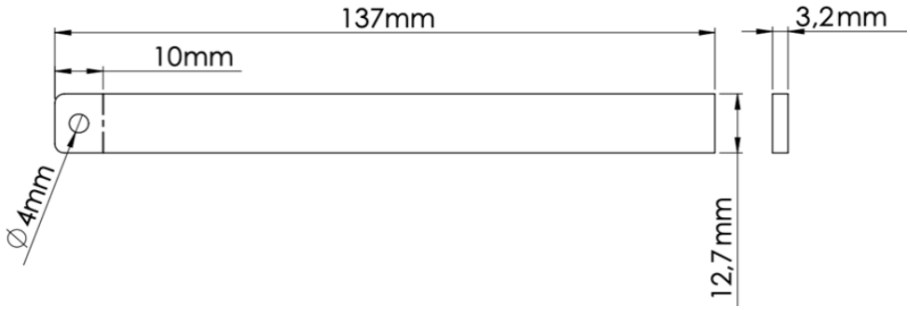


Figure 3.7: Representation of the printed samples with a 100% infill density.

Each printing session consisted of printing seven samples that were then grouped to a specific degradation condition.

Because there were seven scenarios to study, 49 flexural samples (7×7) per percentage fill were printed for exposition. To differentiate each of these samples, an identification code was created based on the nomenclature shown in Figure 3.8.

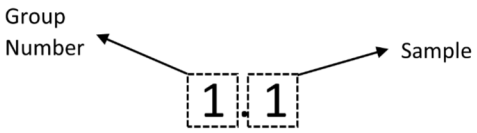


Figure 3.8: Identification code nomenclature.

The degradation study consists of fully submerging 98 printed samples (49 with a 2% infill density and 49 with a 100% infill density) into two liquid environments:

- Water
- Citric Acid Solution (CA)

The water used in the experiments was tap water. This choice was made to more accurately simulate the effect of water on PLA-based everyday items, such as reusable water bottles and kitchen containers, thereby better reflecting real-world conditions.

The CA degradation study was conducted for two different CA concentrations. The CA [1] solution was prepared by dissolving 15g of citric acid from STARWAX into 500 ml of water, while the CA [2] solution was prepared by dissolving 7.5g of citric acid from STARWAX into 500 ml of water.



Figure 3.9: STARWAX Citric Acid.

The samples, both 49 with 2% infill density and the 49 with 100% infill density, were submitted to 7 different conditions:

1. Water study: Room Temperature;
2. Water study: 60 °C;
3. Water study: 90 °C;
4. Citric acid solution [1] study: Room Temperature;
5. Citric acid solution [1] study: 90 °C;
6. Citric acid solution [2] study: Room Temperature;
7. Citric acid solution [2] study: 90 °C.

The code "[1]" represents the citric acid solution with a concentration of 2.9%, while the code "[2]" corresponds to the solution with a concentration of 1.4%.

Samples maintained at RT were stored in 500 mL plastic bottles, while those exposed to 60°C and 90°C were placed in 500 mL glass containers. Both recipients are illustrated in Figure 3.17 and the topic is further discussed in section 3.3.3.

The samples were then kept at room temperature in a controlled laboratory environment within the Faculty of Engineering at the University of Porto (FEUP), while those maintained at 60°C and

90°C were placed in an SLW 53 STD Pol-Eko-Aparatura SP drying oven, located within the same laboratory.

To evaluate the impact of these adverse conditions on the mechanical properties of the flexural samples, an additional set of samples, referred to as the 'control group,' was printed and tested. The mechanical results of these samples will serve as a reference for comparing the results obtained from the degraded samples.

The identification code was written using a permanent ink pen. The permanent ink was chosen for its durability and resistance to water, preventing the loss of crucial information. This way, each sample was accurately tracked throughout the experiment.

To characterize the samples subjected to a degradation mechanism, a series of analyses were conducted on each sample. These analyses, which will be detailed in this section, included FTIR analysis, mass measurement, dimensional measurement, and flexural test.

3.3.1.1 FTIR Analysis

One test sample was retained from each slot subjected to degradation conditions. These samples were analyzed for spectrum identification, with a wavelength between 4000 to 650 cm^{-1}, to verify that no molecules had been lost.

The test was conducted at the Lubricants Laboratory (CETRIB/INEGI) within the Faculty of Engineering at the University of Porto (FEUP). The experiment utilized an Agilent Technologies Cary 630 FTIR, as shown in the following Figure 3.10.



Figure 3.10: Cary 630 FTIR [41].

3.3.1.2 Mass Measurement

The mass measurement of the samples was performed on a Scale House HLD300 digital scale with a resolution of ± 0.005g, as shown in Figure 3.11.



Figure 3.11: Digital Scale House HLD300.

The mass of all degradation samples was measured prior to, during, and after the degradation period. The primary objective was to determine whether there was any water absorption or potential material loss resulting from the degradation mechanisms to which the polymers were exposed.

The pre-exposure measurement of the samples was straightforward, with each sample being measured individually and its mass recorded. During the exposure process, the measurement approach differed between the 2% and 100% infill density samples. The 2% infill density samples, being highly porous, allowed water to become trapped within the internal voids of the infill pattern. This caused inaccuracies in the mass measurements, as it was impractical to manually expel the trapped water within a timeframe that would not interfere with the study, particularly at elevated oven temperatures. Consequently, it was decided to measure the 2% infill density samples only once, after a prolonged exposure period, allowing them to dry naturally at room temperature to obtain their final accurate mass.

In contrast, the 100% infill density samples, being fully filled, did not retain water internally. These samples were easier to measure, as no water became trapped inside. During exposure, and until reaching saturation or experiencing structural failure, each sample was gently dried to remove external moisture using drying paper and immediately weighed before being returned to its container.

3.3.1.3 Dimensional Measurement

The thickness and width of each sample were measured using an AUTOUTLET digital micrometer (Figure 3.12) with a resolution of 0.001 mm and an accuracy of 0.002 mm.



Figure 3.12: Digital micrometer used.

The length of each sample was measured using a digital caliper from ZHJAN (figure 3.13) with a resolution of 0.01 mm and an accuracy of ±0.02 mm.



Figure 3.13: Digital caliper used.

The dimensional measurement of the printed samples was performed at five different points for both thickness and width and at three different points for length, as shown in Figure 3.14.

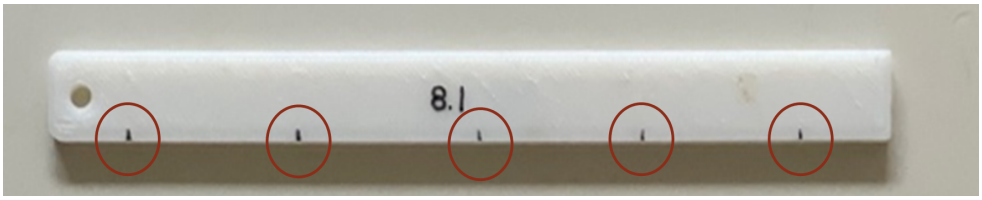


Figure 3.14: Measuring points.

The length was measured along the x-axis, the thickness along the y-axis, and the width along the z-axis. An average measurement for each axis was subsequently calculated. Each degradation sample was measured once before and once after the degradation test to assess the effects on dimensional variations and the hygroscopic properties of each specimen.

3.3.1.4 Mechanical Tests

Each flexural test is based on a three-point loading system where the load is applied from one point and the part acts as a supported beam. These flexural tests were carried out in a material testing machine composed of a dynamometer with a 2.5 kN load cell - AFG (Advanced Force Gauge) 2500N – coupled to a multitest 2.5 - Dv displacement column model (displacement resolution of 0.001mm) of the Mecmesin brand. The tests were carried out at a speed of 5 mm/min and with a distance between supports of 61.5 mm to ensure comparability of the results with other studies in the field ([41]). This setup is shown in figure 3.15.



Figure 3.15: Bending Test Machine in LPDS [5].

3.3.1.5 Heating Process

In the degradation study, the samples exposed to 60°C and 90°C were placed in an SLW 53 STD oven from Pol-Eko-Aparatura SP. J, shown in the Figure 3.16. The samples with a 100% infill density were removed several times from the oven for mass measurement throughout the study. However, the samples with a 2% infill density were weighed only before and after the degradation study. Due to their high porosity, these samples allowed water to become trapped within the internal voids of the infill pattern, resulting in inaccuracies in mass measurements. Manually expelling the trapped water within a timeframe that would not interfere with the study was impractical, particularly at elevated oven temperatures, as detailed in section 3.3.1.2.

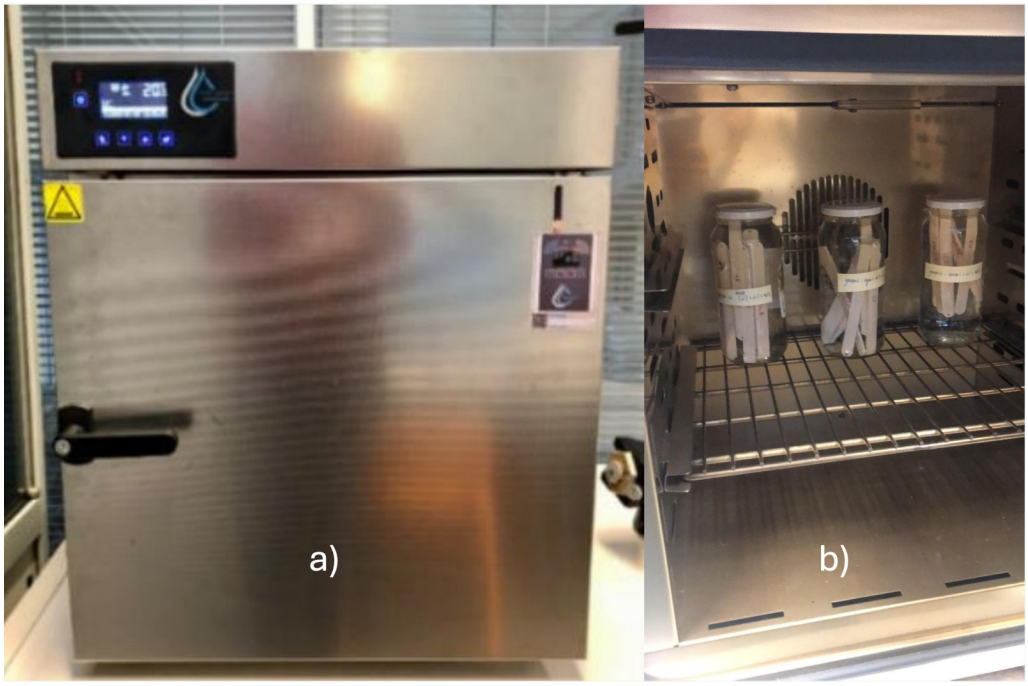


Figure 3.16: (a) Oven [5]; (b) Samples inside the oven.

The oven's technical specifications are presented in Table 3.5 below.

Table 3.5: SLW 53 Oven Specifications

Oven Specifications	
Power Supply	230V 50-60Hz
Nominal Power	1700W
Chamber Capacity	56L
Maximum Temperature	300°C

3.3.2 After Printing Study

The primary objective of the post-printing study is to assess the mechanical properties, mass, and dimensions of the flexural samples following the printing process. The parameters used to print these samples were the same as in Table 3.3.

The data obtained provided a baseline for comparing these results with those obtained after the degradation mechanisms. Consequently, it was possible to determine whether the degraded flexural samples experienced any loss or gain in mass and mechanical properties.

3.3.3 Water Study

The goal of the water study is to trigger degradation mechanisms in polymers induced by water, for three different temperatures and two different infill densities. For this experiment, two plastic bottles (room temperature) and four glass containers (60°C and 90°C) were filled with water. Each set of seven (7) printed samples, with two different infill densities, was labeled and submerged. Figure 3.17 represents the immersion of the samples inside a plastic bottle and a glass container.

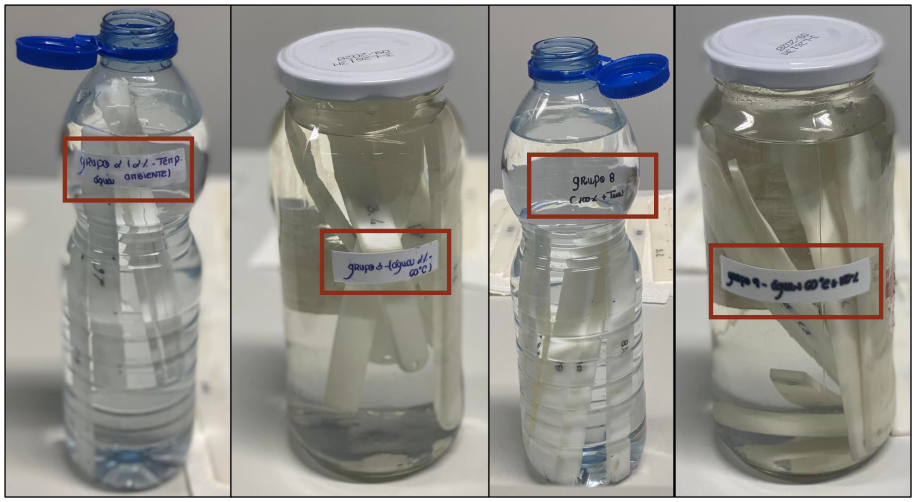


Figure 3.17: Representation of the immersion of the samples inside a plastic bottle and a glass container.

The flexural samples were exposed until either reaching the saturation point or breaking. During this period, the mass of the samples was measured, on a Scale House HLD300 digital scale. The samples with a 2% infill density were also measured 72 hours after exposition so that any excess water could be eliminated.

3.3.4 Citric Acid Study

The goal of the citric acid study is to trigger degradation mechanisms in polymers induced by citric acid, for three different temperatures, two different infill densities, and two different concentrations of CA. For this experiment, two plastic bottles (RT) and two glass containers (90°C) were filled

with citric acid solution with a concentration of 2,9% of citric acid, and two plastic bottles (RT) and two glass containers (90°C) were filled with citric acid solution with a concentration of 1,4% of citric acid. In summary, a total of four plastic bottles and four glass containers were used. Each set of seven (7) printed samples, with two different infill densities, was labeled and submerged. Figure 3.18 represents the immersion of the samples inside a plastic bottle.

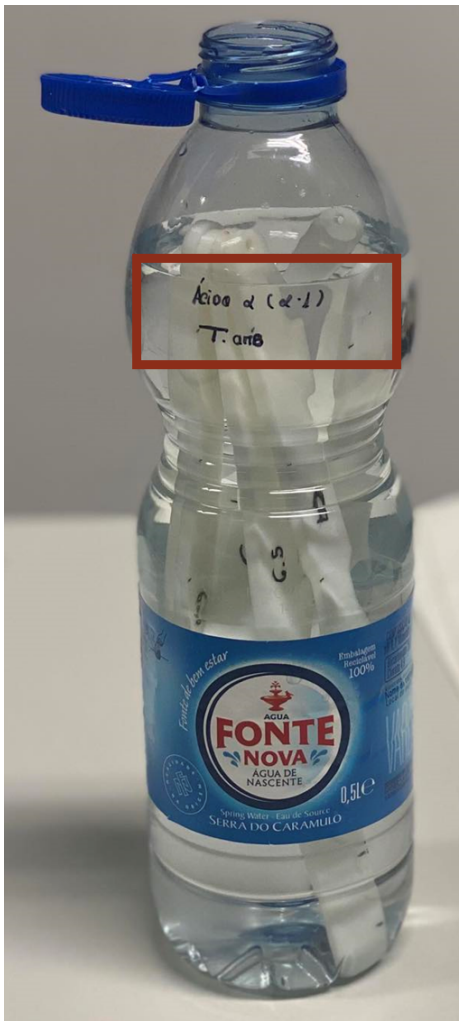


Figure 3.18: Bottles containing the citric acid solution [2] and the labeled samples.

The same experimental procedure applied to the samples that were submitted to water degradation was implemented to check the effects of the citric acid on PLA's mechanical properties.

Chapter 4

Analysis and comparison of the results

4.1 Filament Characterization Results

This chapter will discuss the results obtained from the Fourier Transform Infrared Spectroscopy (FTIR) and flexural tests, used to characterize the samples.

4.1.1 FTIR

FTIR spectroscopy was employed to examine the molecular composition of PLA samples with 2% and 100% filling percentages. The results were then compared with similar materials studied in the literature to confirm the identification of PLA polymer through FTIR analysis. Section 3.3.1.1 provides details on the test parameters and analysis equipment used in these experiments.

The curves obtained for each filling percentage control group can be seen in Figure 4.1. Each curve is characterized by its peaks, which are delimited by one of the five highlighted regions (I, II, III, IV, and V). Each one of these peaks is associated with a molecular functional group that will be further discussed in this section.

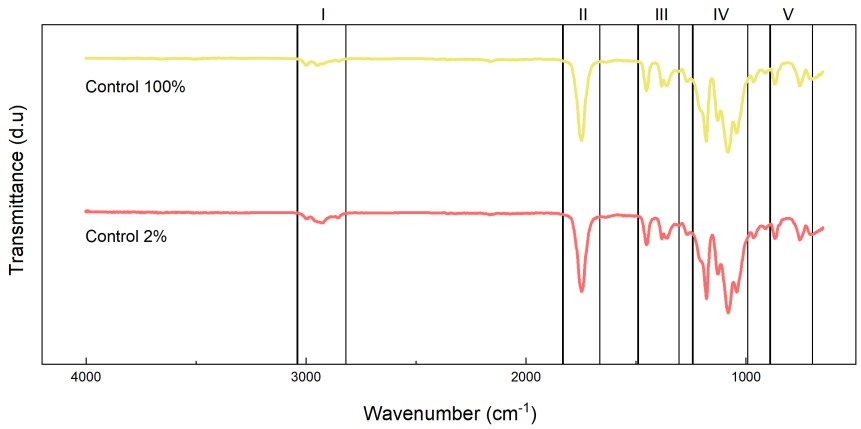


Figure 4.1: FTIR analysis curves obtained from group 7 (control group 100%) and group 1 (control group 2%).

The Table 4.1 provides the main peaks and wave numbers, identified in the spectroscopy test, and represented in the regions delimited by the rectangles (I to V) (Figure 4.1). All regions are defined by two or three peaks except for zone II which is defined by only one peak. Test studies on the composition of PLAs will be used to help interpret the curves resulting from the FTIR spectroscopy.

Table 4.1: Results of FTIR analysis by regions delimited in the curves.

Infill	Wavenumber (cm^{-1})				
	Zone I	Zone II	Zone III	Zone IV	Zone V
2%	2996;2924;2854	1747	1452;1381;1361	1180;1127;1081;1042	865;755
100%	2997;2947	1747	1452;1383;1359	1182;1130;1083;1042	867;757

To summarize the main molecules found on a specific band, Table 4.2 was created to help interpret the FTIR results.

Table 4.2: Relationship between the Wavenumber (cm^{-1}) and the functional group [5].

Wave Number (cm^{-1})	**Functional Group**
2400 - 3400	-OH (COOH)
2850 – 3000	-CH (CH_3)
1650 – 1750	-C=O
1450 – 1500	C-H
1345 – 1450	-CH_3
1000 – 1300	-C-O (COOH)
754 – 800	C-H

The FTIR results obtained in Table 4.1 indicate that the filament that we use to print the samples, both the ones with a filling percentage of 2% and the ones with a filling percentage of 100%, have a similar molecular structure to that described in the literature as it is in the work of [44].

The peaks in region I of the graph in Figure 4.1 (2843 to 2997 cm^{-1}) correspond to the stretching -CH group. The bands in region II (1747 to 1949 cm^{-1}) are associated with the -C=O stretching of the ester group, which belongs to the polylactic acid chain. In region III there are two peaks that correspond to the -CH3 stretching whereas the other one is associated with the C-H. In region IV are found spectra classified as C-O-C stretching. Finally, region V features a band at 755 cm^{-1}) which represents the crystalline portion of PLA, and another band at 867 cm^{-1}) associated with the amorphous portions of PLA [5].

The filaments correspond to PLA polymers and did not suffer any significant change in their molecular structure either as no unconventional band has been identified. Additionally, the characterization study indicated that the filaments exhibit semi-crystalline structure, as evidenced by

the peaks observed in zone V. As a result, the printed samples could be susceptible to thermal variations introduced during the printing process.

4.1.2 Mass Measurements

To define a baseline for the subsequent study of the degradation mechanisms on the variation of mass, the first step was to calculate the average mass, standard deviation, and coefficient of variance of the control groups. The results are shown in Table 4.3.

Table 4.3: Control groups mass measurement [1].

	Gr.1	**Gr.7**
Mean (g)	3.29	6.78
Std. Dev. (g)	0.009	0.013
CV (%)	0.27	0.19

4.1.3 Dimensional Measurements

Same as with the mass measurements, Table 4.4 shows the average dimensions of the control groups of 2% and 100% infill densities, group 1 and group 7[1].

Table 4.4: Dimensions of the control samples [1].

	Width (mm)		**Height (mm)**		**Length (mm)**	
	Gr.1	**Gr.7**	**Gr.1**	**Gr.7**	**Gr.1**	**Gr.7**
Mean (mm)	12.61	12.82	3.00	3.29	133.16	136.87
Std.Dev. (mm)	0.035	0.021	0.026	0.008	0.009	0.010
CV (%)	0.28	0.16	0.86	0.25	0.007	0.007

4.1.4 Flexural Tests

The flexural tests were conducted on the control groups with two different infill densities, 100%, and 2%. The results were then compared with those obtained from the specimens subjected to degradation mechanisms (water and citric acid). In this way, it was possible to conclude how the studied degradation mechanisms influenced the mechanical properties of PLA. 3.3.1.4 provides details on the test parameters and analysis equipment used in these experiments.

Table 4.5 presents the MFS and FM responses, along with the average responses, standard deviation, and coefficient of variation for the control groups.

According to the data provided in Appendix C, the expected MFS for the PLA used is approximately 68 MPa, while the FM is approximately 2.120 GPa, though specific values might differ

[1] Gr.1 - Control group 2%; Gr.7 - Control group 100%

Table 4.5: Mechanical tests responses from the control groups.

Infill	MFS (MPa)			FM (GPa)		
	Mean	**Std. Dev**	**CV (%)**	**Mean**	**Std. Dev**	**CV (%)**
2% (Gr. 1)	41.55	2.66	6	1.95	0.17	9
100% (Gr. 7)	79.01	0.84	1	2.56	0.07	3

slightly based on the exact conditions under which the material is printed and tested. When PLA is printed with a very low infill density, such as 2%, it is anticipated that both the MFS and the FM will significantly decrease compared to a part with full density (100% infill).

Thus, the results presented in Table 4.5 indicate that the mechanical tests responses from the control groups aligns with the expected outcomes.

4.2 Degradation Study

In this section, the impact of the exposure to water and citric acid, on mass, mechanical properties, and the diffusion coefficient will be addressed. Each one of the following subsections will discuss the results obtained by each filling percentage.

At RT (below the PLA's T_g) the PLA polymer is in a glassy state, where the mobility of amorphous chains is restricted. But, when the temperature is higher than the PLA's T_g (60 °C and 90 °C), we expect to see an increase in mobility of the amorphous chains [37, 45].

Moisture absorption analysis was performed according to ASTM standard D570.

4.2.1 Filling Percentage: 2%

4.2.1.1 Mass Analysis

To study the influence of the degradation mechanisms on the variation of mass, the first step was to calculate the average mass, standard deviation, and coefficient of variance as it was explained in 4.1.2. The mass measurements obtained by all the degradation mechanisms are shown in table 4.6.

Table 4.6: 2% filling percentage conditions mass measurement [1].

	After-Printing			After-Degradation			After-Drying		
Water									
	Gr.2	**Gr.3**	**Gr.4**	**Gr.2**	**Gr.3**	**Gr.4**	**Gr.2**	**Gr.3**	**Gr.4**
Mean (g)	3.275	3.319	3.268	4.865	4.810	-	3.300	3.260	-
Std. Dev. (g)	0.010	0.010	0.013	0.220	0.511	-	0.016	0.077	-
CV (%)	0.249	0.168	0.394	4.521	10.641	-	0.478	2.359	-
Citric Acid [1]									
	Gr.5	**Gr.11**		**Gr.5**	**Gr.11**		**Gr.5**	**Gr.11**	
Mean (g)	3.280	3.293		5.150	-		3.300	-	
Std. Dev. (g)	0.014	0.010		0.214	-		0.018	-	
CV (%)	0.413	0.246		4.153	-		0.545	-	
Citric Acid [2]									
	Gr.6	**Gr.12**		**Gr.6**	**Gr.12**		**Gr.6**	**Gr.12**	
Mean (g)	3.269	3.307		5.000	-		3.290	-	
Std. Dev. (g)	0.011	0.010		0.191	-		0.022	-	
CV (%)	0.327	0.260		3.817	-		0.666	-	

Continuous mass measurements were avoided during the exposure of the samples with an infill density of 2% due to the reasons specified at 3.3.1.2 with the entrapment of water with the low infill density specimens. Therefore, mass measurements were performed only after printing, after exposure, and after a 72-hour drying period to determine the weight and absorption rate of the samples more accurately. The samples with 2% infill density did not show significant mass changes, with a small increase in mass, proving the hygroscopic properties of the FILKEMP PLA-N supplier.

[1] Gr.2 - Water at RT; Gr.3 - Water at 60°C; Gr.4 - Water at 90°C; Gr.5 - Citric acid solution [1] at RT; Gr.11 - Citric acid solution [1] at 90°C; Gr.6 - Citric acid solution [2] at RT; Gr.12 - Citric acid solution [2] at 90°C

Figure 4.2 represents the differences in mass before and after exposure of the 2% infill samples and the respective standard deviation.

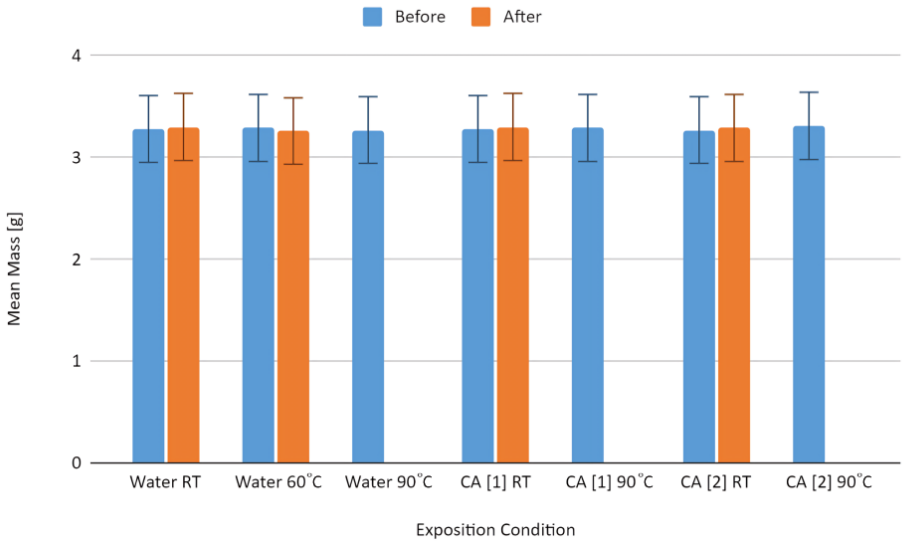


Figure 4.2: Graph of mean mass measurement difference obtained for 2% filling percentage samples.

With the help of Figure 4.2, it is possible to easily conclude that the group 6[1] samples were the most affected by increase of mass. However, it is important to understand the scale of the mean mass increase. As it is represented in Table 4.7 below, the increasing percentage is very low, an increase lower than 1% is not significant.

Table 4.7: Mean increase for 2% filling percentage samples [1].

	Gr.2 (Water at RT)	**Gr.5 (CA 1 at RT)**	**Gr.6 (CA 2 at RT)**
Mean Increase (%)	0.68	0.72	0.79

In group 3 (water at 60°C), we observed an initial average mass higher than the average mass after exposure and drying. This may be because almost all samples from group 3[1] broke after the exposure process (Figure 4.3), causing the final weighing to be not entirely accurate. The samples became so brittle after exposure that handling them for mass and dimensional measurements caused them to break at the slimmest pressure.

[1] Gr.2 - Water at RT; Gr.3 - Water at 60°C; Gr.5 - Citric acid solution [1] at RT; Gr.6 - Citric acid solution [2] at RT;

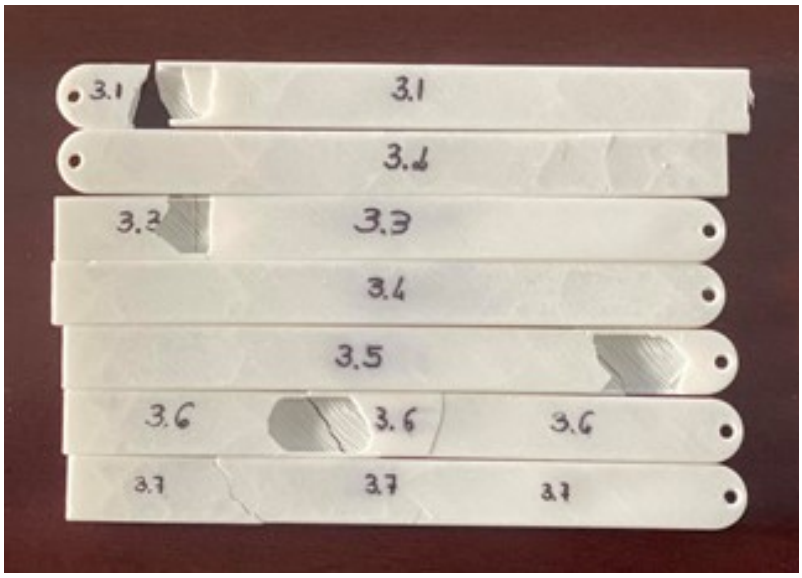


Figure 4.3: Group 3 samples after exposure.

After subjecting the samples from groups 4, 11, and 12 [1] to 489 hours of exposure to 90°C, all three groups exhibited failure. Due to their destruction, drawing definitive conclusions about their final properties was not possible.

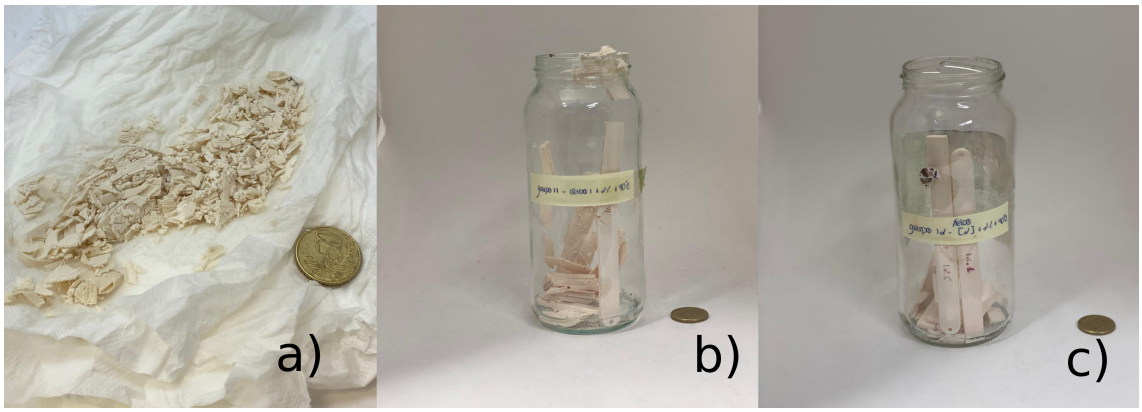


Figure 4.4: Groups: a) 4; b) 11 and c) 12 samples after exposure [1].

Due to the samples being submitted to these conditions for a short period of time and the increase is so small, there might not have been enough time for significant absorption to occur. Another possibility for the small increase in the overall mass of each sample is the low infill density. With only 2% infill, most of the interior of the sample is empty space or air. This means there is very little material inside to absorb or interact with the liquid. However, the same comparison will be discussed for group samples with 100% infill densities, where it may be possible to see a higher increase in the mass.

[1] Gr.4 - Water at 90°C; Gr.11 - Citric acid solution [1] at 90°C; Gr.12 - Acid citric [2] at 90°C

4.2.1.2 Diffusion Coefficient

After calculating the percentage of liquid absorbed by each sample, the diffusion coefficient was calculated using Equation 2.3. The results for each one of the groups are summarized in Table 4.8.

Table 4.8: Diffusion Coefficient for each group with 2% infill [1].

Parameters	**Group**		
	2	**5**	**6**
$D\ (m^2/s)$	$2{,}87 \times 10^{-10}$	$3{,}73 \times 10^{-11}$	$5{,}49 \times 10^{-11}$

It was not possible to calculate the percentage of liquid absorbed and therefore the diffusion coefficient, for the samples of groups 3, 4, 11, and 12[1], as these groups experienced rupture. The PLA specimens with a filling percentage of 2% have an average diffusion coefficient of $\sim 1.26 \times 10^{-10}$ m^2/s, at RT.

The calculated diffusion coefficient for group 2[1] has the highest value, indicating that the diffusion of water molecules in PLA occurs more rapidly than the diffusion of citric acid molecules (groups 5 and 6)[1]. A lower concentration of citric acid (1.4418%) results in a slightly higher diffusion coefficient compared to a higher concentration (2.8647%), though both values remain within the same order of magnitude. This result suggests that, within the range of concentrations studied, the penetration of citric acid into PLA is not significantly affected by variations in the acid concentration.

4.2.1.3 Dimensional Analysis

In this subsection, the dimensions of the samples measured before and after the immersion will be analyzed. As previously concluded, samples experienced a small mass increase, with some exhibiting more significant changes than others. The dimensions measurements obtained before and after immersion are shown in Table 4.9.

For groups 3, 4, 11, and 12[1], it was not possible to draw any conclusions regarding the dimensional variance of the samples, as observed in Table 4.9. This was because the samples fractured after exposure, making it impossible to measure them (see Figure 4.4).

Regarding all the other groups, it can be observed that after exposure the samples exhibited a slight increase in all dimensions (height, width, and length). Considering the short immersion period of approximately 13 days, and the minimal increase in mass, it was anticipated that the dimensions of the samples would remain relatively stable.

[1] Gr.2 - Water at RT; Gr.3 - Water at 60°C; Gr.4 - Water at 90°C; Gr.5 - Citric acid solution [1] at RT; Gr.6 - Citric acid solution [2] at RT; Gr.11 - Citric acid solution [1] at 90°C; Gr.12 - Citric acid solution [2] at 90°C;

Table 4.9: Dimensions of the samples with a 2% infill density before and after exposition [1].

	Width (mm)				Height (mm)				Length (mm)			
	After - Printing			After - Deg.	After - Printing			After - Deg.	After - Printing			After - Deg.
	Water											
	Gr.2	Gr.3	Gr.4	Gr.2	Gr.2	Gr.3	Gr.4	Gr.2	Gr.2	Gr.3	Gr.4	Gr.2
Mean (mm)	12.60	12.59	12.61	12.63	2.86	2.89	3.09	3.07	133.05	133.16	133.13	133.12
Std.Dev. (mm)	0.114	0.005	0.017	0.018	0.095	0.067	0.034	0.031	0.016	0.019	0.018	0.016
CV (%)	0.114	0.039	0.132	0.144	3.336	2.332	1.115	0.993	0.012	0.014	0.014	0.012
	Citric Acid [1]											
	Gr.5	Gr.11		Gr.5	Gr.5	Gr.11		Gr.5	Gr.5	Gr.11		Gr.5
Mean (mm)	12.59	12.56		12.62	2.98	2.80		3.10	133.12	133.09		133.18
Std.Dev. (mm)	0.014	0.016		0.014	0.049	0.045		0.035	0.027	0.0148		0.043
CV (%)	0.114	0.125		0.112	1.644	1.597		1.132	0.021	0.011		0.032
	Citric Acid [2]											
	Gr.6	Gr.12		Gr.6	Gr.6	Gr.12		Gr.6	Gr.6	Gr.12		Gr.6
Mean (mm)	12.60	12.61		12.62	2.95	2.81		3.10	133.13	133.16		133.17
Std.Dev. (mm)	0.013	0.026		0.011	0.072	0.035		0.023	0.02	0.056		0.034
CV (%)	0.101	0.21		0.09	2.446	1.257		0.749	0.015	0.042		0.023

4.2.1.4 Mechanical Test Analysis

To analyze the influence in the MFS and FM responses of the specimens, the average responses, standard deviation, and coefficient of variance for each group were calculated. As we can see in Table 4.10, the groups subjected to temperatures of 60°C and 90°C (3, 4, 11 and 12)[1] were not tested because they experienced rupture after exposure. Therefore, only the samples that were exposed to RT will be analyzed. The samples were exposed for approximately 15 days.

Table 4.10: Mechanical tests responses from the samples with a 2% filling percentage.

	MFS (MPa)			FM (GPa)		
	Mean	**Std. Dev**	**CV (%)**	**Mean**	**Std. Dev**	**CV (%)**
No Treatment (Gr. 1)	41.55	2.66	6	1.95	0.17	9
Water at RT (Gr. 2)	58.92	4.95	8	3.85	0.82	21
CA [1] at RT (Gr. 5)	52.51	4.95	8	3.29	4.11	6
CA [2] at RT (Gr. 6)	53.97	4.03	7	3.25	0,4	12

MFS Analysis

The MFS average responses tend to increase when the samples are submersed in both water and citric acid. The samples submerged in water (Group 2) exhibited the most significant change, with an increase of approximately 29%.

Prolonged exposure to water can induce slow hydrolytic degradation, which consequently increases the polymer crystallinity [46]. This can be explained by the fact that hydrolytic chain cleavage occurs preferentially in the amorphous regions, leading to an increase in the polymer´s global crystallinity [46]. Crystalline regions are more ordered and provide better mechanical stability.

A higher degree of crystallinity results in harder, stiffer, and less ductile behavior [47], providing better structural integrity and leading to improved flexural strength. The samples with a 2% filling percentage were left to rest for 72 hours to dry. As the samples dry, the decrease in water content within the specimen (desorption) results in a temporary increase in yield strength recovery [39], and consequently an improved flexural strength.

In addition, the process of water absorption and subsequent drying can reduce the molecular porosity of the material, so we expect to see a porosity decrease on the 2% filling percentage samples, and consequently an improvement of the PLA's mechanical properties [48].

The increase in the mechanical flexural strength (MFS) of PLA samples submerged at room temperature can be explained by the preferential hydrolytic degradation in the amorphous regions, which leads to increased crystallinity.

Additionally, the reduction in porosity due to water absorption strengthens the material, resulting in improved flexural strength.

Figure 4.5 shows the MFS response from the 2% filling percentage samples before and after exposure to RT conditions.

[1] Gr.2 - Water at RT; Gr.3 - Water at 60°C; Gr.4 - Water at 90°C; Gr.5 - Citric acid solution [1] at RT; Gr.6 - Citric acid solution [2] at RT; Gr.11 - Citric acid solution [1] at 90°C; Gr.12 - Citric acid solution [2] at 90°C;

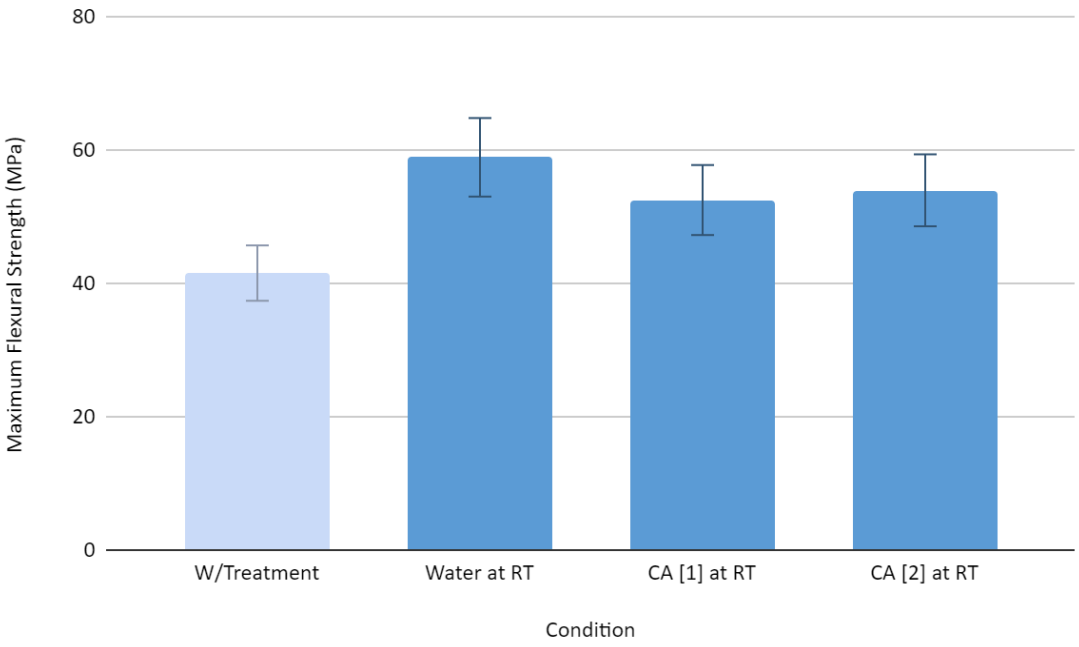


Figure 4.5: MFS response from the 2% filling percentage samples.

The values of the last three conditions in the graph can be considered statistically equivalent due to the high dispersion indicated by the error bars. This large variability suggests that the exposure to different environments (water and citric acid solutions) had little influence on the results of maximum flexural strength when compared to one another. Therefore, although the exposure conditions did increase the maximum flexural strength when compared to the control group, the observed differences between the mean values of the exposed conditions are not statistically significant enough to conclude that the individual exposure to water or either citric acid solutions had a more substantial impact on the mechanical properties of the materials than the other.

FM Analysis

As we can see in Figure 4.6, the flexural modulus increased. This can be explained by the fact that hydrolytic chain cleavage occurs preferentially in the amorphous regions, leading to an increase in the polymer´s global crystallinity [46].

Consequently, a higher degree of crystallinity results in harder, stiffer, and less ductile behavior [47], providing better structural integrity. Samples submerged in water at room temperature were the ones that obtained the biggest difference when compared to the group samples with no treatment.

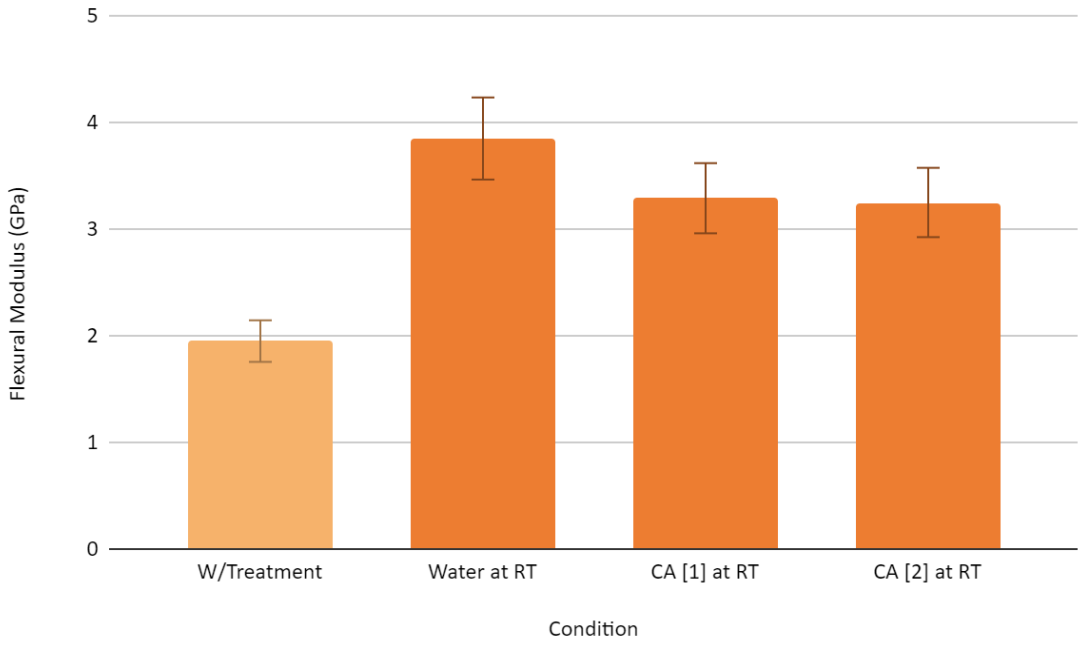


Figure 4.6: FM response from the 2% filling percentage samples.

The values of the last three conditions in the graph can be considered statistically equivalent due to the high dispersion indicated by the error bars. This large variability suggests that the exposure to different environments (water and citric acid solutions) had little influence on the results of the flexural modulus when compared to one another. Therefore, although the exposure conditions did increase the flexural modulus when compared to the control group, the observed differences between the mean values of the exposed conditions are not statistically significant enough to conclude that the individual exposure to water or either citric acid solutions had a more substantial impact on the mechanical properties of the materials than the other.

4.2.1.5 FTIR Analysis

A FTIR analysis was conducted to identify any new peaks or changes in existing ones, for that a FTIR spectroscopy was performed on one sample from each group.

In the figures below (Figure 4.7 and Figure 4.8) are represented the curves obtained for the samples with a 2% infill density, before and after being subjected to the degradation solutions, at room temperature (RT).

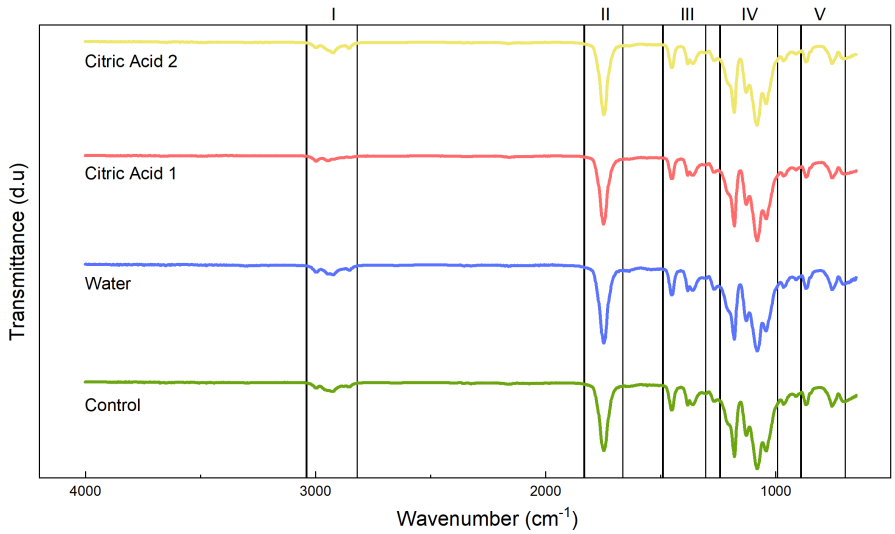


Figure 4.7: FTIR curves before immersion of each sample group with a 2% infill density at RT.

To complement the results presented in Figure 4.7, Table 4.11 below highlights the main peaks in each zone along with their corresponding wavenumbers identified in the spectroscopy test.

Table 4.11: Peaks of FTIR curves and its relative wavenumbers before immersion of each sample group with a 2% infill density at RT.

Solution	**Wavenumber (cm^{-1})**				
	Zone I	**Zone II**	**Zone III**	**Zone IV**	**Zone V**
Water	2996;2923;2852	1747	1450;1381;1363	1180;1128;1079;1042	867;755
AC 1	2998;2945	1748	1452;1381;1359	1180;1127;1081;1042	867;755
AC 2	2995;2923;2854	1747	1452;1381;1359	1180;1128;1083;1042	867;755

Based on the results presented in Table 4.11 above, it can be concluded that the peaks and their corresponding wavenumbers were very similar to those obtained with the filaments (see Table 4.1). This indicates that there were no significant changes in the molecular composition during the FFF manufacturing process.

Figure 4.8 shows the FTIR curves obtained for the same samples of each group after immersion.

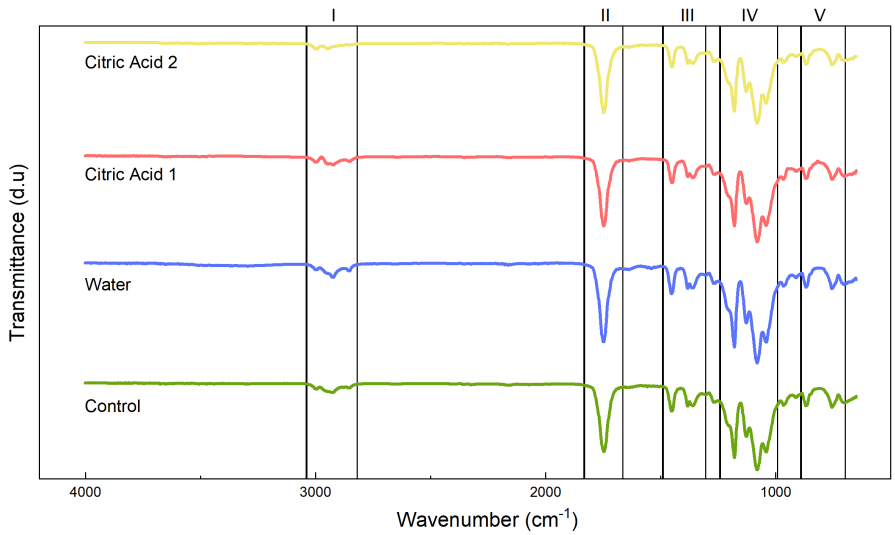


Figure 4.8: FTIR curves after immersion of each sample group with a 2% infill density at RT.

To complement the results presented in Figure 4.8 for the samples of each solution group after the immersion period, Table 4.12 below highlights the main peaks in each zone along with their corresponding wavenumbers, identified in the spectroscopy test.

Table 4.12: Peaks of FTIR curves and its relative wavenumbers after immersion of each sample group with a 2% infill density at RT.

Solution	**Wavenumber (cm^{-1})**				
	Zone I	**Zone II**	**Zone III**	**Zone IV**	**Zone V**
Water	2996;2923;2852	1748	1452;1383;1362	1180;1128;1081;1042	867;757
AC 1	2996;2945;2852	1747	1450;1381;1359	1180;1128;1081;1042	867;755
AC 2	2996;2945	1747	1450;1381;1361	1180;1128;1081;1042	867;755

Comparing the FTIR results obtained in Table 4.12 above with those in Table 4.11, it is evident that the FTIR curves remained very similar, indicating no significant changes in molecular composition. This further confirms the lack of substantial alterations during the test.

Figure 4.9 below displays the FTIR spectra for the samples with a 2% infill density, both before and after exposure to the degradation solutions, at 60°C.

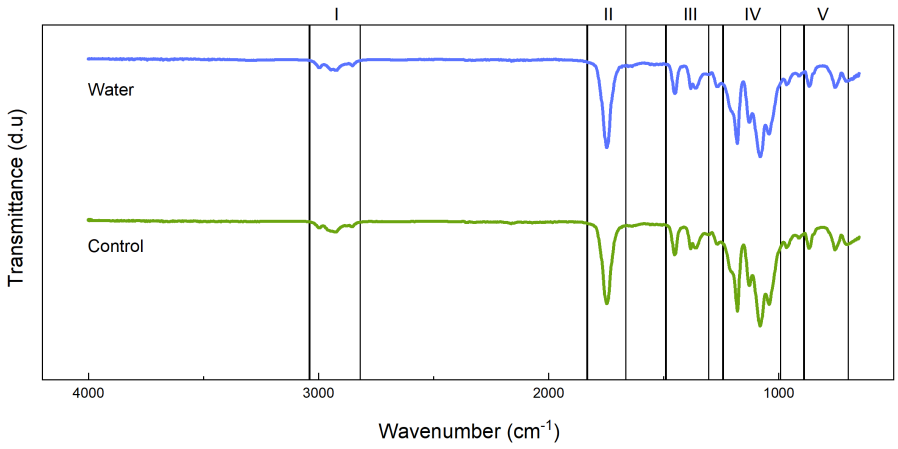


Figure 4.9: FTIR curves before immersion of each sample group with a 2% infill density at 60°C.

To complement the results shown in Figure 4.9 above, Table 4.13 below highlights the main peaks identified in each zone, along with their corresponding wavenumbers as determined by the spectroscopy test.

Table 4.13: Peaks of FTIR curves and its relative wavenumbers before immersion of each sample group with a 2% infill density at 60°C.

Solution	**Wavenumber (cm^{-1})**				
	Zone I	**Zone II**	**Zone III**	**Zone IV**	**Zone V**
Water	2996;2923;2852	1747	1450;1381;1362	1180;1128;1079;1042	867;755

The results in Table 4.13 above show that the peaks and their corresponding wavenumbers closely match those of the filaments (Table 4.1). This similarity indicates that no significant changes occurred in the molecular composition during the FFF manufacturing process.

Figure 4.10 below displays the FTIR spectra for the samples with a 2% infill density before and after exposure to the degradation solutions, at 60°C.

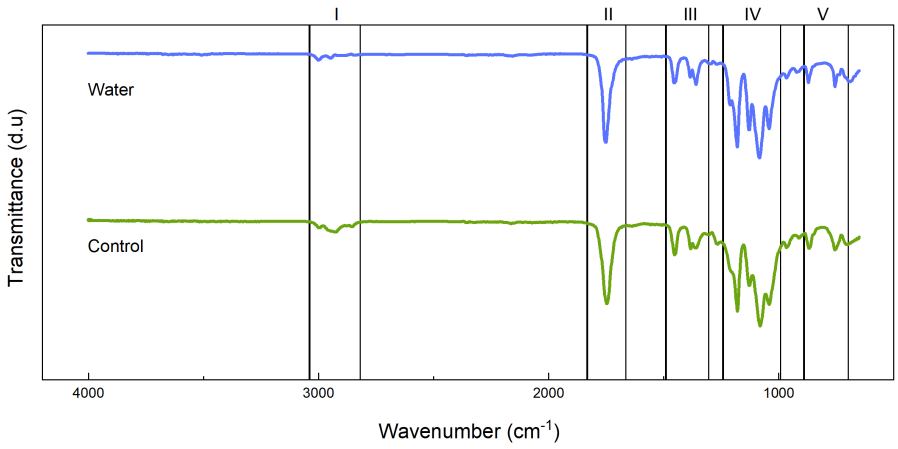


Figure 4.10: FTIR curves after immersion of each sample group with a 2% infill density at 60°C.

To complement the results shown in Figure 4.10 above, Table 4.14 below summarizes the main peaks and their corresponding wavenumbers identified in the spectroscopy test for each zone.

Table 4.14: Peaks of FTIR curves and its relative wavenumbers after immersion of each sample group with a 2% infill density at 60°C.

Solution	**Wavenumber (cm^{-1})**				
	Zone I	**Zone II**	**Zone III**	**Zone IV**	**Zone V**
Water	2996;2947	1752	1456;1385;1359	1180;1130;1085;1042	870;755

Comparing the FTIR results presented in Table 4.14 above with those in Table 4.13, it is evident that the FTIR curves remained very similar, but showed a subtle change in 5 peaks (1 in Zone I, 1 in Zone II, 2 in Zone III and another in Zone IV) of around $4cm^{-1}$, which can indicate changes in the molecular environment or chemical structure of the material. This can be explained by changes in bond strength between existing molecules, new molecular interactions, or due to experimental conditions.

FTIR instruments typically have a resolution of 1-$4cm^{-1}$cm, and, due to this, a change above this value can be significant depending on the context.

Figures 4.11 and 4.12 show the FTIR curves obtained for the samples with a 2% infill density, before and after being subjected to the degradation solutions, at 90°C.

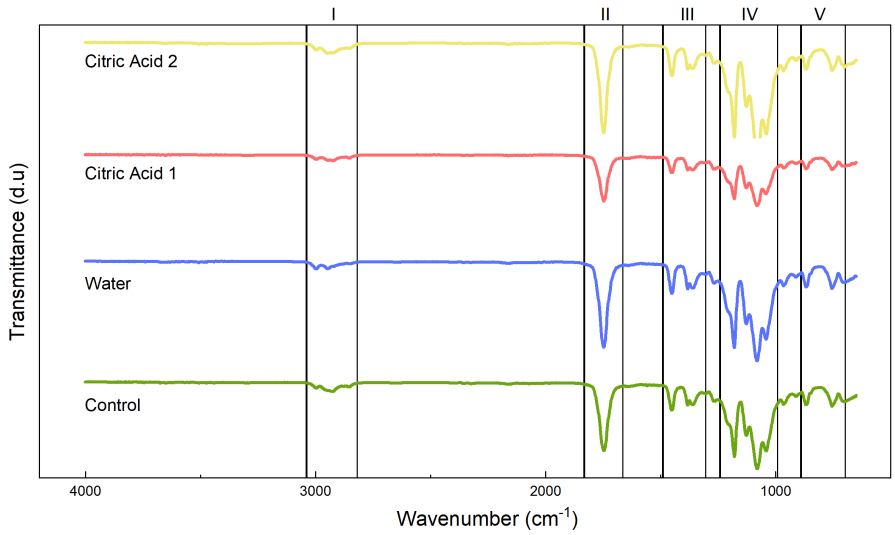


Figure 4.11: FTIR curves before immersion of each sample group with a 2% infill density at 90°C.

To complement the results presented in Figure 4.11, Table 4.15 below highlights the main peaks in each zone along with their corresponding wavenumbers identified in the spectroscopy test.

Table 4.15: Peaks of FTIR curves and its relative wavenumbers before immersion of each sample group with a 2% infill density at 90°C.

Solution	**Wavenumber (cm^{-1})**				
	Zone I	**Zone II**	**Zone III**	**Zone IV**	**Zone V**
Water	2998;2947	1747	1452;1383;1363	1180;1128;1081;1042	867;757
AC 1	2996;2945	1747	1450;1381;1360	1180;1128;1079;1042	867;753
AC 2	2996;2947	1748	1452;1381;1362	1180;1128;1081;1042	867;755

The results in Table 4.15 above demonstrate that the peaks and their corresponding wavenumbers closely match those of the filaments (see Table 4.1). This similarity suggests that there were no significant changes in the molecular composition during the FFF manufacturing process.

Figure 4.12 shows the FTIR curves obtained for the same samples of each group after immersion.

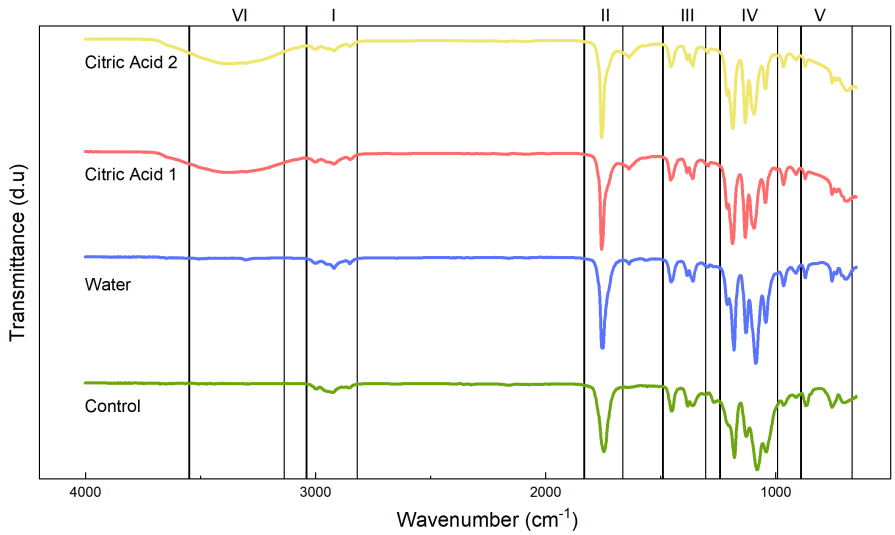


Figure 4.12: FTIR curves after immersion of each sample group with a 2% infill density at 90°.

To complement the results shown in Figure 4.12, Table 4.16 below summarizes the main peaks and their corresponding wavenumbers identified in the spectroscopy test for each zone.

Table 4.16: Peaks of FTIR curves and its relative wavenumbers after immersion of each sample group with a 2% infill density at 90°C.

Solution	**Wavenumber (cm^{-1})**					
	Zone I	**Zone II**	**Zone III**	**Zone IV**	**Zone V**	**Zone VI**
Water	2998;2919;2850	1754	1456;1385;1361	1182;1130;1087;1044	872;755;697	
AC 1	2999;2919;2849	1756	1456;1385;1361	1187;1131;1094;1046	872;755;694	3369
AC 2	2999;2919;2850	1756	1456;1385;1361	1187;1131;1094;1046	872;755;695	3370

By comparing the FTIR results shown in Table 4.16 with those in Table 4.15, some conclusions can be taken:

- a new zone (VI) can be seen in the curves related to exposure to citric acid for both concentrations, indicating changes in the molecular structure. The broad peaks around 3200-3500 cm^{-1} are primarily associated with the O – H from hydroxyl groups, as evidenced by Table 4.2, a common feature in molecules with strong hydrogen bonding networks. Citric Acid has multiple hydroxyl (-OH) and carboxylic acid (-COOH) groups that are prone to forming extensive hydrogen bonds. The less pronounced O-H stretching bands around 3200-3500 cm^{-1} in the other groups are due to the absent or weakened hydrogen bonding. This suggests that hydrogen bonding is a key factor contributing to the broad peaks in the CA samples [49, 50, 51].

- the temperature also plays an important role, since the samples with the same concentration of citric acid but maintained at room temperature do not show this peak, as shown in Figure 4.12. Furthermore, the two concentrations of citric acid used were sufficient to induce the formation of these peaks, at 90°C.

4.2.2 Filling Percentage: 100%

4.2.2.1 Mass Analysis

The next step in the degradation study was to evaluate how the degradation of the samples with a 100% filling percentage progressed. The groups were immersed in water and citric acid at two different concentrations. The samples submerged in water were subjected to three different temperatures: room temperature, 90°C, and 60°C, while those submerged in acid were only subjected to room temperature and 90°C. The results obtained for each condition are shown in Table 4.17.

Table 4.17: 100% filling percentage conditions mass measurement [1].

	After-Printing			**After-Degradation**		
			Water			
	Gr.8	**Gr.9**	**Gr.10**	**Gr.8**	**Gr.9**	**Gr.10**
Mean (g)	6.780	6.912	6.840	6.830	-	-
Std. Dev. (g)	0.020	0.011	0.011	0.019	-	-
CV (%)	0.289	0.161	0.157	0.282	-	-
			Citric Acid [1]			
	Gr.13	**Gr.14**		**Gr.13**	**Gr.14**	
Mean (g)	6.850	6.870		6.890	-	
Std. Dev. (g)	0.018	0.022		0.020	-	
CV (%)	0.270	0.324		0.0292	-	
			Citric Acid [2]			
	Gr.15	**Gr.16**		**Gr.15**	**Gr.16**	
Mean (g)	6.930	6.850		6.960	-	
Std. Dev. (g)	0.010	0.010		0.010	-	
CV (%)	0.149	0.150		0.142	-	

To better visualize the evolution of the mass of the 100% infill printed samples, the graph in Figure 4.13 was created where we can see how the mean mass was affected per group.

[1] Gr.8 - Water at RT; Gr.9 - Water at 60°C; Gr.10 - Water at 90°C; Gr.13 - Citric acid solution [1] at RT; Gr.14 - Citric acid solution [1] at 90°C; Gr.15 - Citric acid solution [2] at RT; Gr.16 - Citric acid solution [2] at 90°C;

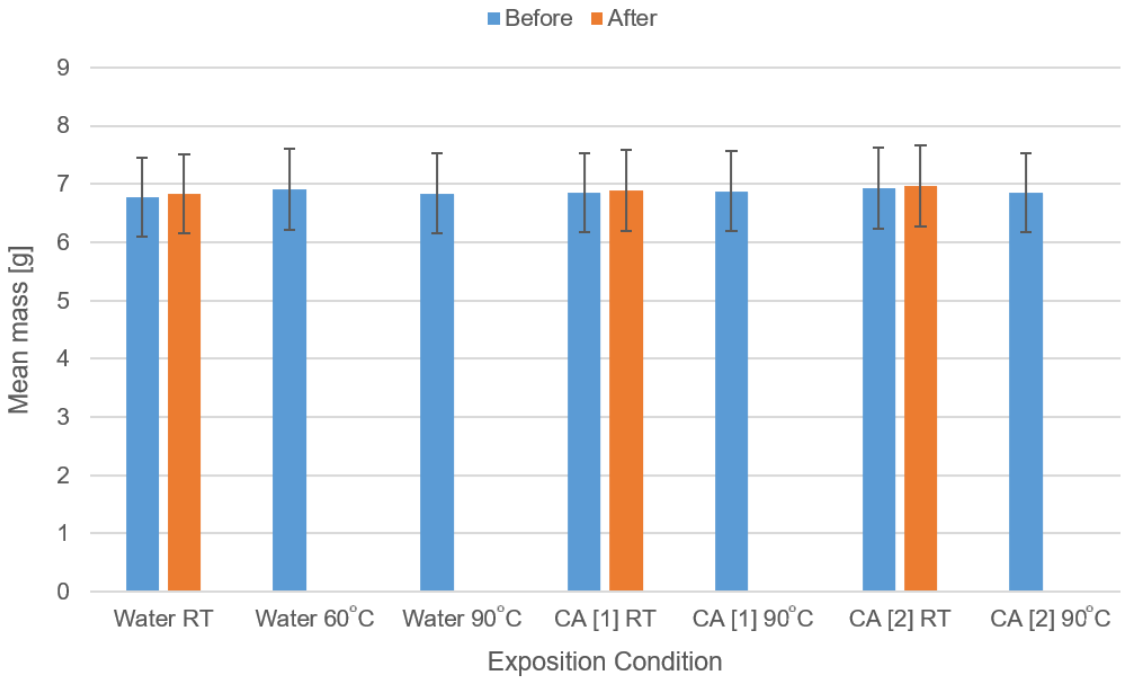


Figure 4.13: Mean mass evolution of the 100% infill samples before and after submersion.

With the help of Figure 4.13 above, it is possible to easily conclude that group 13 samples were the most affected by increase of mass. However, it is important to understand the scale of the mean mass increase. As it is represented in Table 4.18 below, the increasing percentage is meager, an increase lower than 1% is not significant.

Table 4.18: Mean increase for 100% filling percentage samples.

	Gr.8 (Water at RT)	**Gr.13 (CA 1 at RT)**	**Gr.15 (CA 2 at RT)**
Mean Increase (%)	0.51	0.52	0.46

The findings from the exposure of Polylactic Acid (PLA) to water present a comprehensive understanding of the material's behavior under specific conditions. After 317.5 hours of exposition at room temperature, the PLA samples demonstrated a consistent, slow increase in mass, reaching a saturation point, as we can see in Figure 4.14.

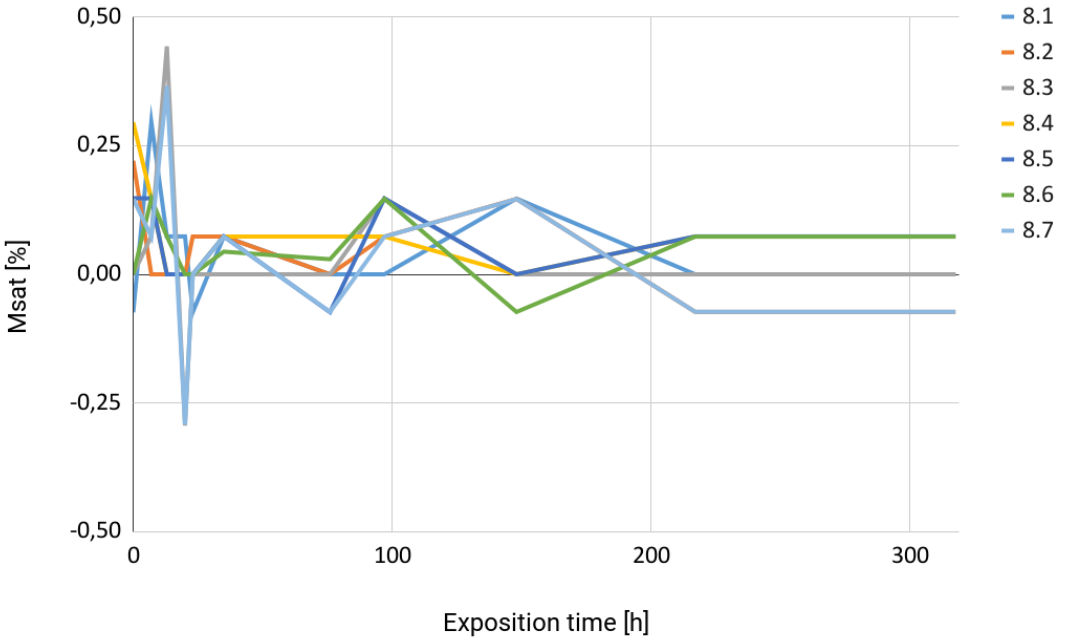


Figure 4.14: Mass over time for group 8 samples.

This observed saturation indicates that PLA undergoes a controlled process of water absorption and the calculated medium absorption rate of 0.514% sheds light on the material's modest but discernible affinity for moisture. The experiments were conducted at room temperature, providing insights into the behavior of PLA in conditions commonly encountered in various applications. The filling percentage of 100% signifies that the PLA samples were fully exposed to water, allowing a thorough assessment of the material's response. These detailed results offer valuable information for industries seeking materials with predictable and controlled moisture absorption properties, aiding in the informed selection and application of PLA in environments with sustained exposure to water at room temperature.

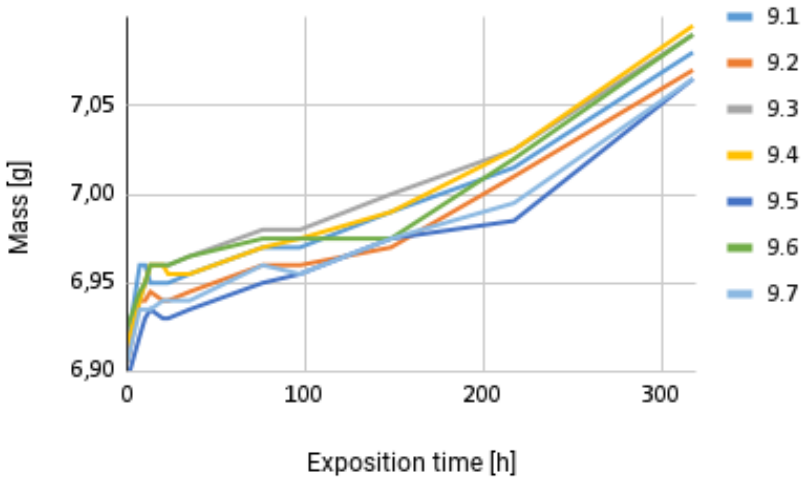


Figure 4.15: Mass over time for group 9 samples.

The samples exposed to water at 60°C did not attain equilibrium, as we can see in Figure 4.15, due to structural limitations; instead, they began to break (see Figure 4.16). The samples underwent a degradation process closely linked to the exposure temperature. Since 60°C is near the glass transition temperature of PLA, the material begins to lose rigidity, and the mobility of its polymer chains increases. This heightened chain mobility facilitates water penetration into the material, accelerating degradation mechanisms. As a result, proximity to the glass temperature transition of PLA makes the material more prone to degradation, especially in humid or aqueous environments, as observed in the samples exposed to water at 60°C.

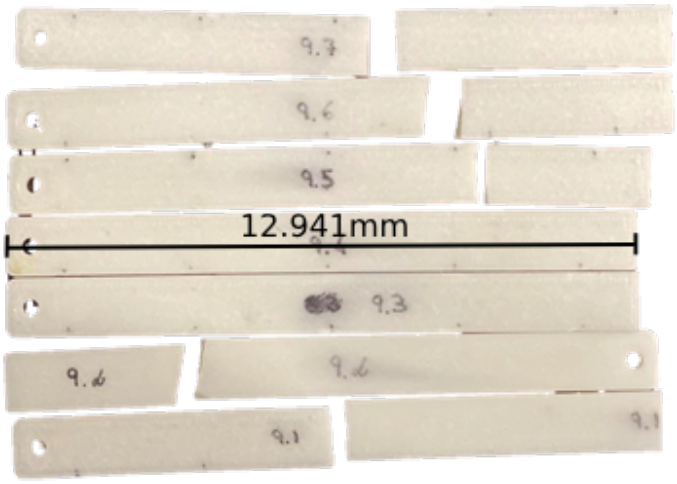


Figure 4.16: Group 9 samples after exposure.

This unexpected result indicates that the PLA samples experienced a stress-induced failure, possibly associated with the combination of water exposure at an elevated temperature of 60°C. Despite the structural challenges, the mass of the samples consistently increased in every measurement, suggesting a continuous water absorption process. The calculated medium absorption rate of 2.418% indicates a significant affinity for water, emphasizing the material's susceptibility to degradation or structural compromise under the specific exposure conditions. These findings provide crucial insights into the limits of PLA's resilience in hot water environments and emphasize the importance of considering both mass changes and structural integrity when evaluating the material's performance in applications demanding sustained exposure to elevated temperatures and high filling percentages.

The graphs in Figure 4.17 depict the evolution of the mass of samples from groups 13 and 15[1] over a 489-hour exposure to citric acid [1] and [2], respectively, while submerged and at room temperature. After this period, all samples reached saturation. During this time the mass average absorption rate was 0.521% for group 13[1] samples and 0.464% for group 15[1] samples.

From 157 hours of exposure onwards, the average mass of the group 13[1] samples remained almost unchanged, suggesting they reached a point of stabilization regarding citric acid [1] absorption. Figure 4.17 - a) clearly shows this stabilization, indicating that additional citric acid absorption decreased significantly after this point.

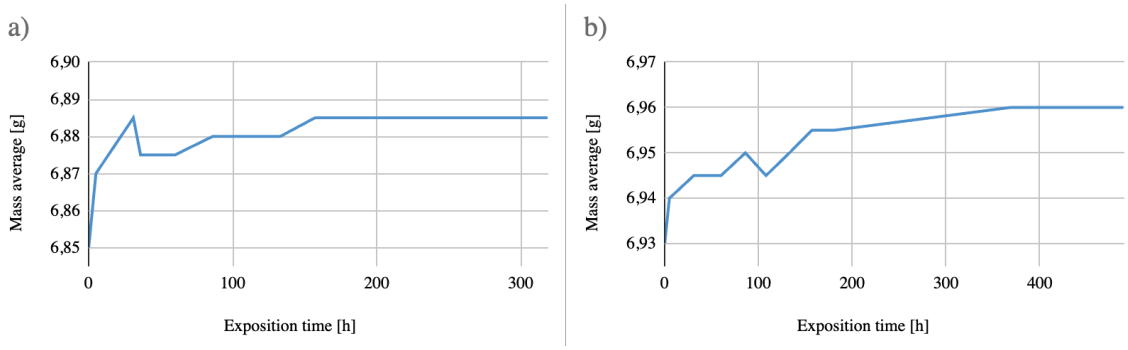


Figure 4.17: Mass average over time for groups: a) 13[1]: b) 15[1].

Over the 489 hours, the average mass of the group 13[1] samples increased by 0.58%, and the average mass of the group 15[1] samples increased by 0.43%. This suggests that while citric acid absorption initially occurred at a relatively high rate, the process slowed considerably as the samples reached saturation, resulting in a slower mass increase in the subsequent period.

The specimens from groups 10, 14, and 16[1], subjected to a temperature of 90°C, experienced failure after 31, 31, and 36 hours of exposure, respectively.

The specimens broke when exposed to 90°C likely due to the material's thermal properties. PLA has a glass transition temperature (T_g) typically around 60 - 65°C. When PLA is exposed to temperatures above its T_g, it becomes increasingly soft and loses its structural integrity, eventually

[1]Gr.8 - Water at RT; Gr.10 - Water at 90°C; Gr.13 - Citric acid solution [1] at RT; Gr.14 - Citric acid solution [1] at 90°C; Gr.15 - Citric acid solution [2] at RT; Gr.16 - Citric acid solution [2] at 90°C;

leading to deformation or failure. At 90°C, PLA would be significantly above its T_g, causing it to soften and ultimately break under stress. Additionally, prolonged exposure to high temperatures can accelerate degradation processes, further compromising the mechanical properties of the material and leading to failure.

4.2.2.2 Diffusion Coefficient

Similar to what was done for the samples group with a filling percentage of 2%, after calculating the percentage of water absorbed by each of the samples, the diffusion coefficient was calculated using Equation 2.3. The results for each one of the groups are summarized in Table 4.19.

Table 4.19: Diffusion Coefficient for each 100% infill group [1].

Parameters	**Group**		
	8	**13**	**15**
$D\ (m^2/s)$	$3{,}32 \times 10^{-10}$	$2{,}22 \times 10^{-10}$	$2{,}94 \times 10^{-10}$

The PLA specimens with a filling percentage of 100% have an average diffusion coefficient, at RT, of $\sim 2.83 \times 10^{-10}$ m^2/s. It was not possible to calculate the percentage of liquid absorbed and therefore the diffusion coefficient, for the samples of groups 9, 10, 14, and 16 [1], as these groups experienced rupture.

Similar to the results observed with the groups having 2% infill density, group 8 (water) exhibits the highest diffusion coefficient, further supporting the indication that water molecules diffuse more rapidly than citric acid molecules in PLA. As observed on the PLA's samples with an infill of 2%, the diffusion coefficient obtained for both concentrations of citric acid (2.8647% and 1.4418%) are close to each other, indicating that the acid penetration into the PLA is not strongly dependent on the acid concentration, between the studied concentration values.

In [39], a diffusion coefficient of 5.73×10^{-10} m^2/s was calculated for a PLA specimen with 100% infill density immersed at 21°C. This value is significantly higher than the diffusion coefficients obtained. Several factors could explain this discrepancy, but the difference in solvents used could have a significant impact. The literature value was obtained using deionized water while, in this thesis, tap water was used. Tap water contains various dissolved minerals and impurities that could enhance the interaction between the water and the PLA, potentially increasing the diffusion rate.

In summary, the samples with 100% infill density exhibit higher diffusion coefficients for citric acid (at both concentrations) compared to the samples with 2% infill density. This indicates that the more compact structure of PLA with 100% infill density facilitates the diffusion of citric acid molecules. Conversely, the difference in water diffusion between the two infill densities is smaller, suggesting that water diffusion is less affected by infill density than citric acid diffusion.

[1] Gr.8 - Water at RT; Gr.9 - Water at 60°C; Gr.10 - Water at 90°C; Gr.13 - Citric acid solution [1] at RT; Gr.14 - Citric acid solution [1] at 90°C; Gr.15 - Citric acid solution [2] at RT; Gr.16 - Citric acid [2] at 90°C;

4.2.2.3 Dimensional Analysis

In this subsection, the dimensions of the samples measured before and after the immersion will be analyzed. Table 4.20 shows the measurements of the dimensions obtained before and after immersion.

Similar to what happened to the samples with a filling percentage of 2%, for the groups subjected to temperatures of 60°C and 90°C (groups 9, 10, 14, and 16)[1] it was not possible to draw any conclusions regarding the dimensional variance of the samples, as observed in Table 4.20. This was because the samples fractured after exposure, making it impossible to measure them.

[1] Gr.9 - Water at 60°C; Gr.10 - Water at 90°C; Gr.14 - Citric acid solution [1] at 90°C; Gr.16 - Citric acid [2] at 90°C;

Table 4.20: Dimensions of the samples with a 100% infill density before and after exposition.

	Width [mm]				**Height (mm)**				**Length (mm)**			
	After - Printing			**After - Deg.**	**After - Printing**			**After - Deg.**	**After - Printing**			**After - Deg.**
	Water											
	Gr.8	**Gr.9**	**Gr.10**	**Gr.8**	**Gr.8**	**Gr.9**	**Gr.10**	**Gr.8**	**Gr.8**	**Gr.9**	**Gr.10**	**Gr.8**
Mean (mm)	12.89	12.84	12.87	12.90	3.28	3.37	3.35	3.31	136.88	136.86	136.92	137.05
Std.Dev. (mm)	0.053	0.027	0.027	0.026	0.015	0.007	0.03	0.012	0.025	0.029	0.027	0.012
CV (%)	0.411	0.209	0.213	0.199	0.458	0.206	0.213	0.354	0.019	0.022	0.02	0.009
	Citric Acid [1]											
	Gr.13	**Gr.14**		**Gr.13**	**Gr.13**	**Gr.14**		**Gr.13**	**Gr.13**	**Gr.14**		**Gr.13**
Mean (mm)	12.96	12.95		12.96	3.37	3.40		3.36	137.00	136.98		136.84
Std.Dev. (mm)	0.018	0.012		0.009	0.014	0.034		0.009	0.037	0.035		0.201
CV (%)	0.138	0.096		0.071	0.42	0.992		0.281	0.027	0.025		0.147
	Citric Acid [2]											
	Gr.15	**Gr.16**		**Gr.15**	**Gr.15**	**Gr.16**		**Gr.15**	**Gr.15**	**Gr.16**		**Gr.15**
Mean (mm)	12.92	12.95		12.93	3.38	3.40		3.38	136.87	136.98		136.92
Std.Dev. (mm)	0.017	0.012		0.004	0.012	0.034		0.016	0.037	0.035		0.025
CV (%)	0.133	0.096		0.03	0.37	0.992		0.466	0.027	0.025		0.0184

4.2.2.4 Mechanical Test Analysis

In order to analyze the influence in the MFS and FM responses, the average responses, standard deviation, and coefficient of variance for each group were calculated. As we can see in Table 4.21, the groups subjected to temperatures of 60°C and 90°C (9, 10, 14, and 16)[1] were not tested because they experienced rupture after exposure. Therefore, only the samples that were exposed to RT were analyzed.

Table 4.21: Mechanical tests responses from the samples with a 100% filling percentage.

	MFS (MPa)			FM (GPa)		
	Mean	**Std. Dev**	**CV (%)**	**Mean**	**Std. Dev**	**CV (%)**
No Treatment (Gr. 7)	79.01	0.84	1	2.56	0.07	3
Water at RT (Gr. 8)	73.98	0.93	1	2.58	0.17	7
CA [1] at RT (Gr. 13)	76.98	0.92	1	2.65	0.04	2
CA [2] at RT (Gr. 15)	77.47	0.44	1	2.69	0.05	2

MFS Analysis

As Table 4.21 shows, the average responses tend to decrease when the samples with a 100% filling percentage are submitted to the solutions. However, the graphic represented in Figure 4.18, shows that the values of all conditions can be considered statistically equivalent due to the high dispersion indicated by the error bars and the base value.

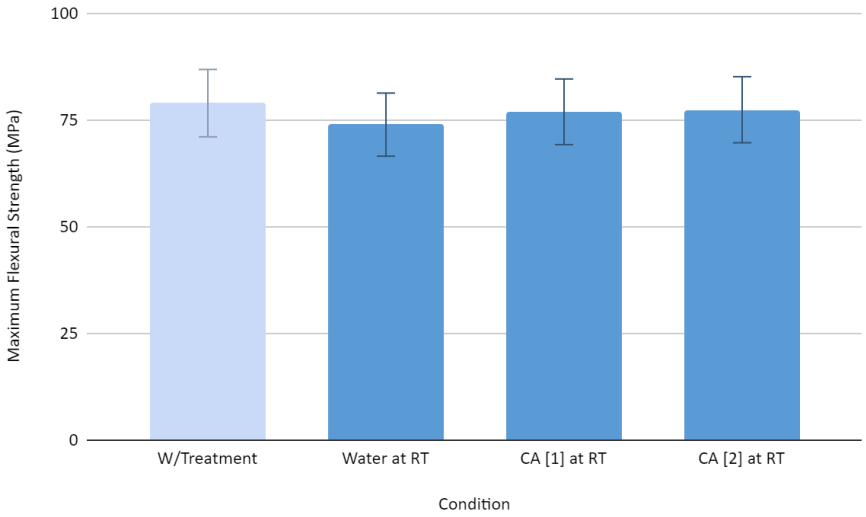


Figure 4.18: MFS response from the 100% filling percentage samples.

This large variability suggests that the exposure to different environments (water and citric acid solutions) had little influence on the results of maximum flexural strength when compared to

[1]Gr.9 - Water at 60°C; Gr.10 - Water at 90°C; Gr.14 - Citric acid solution [1] at 90°C; Gr.16 - Citric acid [2] at 90°C;

the control groups. Therefore, the observed differences between the mean values of the exposed conditions are not statistically significant enough to conclude that individual exposure to water or either citric acid solutions had a substantial impact on the mechanical properties of the materials.

FM Analysis

As Table 4.21 shows, the average responses tend to slightly increase when the samples with a 100% filling percentage are submitted to the solutions. However, the graphic represented in Figure 4.19, shows that the values of all conditions can be considered statistically equivalent due to the high dispersion indicated by the error bars and the base value. This large variability suggests that the exposure to different environments (water and citric acid solutions) had little influence on the results of the flexural modulus when compared to the control groups. Therefore, the observed differences between the mean values of the exposed conditions are not statistically significant enough to conclude that individual exposure to water or either citric acid solutions had a substantial impact on the mechanical properties of the materials.

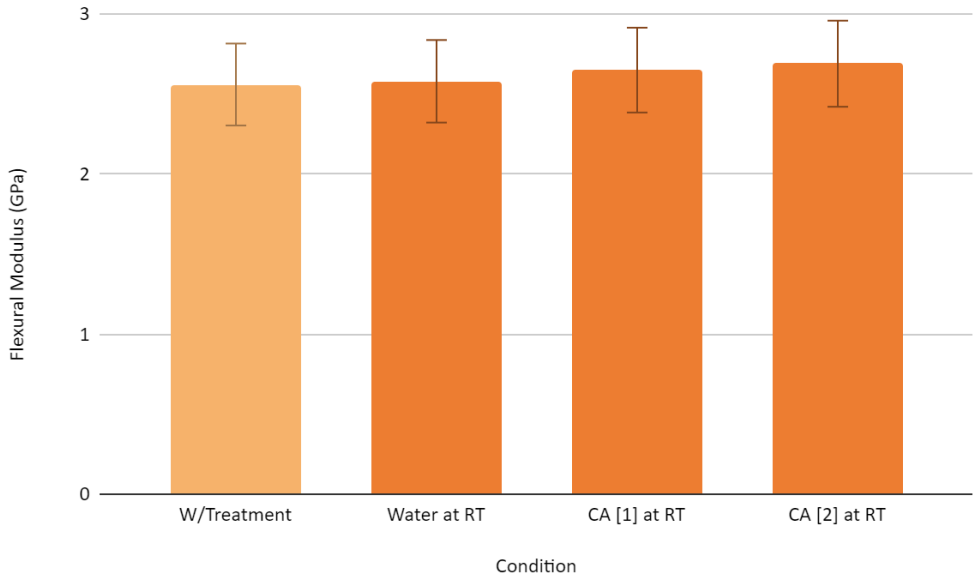


Figure 4.19: FM response from the 100% filling percentage samples.

4.2.2.5 FTIR Analysis

Similar to what was done for the samples with a 2% infill density, an FTIR analysis was conducted to identify any new peaks or changes in existing peaks. A FTIR spectroscopy was performed on one sample from each group. In Figures 4.20 and 4.21 are represented the curves obtained for the samples with a 100% infill density, before and after being subjected to the degradation solutions, at room temperature (RT).

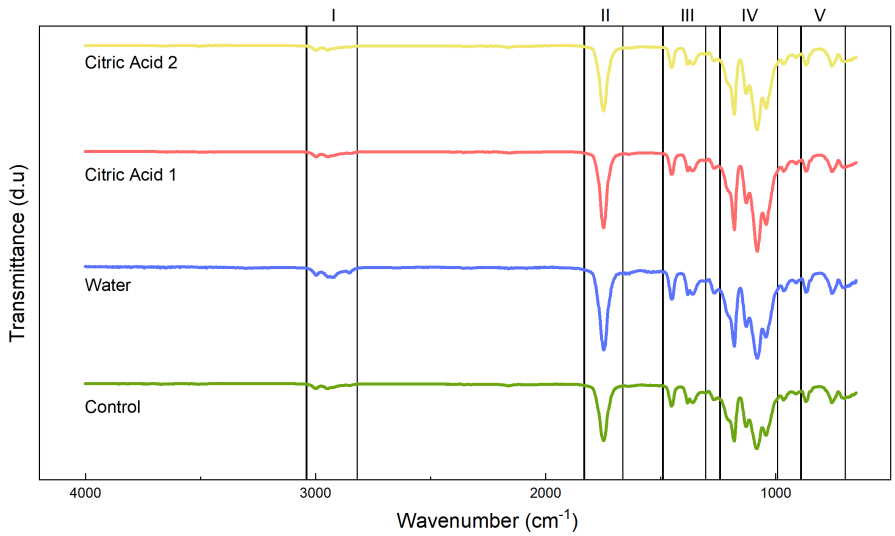


Figure 4.20: FTIR curves before immersion of each sample group with a 100% infill density at RT.

To complement the results presented in Figure 4.20, Table 4.22 highlights the main peaks in each zone along with their corresponding wavenumbers identified in the spectroscopy test.

Table 4.22: Peaks of FTIR curves and their relative wavenumbers before immersion of each sample group with a 100% infill density at RT.

Solution	**Wavenumber (cm^{-1})**				
	Zone I	**Zone II**	**Zone III**	**Zone IV**	**Zone V**
Water	2996;2945;2852	1747	1450;1381;1362	1180;1128;1079;1042	867;755
AC 1	2996;2945	1748	1452;1381;1361	1180;1128;1081;1042	867;755
AC 2	2996;2947	1748	1452;1383;1359	1180;1128;1081;1042	867;755

Based on the results presented in the table above, it can be concluded that the peaks and their corresponding wavenumbers were very similar to those obtained with the filaments (see Table 4.1). This indicates that there were no significant changes in the molecular composition during the FFF manufacturing process.

Figure 4.21 shows the FTIR curves obtained for the same samples of each group after immersion.

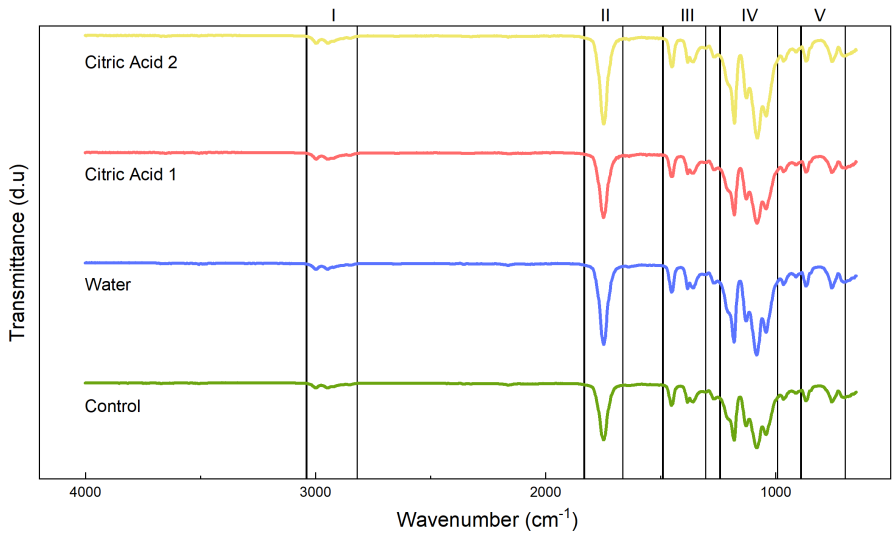


Figure 4.21: FTIR curves after immersion of each sample group with a 100% infill density at RT.

In order to complement the results presented in Figure 4.21, Table 4.23 highlights the main peaks in each zone along with their corresponding wavenumbers identified in the spectroscopy test.

Table 4.23: Peaks of FTIR curves and their relative wavenumbers after immersion of each sample group with a 100% infill density at RT.

Solution	**Wavenumber (cm^{-1})**				
	Zone I	**Zone II**	**Zone III**	**Zone IV**	**Zone V**
Water	2998;2947	1747	1452;1383;1359	1182;1130;1083;1042	867;757
AC 1	2996;2945	1748	1450;1381;1363	1180;1128;1081;1042	867;757
AC 2	2996;2945	1747	1450;1381;1363	1180;1128;1081;1042	867;755

By comparing the FTIR results shown in Table 4.23 with those in Table 4.22, it is possible to conclude that the FTIR curves represented in Figure 4.21 remained nearly identical, indicating no changes in the molecular composition. This further confirms the absence of significant alterations in the PLA samples, with a 100% infill density.

Figure 4.22 below displays the FTIR spectra for the samples with a 100% infill density, both before and after exposure to the degradation solutions, at 60°C.

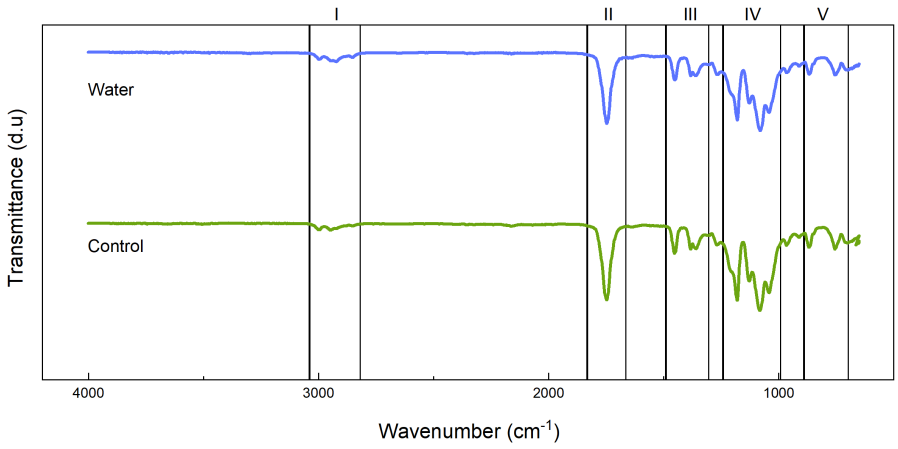


Figure 4.22: FTIR curves before immersion of each sample group with a 100% infill density at 60°C.

To complement the results shown in Figure 4.22 above, Table 4.24 below highlights the main peaks identified in each zone, along with their corresponding wavenumbers as determined by the spectroscopy test.

Table 4.24: Peaks of FTIR curves and its relative wavenumbers before immersion of each sample group with a 100% infill density at 60°C.

Solution	**Wavenumber (cm^{-1})**				
	Zone I	**Zone II**	**Zone III**	**Zone IV**	**Zone V**
Water	2996;2923;2852	1747	1450;1381;1362	1180;1128;1081;1042	867;755

By comparing the FTIR results shown in Table 4.24 with those in Table 4.1, it is possible to conclude that the FTIR curves represented in Figure 4.22 remained nearly identical, indicating no changes in the molecular composition. This further confirms the absence of significant alterations in the PLA samples, with a 100% infill density.

Figure 4.23 below displays the FTIR spectra for the samples with a 100% infill density, both before and after exposure to the degradation solutions, at 60°C.

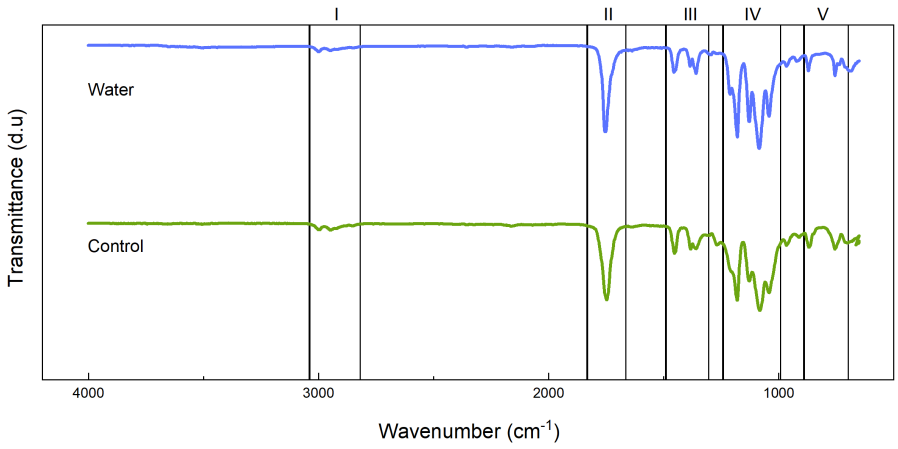


Figure 4.23: FTIR curves after immersion of each sample group with a 100% infill density at 60°C.

To complement the results shown in Figure 4.23 above, Table 4.2.2.5 below summarizes the main peaks and their corresponding wavenumbers identified in the spectroscopy test for each zone.

Table 4.25: Peaks of FTIR curves and its relative wavenumbers after immersion of each sample group with a 100% infill density at 60°C.

Solution	**Wavenumber (cm^{-1})**				
	Zone I	**Zone II**	**Zone III**	**Zone IV**	**Zone V**
Water	2997;2947	1752	1456;1385;1359	1180;1128;1085;1042	870;755

Comparing the FTIR results presented in Table 4.2.2.5 above with those in Table 4.24, it is evident that the FTIR curves remained very similar but showed a subtle change in 2 peaks (1 in Zone II and another in Zone III) of around $4cm^{-1}$, which can indicate changes in the molecular environment or chemical structure of the material. This can be explained by changes in bond strength between existing molecules, new molecular interactions, or due to experimental conditions.

Figures 4.24 and 4.25 show the FTIR curves obtained for the samples with a 100% infill density, before and after being subjected to the degradation solutions, at 90°C.

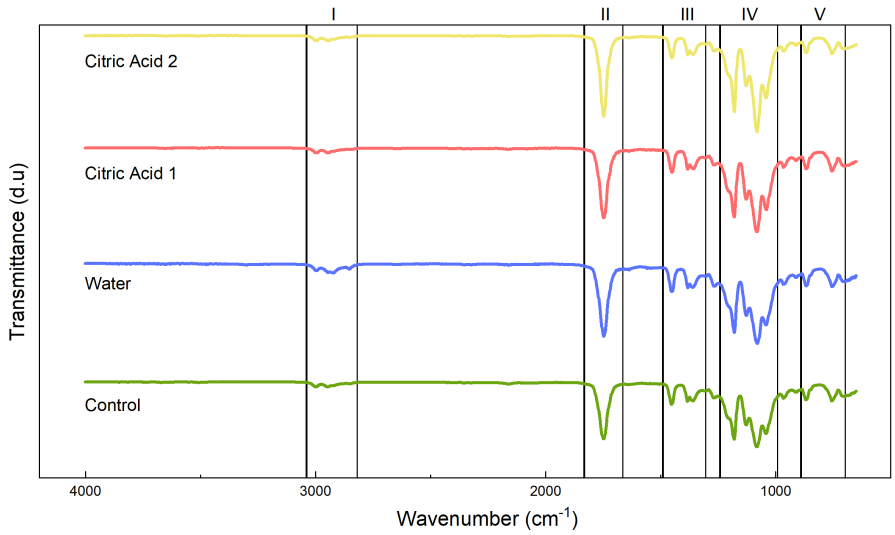


Figure 4.24: FTIR curves before immersion of each sample group with a 100% infill density at 90°.

To complement the results presented in Figure 4.24, Table 4.26 highlights the main peaks in each zone along with their corresponding wavenumbers identified in the spectroscopy test.

Table 4.26: Peaks of FTIR curves and their relative wavenumbers before immersion of each sample group with a 100% infill density at 90°.

Solution	**Wavenumber (cm^{-1})**				
	Zone I	**Zone II**	**Zone III**	**Zone IV**	**Zone V**
Water	2996;2945;2852	1747	1450;1381;1363	1180;1127;1079;1042	867;755
AC 1	2996;2947	1747	1450;1381;1357	1182;1128;1083;1042	867;757
AC 2	2996;2945	1747	1450;1381;1359	1180;1128;1081;1042	867;755

Based on the results presented in the table above, it can be concluded that the peaks and their corresponding wavenumbers were very similar to those obtained with the filaments (see Table 4.1). This indicates that there were no significant changes in the molecular composition during the FFF manufacturing process

Figure 4.25 shows the FTIR curves obtained for the same samples of each group after immersion.

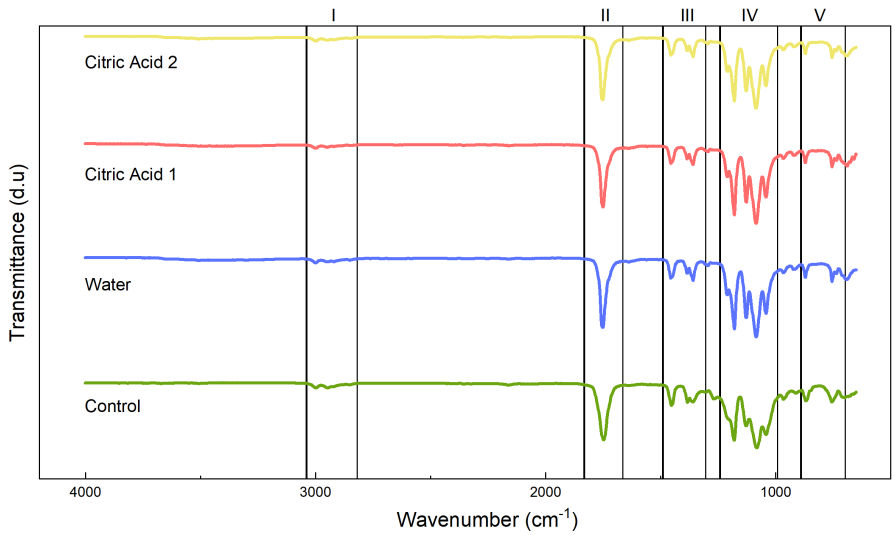


Figure 4.25: FTIR curves after immersion of each sample group with a 100% infill density at 90°.

We can observe the emergence of a new region before Zone I, similar to that seen in the 2% infill density samples at 90°C groups (see Figure 4.16). However, possibly due to the short exposure time and their compact infill density, it was not sufficient for this new region to fully develop.

In order to complement the results presented in Figure 4.25, Table 4.27 highlights the main peaks in each zone along with their corresponding wavenumbers identified in the spectroscopy test.

Table 4.27: Peaks of FTIR curves and their relative wavenumbers before immersion of each sample group with a 100% infill density at 90°.

Solution	**Wavenumber (cm^{-1})**				
	Zone I	**Zone II**	**Zone III**	**Zone IV**	**Zone V**
Water	2999;2947	1752	1456;1385;1359	1180;1130;1083;1042	870;755
AC 1	2999;2947	1750	1456;1385;1359	1180;1128;1085;1042	870;755
AC 2	2999;2947	1752	1456;1385;1359	1180;1128;1085;1044	870;755

By comparing the FTIR results shown in Table 4.27 with those in Table 4.26, it is possible to conclude that the FTIR curves represented in Figure 4.25 remained nearly identical, indicating no changes in the molecular composition. This further confirms the absence of significant alterations in the PLA samples, with a 100% infill density when submitted to a temperature of 90°C.

Chapter 5

Conclusions and Future Work

5.1 Conclusions

With the conclusion of this thesis, a deeper understanding of the complex aspects of additive manufacturing through fused filament fabrication (FFF) has been achieved. As this technology becomes more widespread due to its low cost and ease of use, it is crucial to explore and understand the more intricate challenges it presents. One such challenge is the degradation of polymers, which remains an area of ongoing research aimed at understanding its effects on FFF-produced materials. This study focused on examining the effects of fully immersing flexural samples, produced via 3D printing with FFF, in water and citric acid solutions at different temperatures. Citric acid was selected for this investigation because it is a commonly used acid in real-life applications. This makes it a relevant choice for evaluating the material's resistance in conditions that mimic everyday exposure to acids.

This study investigated the effects of the infill density, moisture, and temperature on the behavior of a commonly used 3D printing semicrystalline polymer: polylactic acid (PLA). 3D printed specimens, with a filling percentage of 2% and 100%, were immersed in water at RT, 60°C, and 90°C and in citric acid, with two different concentrations, at RT and 90°C, and changes in their chemical and mechanical behavior were evaluated.

The groups exposed to temperatures of 60°C and 90°C, whether submerged in water or citric acid, experienced fracture.

The glass transition temperature (T_g) of polylactic acid (PLA) typically falls within the range of 55-60°C. Above this threshold, PLA undergoes a transition from a glassy, rigid state to a rubbery, more flexible state. However, as temperatures exceed T_g, PLA can experience thermal degradation, leading to increased softening and susceptibility to deformation. This degradation process can ultimately render PLA brittle and prone to fracture, as observed in the case of the PLA samples exposed to temperatures of 60°C and 90°C.

Proceeding to the groups that were exposed to room temperature (RT):

- The mass analysis did not reveal a significant increase in the samples after exposure. However, the samples with 2% infill density exhibited the highest mass gain, although this in-

crease was minimal, amounting to only 0,79%, at most. It is also important to note that the measurements for the samples with 100% infill density were more reliable. In contrast, the samples with 2% infill density presented challenges in accurately determining the actual mass gained after exposure. Additionally, the solvent to which the samples were exposed—either water or citric acid—did not emerge as a differentiating factor in the mass analysis. This suggests that while the overall mass change is negligible, higher infill density is crucial for ensuring the accuracy and consistency of the measurements, independent of the solvent used;

- The highest diffusion coefficient was observed in the samples with 100% infill density when submerged in water at room temperature (group 8). The 100% infill density samples showed higher diffusion coefficients for citric acid (at both concentrations) compared to those with 2% infill density. This suggests that the more compact structure of PLA with 100% infill density facilitates the diffusion of citric acid molecules. On the other hand, the difference in water diffusion between the two infill densities is smaller, indicating that water diffusion is less influenced by infill density compared to citric acid diffusion;

- The dimensional analysis exhibited the same trend as the mass analysis;

- For the samples with 2% infill density, an increase in Maximum Flexural Strength (MFS) and Flexural Modulus (FM) was observed following exposure. This enhancement in the MFS of PLA samples can be attributed to preferential degradation occurring in the amorphous regions, which results in increased crystallinity. Furthermore, the reduction in porosity due to water absorption enhances the material's structural integrity, thereby leading to improved flexural properties. The samples with 100% infill density all experienced a reduction in maximum flexural strength (MFS) and an increase in flexural modulus (FM), as anticipated.

- Regarding the FTIR analyses conducted, only the groups with 2% infill density exposed to 90°C and citric acid exhibited a change in their molecular structure, as indicated by the appearance of a new absorption band around 3200 - 3500 cm^{-1}, primarily associated with the O - H from hydroxyl groups, a common feature in molecules with strong hydrogen bonding networks, such as hydroxyl (-OH) and carboxylic acid (-COOH) groups, present in citric acid.

In conclusion, the work conducted in this thesis demonstrates that exposing PLA to temperatures exceeding its glass transition temperature induces degradation and fracture of the samples, rendering it impossible to perform certain tests or draw specific conclusions about the groups of samples subjected to such conditions. Additionally, the samples with 100% infill density provide more reliable results and allow for more definitive conclusions.

5.2 Future Work

Although the research presented in this thesis produced noteworthy results, several aspects necessitate further investigation and additional analysis.

For future work, it is advisable to avoid using PLA samples with excessively low infill density, as this may compromise the quality of the results.

Additionally, testing different concentrations of citric acid would help determine its precise effects on the material's properties.

For future work, it would be beneficial to repeat the experiments at temperatures higher than ambient but lower than the glass transition temperature (T_g)) of PLA. This could provide additional insights into the material's behavior under conditions that are more representative of real-world applications.

It would also be interesting to evaluate the samples using techniques such as differential scanning calorimetry (DSC), thermogravimetric analysis (TGA), and dynamic mechanical analysis (DMA) to gain a more detailed insight into their thermal and mechanical characteristics.

References

[1] C. S. Brazel and S. L. Rosen. *Fundamental principles of polymeric materials*, pages 1–5. Wiley, Hoboken, New Jersey, 2012.

[2] TWI. What is a thermoplastic?, (accessed June 6, 2024). https://www.twi-global.com/technical-knowledge/faqs/what-is-a-thermoplastic.

[3] Samanta Castañeda-Rodríguez, Maykel González Torres, Rosa María Ribas-Aparicio, María Prado-Audelo, Gerardo Leyva-Gómez, Eda Sönmez Gürer, and Javad Sharifi-Rad. Recent advances in modified poly (lactic acid) as tissue engineering materials. *Journal of Biological Engineering*, 17:1–3, 03 2023.

[4] Purvi Kikani, Pooja Vithlani, and Sudhir Nema. Enhancement in gas diffusion barrier property of polyethylene by deposition of nano scale siox films by pecvd. page 10, 04 2015.

[5] J. P. Valente Ramalho. Comparison between pla filaments from different suppliers: an analysis of the effects of process parameters and polymeric degradation mechanisms on the quality of fff parts. Dissertação de mestrado, Universidade do Porto, 2022.

[6] A. Samsuri. Degradation of natural rubber and synthetic elastomers. In *Shreir's Corrosion*, pages 2407–2438. Elsevier, 2010.

[7] Y. Zhang and X. Xu. Machine learning glass transition temperature of polymers. *Heliyon*, 6(10):e05055, 2020.

[8] A. Askadskii. Melting point of polymers. In A. Askadskii, editor, *Computational materials science of polymers*, chapter VI, page 398. Cambridge International Science Publishing, Cambridge, England, 2003.

[9] Anshuman Shrivastava. *Introduction to Plastics Engineering*, pages 17–48. Elsevier Inc, 2018.

[10] Sebastião V Canevarolo Jr. *Ciência dos polímeros*, volume 24, pages 149–152. 2002.

[11] R. F. Landel and L. E. Nielsen. *Mechanical Properties of Polymers and Composites*. CRC Press, 1994.

[12] Leonardo Santana. *Avaliação das capacidades da impressão 3D de baixo custo na fabricação de snap-fits: uma relação de reconhecimento usuário-sistema de impressão*. PhD thesis, 2019.

[13] Sunil Bhandari. *Feasibility of using 3D printed molds for thermoforming thermoplastic composites*. PhD thesis, 05 2017.

[14] *Physical, Thermal, and Mechanical Properties of Polymers*, pages 329–344. John Wiley Sons, Ltd, 2014.

[15] MechaniCalc. Mechanical properties of materials. https://mechanicalc.com/reference/mechanical-properties-of-materials, 2024. Accessed: 2024-08-08.

[16] Tim Osswald and Georg Menges. *Mechanical Behavior of Polymers*, pages 339–422. 09 2012.

[17] G. Baschek, G. Hartwig, and F. Zahradnik. Effect of water absorption in polymers at low and high temperatures. *Polymer*, 40(12):3433–3441, jun 1999.

[18] X. Fan, S. H. Lee, and Q. Han. Experimental investigations and model study of moisture behaviors in polymeric materials. *Microelectronics Reliability*, 49(8):861–871, 2009.

[19] Chao Yang, Xiao Xing, Zili Li, and Shouxin Zhang. A comprehensive review on water diffusion in polymers focusing on the polymer–metal interface combination. *Polymers*, 12(1):20–22, 2020.

[20] Nikita A. Bratasyuk, Alexandr V. Latyshev, and Vjacheslav V. Zuev. Water in epoxy coatings: Basic principles of interaction with polymer matrix and the influence on coating life cycle. *Coatings*, 14(1), 2024.

[21] Greg Christensen, Ding Lou, Haiping Hong, and G.P. Peterson. Improved thermal conductivity of fluids and composites using boron nitride (bn) nanoparticles through hydrogen bonding. *Thermochimica Acta*, 700:178–927, 03 2021.

[22] James E. Mark. *Polymer Data Handbook*. Oxford University Press, 2nd edition, 2007.

[23] Nadka Tz Dintcheva. Overview of polymers and biopolymers degradation and stabilization towards sustainability and materials circularity. *Polymer*, 306:127–136, 2024.

[24] Aditivos e Ingredientes. Ácidos alimentares. https://aditivosingredientes.com/upload_arquivos/201609/20160903632200001474476544.pdf, 2016. Accessed: 2024-08-02.

[25] Encyclopaedia Britannica. ph, 2024. Accessed: 2024-07-12.

[26] Shalom Education. Acids and alkalis - gcse chemistry course. https://www.shalom-education.com/courses/gcsechemistry/lessons/chemical-changes/topic/acids-and-alkalis/, n.d. Accessed: 2024-07-08.

[27] Obinna Okolie, Anuj Kumar, Christine Edwards, Linda A. Lawton, Adekunle Oke, Seonaidh McDonald, Vijay Kumar Thakur, and James Njuguna. Bio-based sustainable polymers and materials: From processing to biodegradation. *Journal of Composites Science*, 7(6):3–41, 2023.

[28] Ahmed Akelah. *Polymers in Food Packaging and Protection*, pages 293–347. Springer US, Boston, MA, 2013.

[29] Marius Murariu and Philippe Dubois. Pla composites: From production to properties. *Advanced Drug Delivery Reviews*, 107:17–46, 2016. PLA biodegradable polymers.

[30] Donald Garlotta. A literature review of poly (lactic acid). *Journal of Polymers and the Environment*, 9(2):63–84, April 2001.

[31] Shady Farah, Daniel Anderson, and Robert Langer. Physical and mechanical properties of pla, and their functions in widespread applications - a comprehensive review. *Advanced Drug Delivery Reviews*, 107:367–392, 06 2016.

[32] J.V. Ecker, A. Haider, I. Burzic, A. Huber, G. Eder, and S. Hild. Mechanical properties and water absorption behaviour of pla and pla/wood composites prepared by 3d printing and injection moulding. *Rapid Prototyping Journal*, 25(4):672–678, 2019.

[33] N. Shekhar and A. Mondal. Synthesis, properties, environmental degradation, processing, and applications of polylactic acid (pla): an overview. *Polymer Bulletin*, 81:11421–11457, 2024.

[34] Julia Dreier, Christian Brütting, Holger Ruckdäschel, Volker Altstädt, and Christian Bonten. Investigation of the thermal and hydrolytic degradation of polylactide during autoclave foaming. *Polymers*, 13:2624, 08 2021.

[35] Pei Feng, Jiye Jia, Mingyang Liu, Shuping Peng, Zhenyu Zhao, and Cijun Shuai. Degradation mechanisms and acceleration strategies of poly (lactic acid) scaffold for bone regeneration. *Materials Design*, 210:110066, 2021.

[36] N. A. A. B. Taib, M. R. Rahman, D. Huda, et al. A review on poly lactic acid (pla) as a biodegradable polymer. *Polymer Bulletin*, 80(4):1179–1213, 2023.

[37] Wanwarang Limsukon, Maria Rubino, Muhammad Rabnawaz, Loong-Tak Lim, and Rafael Auras. Hydrolytic degradation of poly(lactic acid): Unraveling correlations between temperature and the three phase structures. *Polymer Degradation and Stability*, 217:110537, 2023.

[38] Arup Dey, Isnala Nanjin Roan Eagle, and Nita Yodo. A review on filament materials for fused filament fabrication. *Journal of Manufacturing and Materials Processing*, 5(3):1–29, 2021.

[39] Adedotun D. Banjo, Vinamra Agrawal, Maria L. Auad, and Asha-Dee N. Celestine. Moisture-induced changes in the mechanical behavior of 3d printed polymers. *Composites Part C: Open Access*, 7:100243, 2022.

[40] Amazon.ae. Filkemp 3df175plan11 generation filament, diameter: 1.75mm, pla. https://www.amazon.ae/Filkemp-3DF175PLAN11-01-Generation-Filament-Diameter/dp/B06XYJGBPM. Accessed: 17 August 2024.

[41] J. L. Silva Sousa. Degradation analysis of pla printed parts by fff exposed to acids present in foods. Dissertação de mestrado, Universidade do Porto, 2023.

[42] F. F. Alvim de Castro. *Análise da influência da pigmentação na qualidade de peças impressas por FFF em PLA e PETG*. Dissertação de mestrado, FEUP, 2021.

[43] American Society for Testing and Materials. *ASTM D790-17: Standard Test Methods for Flexural Properties of Unreinforced and Reinforced Plastics and Electrical Insulating Materials*. ASTM International, West Conshohocken, PA, 2017.

[44] Alves J. L. Sabino Netto A. da C. Merlini C. Santana, L. A comparative study between petg and pla for 3d printing through thermal, chemical and mechanical characterization. *Matéria (Rio de Janeiro)*, 23(4):e–12174, 2018.

[45] W. Limsukon, R. Auras, and S. Selke. Hydrolytic degradation and lifetime prediction of poly(lactic acid) modified with a multifunctional epoxy-based chain extender. *Polymer Testing*, 80:106108, September 2019.

[46] Moataz A. Elsawy, Ki-Hyun Kim, Jae-Woo Park, and Akash Deep. Hydrolytic degradation of polylactic acid (pla) and its composites. *Renewable and Sustainable Energy Reviews*, 79:1346–1352, 2017.

[47] Necmi Dusunceli and Ozgen U. Colak. Modelling effects of degree of crystallinity on mechanical behavior of semicrystalline polymers. *International Journal of Plasticity*, 24(7):1224–1242, 2008.

[48] Yuhan Liao, Chang Liu, Bartolomeo Coppola, Giuseppina Barra, Luciano Di Maio, Loredana Incarnato, and Khalid Lafdi. Effect of porosity and crystallinity on 3d printed pla properties. *Polymers*, 11(9), 2019.

[49] Wenkai Zhang, Lijuan Shi, Yingqiu Liu, Xianrui Meng, Hao Xu, Yuanqing Xu, Baoying Liu, Xiaomin Fang, Hai-Bei Li, and Tao Ding. Supramolecular interactions via hydrogen bonding contributing to citric-acid derived carbon dots with high quantum yield and sensitive photoluminescence. *RSC Adv.*, 7:20345–20353, 2017.

[50] Ana Roda, Filipa Santos, Yeong Zen Chua, Aarti Kumar, Hoang Tam Do, Alexandre Paiva, Ana Rita C. Duarte, and Christoph Held. Unravelling the nature of citric acid:l-arginine:water mixtures: the bifunctional role of water. *Phys. Chem. Chem. Phys.*, 23:1706–1717, 2021.

[51] Volker Strauss, Huize Wang, Simon Delacroix, Marc Ledendecker, and Pablo Wessig. Carbon nanodots revised: the thermal citric acid/urea reaction. *Chem. Sci.*, 11:8256–8266, 2020.

Appendices

Appendix A

Literature Study of Degradation Mechanisms

Título	Ano	Material de impressão analisado	Forma de impressão das peças	Tipo (s) de degradação avaliada	Método (s) de caraterização utilizados	Resultados obtidos
"Mechanical, physical, and degradation properties of 3D printing PLA + Mg composites"	2023	PLA e PLA + 1 wt% Mg	FDM	Biodegradação numa solução de SBF (Simulated Body Fluid).	- Variação da orientação de enchimento (0º,45º, ±45º, e 90º). - Variação da percentagem de Mg nas amostras de PLA.	-The 90º infill orientation samples were the most damaged samples by degradation; -Mg in the crevice forms and locks a local alkaline environment, accelerating degradation; -The presence of Mg particles increases the degradation rate of 3D-printed samples, especially in samples with more exposed fusion interfaces.
"Chemical Degradation of 3D Printed Products"	2020	Bronze-doped PLA	Additive Technology	-Diesel; -Engine oil; -Coolant.	-Tensile strength tests.	- Diesel fuel had the greatest impact on the tensile strength. The strength decreased compared to non-degraded samples by almost half. The degradation factor also had an effect on the plasticity of the material; -The second most aggressive agent is the coolant, which has also substantially reduced the strength of the material; -Engine oil had the smallest effect on mechanical properties.
"Mechanical Degradation of 3D Printed PLA in Simulated Marine Environment"	2020	PLA	FDM	-Mechanical degradation (friction and surface deformation) in a simulated marine environment.	-Tensile test sample (ASTM D638); -Simulated seawater environment (ASTM D1141-98).	-Mainly, the salt content from the seawater has initiated surface degradation, which appeared as tiny pits. However, the degradation is in controlled mode and held partial crystalline properties, and the study is practically useful in the marine industry for contact/non-contact applications.
"Characterization of the Degradation of Polylactic Acid Solid Substrate Environment"	1998	PLA		-Four types of environments were used for this study: (1) a biotic system environment, (2) an abiotic environment, (3) a sterile water environment and (4) a dry oven environment.	-CO2 evolved, weight loss, and molecular weights were measured to evaluate the extent of degradation; -X-ray diffraction and differential scanning calorimetry techniques monitored the morphological changes in the polymer; -FTIR was used as a semi quantitative tool to gather information about the chemistry of the degradative process.	-Neither of the used analytical techniques indicated any difference in the rate or mechanism of degradation attributable to the presence of microorganisms; -The extent of degradation increased at higher process temperatures; -FTIR analysis also indicated that there was no difference in the mechanism of degradation in the presence or absence of microorganisms. -The results confirmed hydrolysis of ester linkage as the primary mechanism of degradation of PLA;
"Hydrolytic degradation of polylactic acid (PLA) and its composites"	2017	PLA		-Erosion; -Bulk degradation.	-Use of a combination of analytical techniques, such as: pH, temperature, autocatalytic behavior of PLA, and ability of water to diffuse into the polymer matrix.	-The degradation of the PLA polymer matrix is restricted to its surface if the temperature remains below the glass transition temperature (T_g) value (60ºC); -The degradation is very fast at highly basic and highly acidic mediums (as compared to neutral conditions); -The properties of PLA can be enhanced by certain modifications. Mixing with Cs has been shown to influence the degradation of PLA.
"Enzimatic degradation study of PLA-based composite scaffolds"	2019	Composite scaffolds (PLA:CaCO3:β-TCP 95:2.5:2.5)	FDM	-Enzimatic degradation using *proteinase K* enzymes.	-Optical microscopy; -Scaning electron microscopy; -Compression testing; -Thermogravimetric analysis; -Calorimetric analysis.	-According to the results, the combination of the PLA matrix with the proposed additives increases the degradation rate of the 3D printed scaffolds, which is an advantage for the application of the composite scaffold in the field of Tissue Engineering. The higher degradation rate of the composite scaffolds could be explained by the release of the additive particles and the statistically higher microporosity of these samples compared to the neat PLA ones.

Figure A.1: Literature research of degradation mechanisms on printed parts (page 1).

Título	Ano	Material de impressão analisado	Forma de impressão das peças	Tipo (s) de degradação avaliada	Método (s) de caraterização utilizados	Resultados obtidos
"Hydrolytic Degradation of 3D-Printed Poly (Lactic Acid) Structures"	2021	PLA	FDM	-3D-printed parts were incubated in deionized water.	-Use of different temperatures.	-Small changes in orthogonal dimensions occurred due to relaxation of printing stresses, but no mass or volume loss were detected over the timeframe of the experiments; -Molecular weight decreased while polydispersity remained constant; -The most sensitive measure of degradation was found to be nondestructive, small-amplitude oscillatory tensile measurements; -A rapid decay of tensile storage modulus was found with an exponential decay time constant of about an hour; -This work demonstrates that practical monitoring of commercially available PLA degradation can be achieve with linear viscoelastic measurements of modulus.
"Safety Assessment of Polylactide (PLA) for Use as a Food-contact Polymer"	1995	PLA		-Aqueous, acidic, and fatty foods that are (a) dispensed and maintained at or below room temperature, or (b) dispensed at temperatures as high as 60ºC, and then allowed to cool to room temperature or below.	-The safety of food-contact polymers is evaluated by considering the identity, toxicological properties and quantities of substances that migrate from the polymers into food during conditions of intended use; -Migration of PLA components was determined in extraction tests in which samples of the polymer were exposed to food-simulating solvents under conditions that reproduced the most severe temperature/time conditions to which food would be exposed while in contact with PLA.	-Very limited migration can be expected from PLA into foods that it contacts during intended conditions of use; -The small amount of any material that might migrate from PLA into food will be lactic acid, or its dimers and oligomers, which will hydrolyze in aqueous systems to lactic acid; -Lactic acid is a common food ingredient that has been shown to be safe in food at levels far in excess o -PLA is safe and "Generally Recognized As Safe" for its intended uses as a polymer for fabricating articles that will hold and/or package food.
"Effects of fused deposition modeling process parameters on tensile, dynamic mechanical properties of 3D printed polylactic acid materials"	2020	PLA	FDM	-Thermal degradation; -Mechanism by which process parameters:namely printing angle, layer thickness, fill rate and nozzle temperature. affect the mechanical properties of printed materials.	-Uniaxial tensile tests; -Dynamic mechanical analysis (Effects of process parameters: namely printing angle, layer thickness, fill rate and nozzle temperature. on the dynamic mechanical properties of FDM-printed materials).	-FDM process parameters will affect the mass of the printed material, the interlayer bonding strength, air gaps,etc; -Printing angle mainly affects the fracture mode of the FDM-printed PLA materials. When the printing angle is less than 45º, the failure mode of the specimen trends to be interlayer fracture, and conversely, the specimen´s failure mode trends to be intra-layer fracture; -Layer thickness mainly affects the interlayer bonding strength of the printed materials. Smaller layer thickness not only strengthen the PLA materials' interlayer bonding strength, but also may have greater restrictions on the movement of adjacent polymer chains in PLA materials; -The fill rate mainly affects the air gap inside the printed material. With the increase of the fill rate, the air gaps in the material decrease rapidly, which makes the material layers and the filaments more tightly bonded, and increses the resistance of the molecular chain of PLA materials. - Nozzle temperature mainly affects the fluidity of extruded material. When the nozzle temperature is too low, the fluidity of the extruded material is poor, which results in weak interlayer bonding strength. When the noozle temperature is to high, the extruded PLA material is almost liquid, and even partial thermal degradation will occur, which is not conducive to printing.

Figure A.2: Literature research of degradation mechanisms on printed parts (page 2).

Título	Ano	Material de impressão analisado	Forma de impressão das peças	Tipo (s) de degradação avaliada	Método (s) de caraterização utilizados	Resultados obtidos
"Mechanical properties of components fabricated with open-source 3-D printers under realistic environmental conditions"	2014	ABS and PLA	3D printing	-Realistic environmental conditions.	-To determine the mechanical properties of 3-D printed parts and the variability in these properties when different user-con- trolled printing and slicing parameters are used, this investigation looked at the relationship between deposition pattern orientation and layer height to tensile strength, strain at tensile strength, and modulus. -This study quantifies the basic tensile strength and elastic modulus of printed components using realistic environmental conditions for standard users of a selection of open-source 3-D printers;	-The results find average tensile strengths of 28.5 MPa for ABS and 56.6 MPa for PLA with average elastic moduli of 1807 MPa for ABS and 3368 MPa for PLA; -Parts printed from tuned, low-cost, open-source RepRap 3-D printers can be considered as mechanically functional in tensile applications as those from commercial vendors.
"Atmospheric pressure cold plasma anti-biofilm coatings for 3D printed food tools"	2020	PLA with acrylic acid (AcAc) and tetraethyl orthosilicate (TEOS) coatings applied by plasma-polymerization.	3D printing	-Once printed, different plasma-polymerization treatments were applied on the PLA, in order to apply AcAc and TEOS coatings to the samples.	-Two liquid precursors (AcAc and TEOS) were utilized with diverse number of passes.	-This study demonstrated that acrylic acid plasma coatings are suitable for decreasing the amount of biofilm generated by different bacteria over 3D printed PLA substrates. -AcAc coatings were more effective than TEOS coatings, and showed up to a 47.7% (L. monocytogenes), 50.4% (P. aeruginosa) and 64.1% (E. coli) relative biofilm production, when compared with untreated samples;
"A Case Study of 3D Printed PLA and Its Mechanical Properties"	2017	PLA	FDM	-Bacterial degradation;	-Micro tensile testing; -Biodegradable test of componente using landfill method.	-The results clearly shows that the strength of the test specimen strongly satisfies which can be further used as any biomedical component; -Land fill test of the specimen over a period of 30 days to 60 days shows good amount of weight reduction which is also a fine outcome of this research work. -Bacterial degradation such as Amycolatopsis coloradensis are able to degrade PLA; -A purified protease from amycolatopsis sp., PLA depolymerise, can also degrade PLA.
"A comparative study between PETG and PLA for 3D Printing through thermal, chemical and mechanical characterization"	2018	PLA e PETG	FDM		-Materials were mechanically analyzed by traction through samples made by 3D printing varying the angles of deposition of the extruded material; -Thermal evaluation by TGA and DSC; -Chemical evaluation by FTIR.	-The results showed that the tensile mechanical properties of the printed components are strongly influenced by the orientation of the fil-aments deposited in the layers and by the mesostructure of the parts; -PLA has mechanical superiority, greater maximum tension and high rigidity, in relation to PETG, in the injected and printed samples. -PETG has shown to be more resistant to thermal degradation, more thermally stable (because it does not show significant changes in its thermal behavior after being processed), and more flexible, which is very interesting for 3D printing applications. -The molecular chemical structure of both polymers was similar to that described in other studies found in the literature and was slightly altered by the manufacturing processes.

Figure A.3: Literature research of degradation mechanisms on printed parts (page 3).

Título	Ano	Material de impressão analisado	Forma de impressão das peças	Tipo (s) de degradação avaliada	Método (s) de caraterização utilizados	Resultados obtidos
"A Study of the Effect of Heat Treatment on 3D Printed PLA Impact Strength"	2019	PLA	3D printing	-Effect of the temperature and humidity on the impact strength of 3D printed PLA plastic.	-Impact tests.	-Impact strength of the PLA increased with an increase in temperature treatment; -The PLA samples had the highest impact strength at higher temperature temperature but only for short treatment times; -At low temperature treatment, the impact strength of PLA samples increased with an increase in treatment time; -The impact strength of PLA is not sustaining with aging of samples. So, heat treatment can change the strength of 3D printed PLA but it was verified upon testing that the initial strength tested right after the heat treatment was not sustained over time as the impact strength of the samples decreased although not to the initial strength prior to heat treatment.
"Chemical Degradation of End-of-Life Poly(lactic acid) into Methyl Lactate by a Zn(II) complex"	2020	PLA	3D printing	-Chemical degradation: Catalysis by a Zn complex -Effect of the temperature on the catalyzed methanolysis of end-of-life PLA products by na ethylenediamine Zn(II) complex to form biodegradable mehtyl lactate	-Additionally, and to develop a predictive kinetic model, kinetic parameters (pre-exponential factor and activation energies) of the PLA transesterification reaction were first obtained from virgin PLA.	-Green solvent methyl lactate was obtained from the chemical degradation of end-of-life poly(lactic acid) catalyzed by a Zn complex. -Three different samples were tested: a cup, a toy, and a 3D printing material, at three temperatures: 70, 90, and 110 °C. -Kinetic parameters were obtained from the experimental data of virgin PLA, and the model was used to predict the conversion, selectivity, and yield of the PLA waste samples from a batch process in which the samples start at a room temperature of 20 °C until they reached the final process temperature. -The deviations between the predicted and experimental values of the end-of-life samples varied depending on temperature, reaction time, and sample. The deviations are overall in good agreement for the cup, which is believed to have the fewest amount of additives. Larger deviations are observed for the toy, which seems to contain the largest amounts of additives as exhibited by their structural strength and by the final mixture containing an insoluble phase. -Despite the large amount of uncertainty in the samples given by additive type and concentration, particle size, manufacturing process, and molecular weight, the kinetic parameters obtained in this work can be used to get a good approximation of the conversion, selectivity, and yield of the methanolysis of end-of- life PLA into methyl lactate to an average deviation of 5, 7, and 12, respectively.
"Extrusion Based 3D Printing: Color Influence on Mechanical Properties of PLA Parts"	2021	PLA	3D printing	-Effect of the inclusion of diferente types of pigments on the quality standard of printed parts; -Annealing treatment (HT).	-Three-point flexural tests. -Measumerents of the mass of the parts, density and analysis of the molecular composition, through FTIR.	-The results showed that the molecular structure of polymers with different colors and its density are similar, thus no conclusion regarding the presence of additives could be made. -The color significantly influenced the mechanical responses and mass of the parts with and without heat treatment. -Annealing increased the maximum flexural strength in all samples. Parts' modulus also slightly increased, indicating that the HT was not adequate to increase crystallization due to the influence of the pigments. -Results suggest that color brings unpredictability to the behavior of printed and post treated parts.
"Development and characterization of pla biofilament combined with perifiton biomass for 3d printing"	2023	PLA (95%) + periphytic biomass (5%)	3D printing	-Simulated soil: three equals parts of black earth, horse manure and coarse sand.	-Scanning Electron Microscopy; -FTIR spectroscopy.	-The biofilament presented mechanical performance similar to pure PLA, becoming slightly more rigid and brittle. -In the biodegradability test, the sample produced with the biofilament showed a greater mass loss, with 63.75%, when compared to the PLA samples, indicating that the presence of microalgae contributed to the degradation of the material.

Figure A.4: Literature research of degradation mechanisms on printed parts (page 4).

Título	Ano	Material de impressão analisado	Forma de impressão das peças	Tipo (s) de degradação avaliada	Método (s) de caraterização utilizados	Resultados obtidos
"Comparative thermal, biological and photodegradation kinetics of polylactide and effect on crystallization rates"	2013	PLA	3D printing	-Biodegradation; -Thermal degradation; -Photodegradation.	-Analyze of the temporal decrease of molar mass. -FTIR; -Thermal rate analysis; -Crystallization rate analysis.	-Under the degradation conditions tested, the degradation rate follows the progression thermal > photo > biological; -For equivalent molar mass, the effect of degradation type on cold crystallization and melting is significant indicating that degradation cannot be explained by a solely outcome of chains breakage and molar mass reduction. This feature is especially prominent when the linear growth rates of specimens subjected to bio or photo degradation are compared. -Anhydride groups that are formed during photodegradation decrease the crystallization rate compared to biodegraded specimens of equivalent molar mass. -The temperature coefficient of the growth rate, analyzed according to secondary nucleation leads to a linear dependence for bio and photodegraded specimens, and to values of the surface free energy of crystallites that decrease with decreasing molar mass. -Combinations of molar mass characterization, FTIR, and thermal and crystallization rate analysis are proven useful strategies to assess and discriminate macroscopic changes of PLA structure induced by different types of degradation. This work also underlines the importance of analyzing the linear growth rates as a parameter that uncovers specific structural changes during degradation.
"Explication of mechanism governing atmospheric degradation of 3D-printed poly(lactic acid) (PLA) with different in-fill pattern and varying in-fill density"	2023	PLA	3D printing	-Water; -Degradation under natural conditions of ultra-violet rays (UV), humidity, fumes,etc.	-Tensile tests.	-It was found that though the performance of PLA deteriorates with the exposure time, the combination of infill pattern and volume plays an important role on the tensile properties and the extent of degradation; -It is concluded herein that with natural exposure, the degradation of PLA occurs in two stages, supported by a side reaction. -Thus, this study offers a new perspective towards the life of components in actual application by exposing PLA to the natural atmosphere and evaluating its strength and structure.
"Degradation of 3D-Printed Porous Polylactic Acid Scaffolds Under Mechanical Stimulus"	2021	PLA	3D Printing			
"Physical and Degradation Properties of Polylactic Acid and Thermoplastic Starch Blends – Effect of Citric Acid and Treatment on Starch Structures"	2017	PLA/thermoplastic starch (TPS)		-Citric Acid	-Tensile strength tests; -FTIR Spectroscopic Analysis; -Elongation tests.	-The tensile strength and Young´s modulus for PLA/TPS blends at (60/40) and (40/60) blends ratio were found to increase after modification with citric acid; -The elongation at break if the (60/40) blend decreased, while elongation at break of the (40/60) blend increased; -TPS chemically interacted with the citric acid at 1721 cm^{-1} ; -The biodegradability properties of PLA/TPS blends were also improved after treatment with citric acid; -The deterioration of PLA/TPS blends was attributed to the incorporation of citric acid; -O_2 from the soil was attracted to the PLA/TPS blends, thus speeding up the degradation process of the blends.

Figure A.5: Literature research of degradation mechanisms on printed parts (page 5).

Appendix B

Calibration Cubes Measurements

Parâmetros/Cubos		1			2			3			4			5		
		1	2	3	1	2	3	1	2	3	1	2	3	1	2	3
Massa (g)		8,955	8,955	8,955	8,995	8,995	8,995	8,790	8,790	8,790	8,815	8,815	8,815	8,800	8,800	8,800
		8,955			**8,995**			**8,790**			**8,815**			**8,800**		
x (mm)		20,03	19,99	20,01	20,04	19,98	20,08	20,05	19,93	20,02	20,11	19,95	20,03	20,03	19,96	20,04
		20,01			**20,03**			**20,00**			**20,03**			**20,01**		
y (mm)		19,96	19,99	20,03	20,00	20,03	29,99	19,97	19,98	19,96	19,98	19,98	19,94	19,97	19,97	19,95
		19,99			**20,01**			**19,97**			**19,97**			**19,96**		
z (mm)		20,13	20,07	20,08	20,14	20,07	20,12	20,03	19,94	20,03	20,08	20,08	20,07	20,09	20,00	20,06
		20,09			**20,11**			**20,00**			**20,08**			**20,05**		

Figure B.1: Calibration cubes measurements.

Appendix C

FILKEMP PLA-N Filament Technical Sheet

Filkemp
Working together for new solutions

PLA for 3D Printing *PLN0*

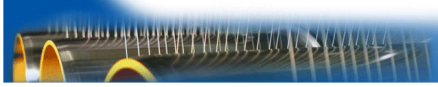
The next generation Biopolymer

- Ideal for tooling, prototyping and general industrial applications
- Ideal material to replace ABS (odourless)
- Machinable
- High mechanical and impact resistance
- Consistent diameter and extremely round
- Reduced breakage for longer printing performance
- High temperature resistance (180°C melting point after annealing)

Size Specifications[a]		Units	Test Method
Nominal Diameter	1.75 / 2.85	mm	-
Diameter Tolerances	±0.05 / ±0.15	mm	-

Mechanical Properties		Units	Test Method
Tensile Modulus	2400 ± 40	MPa	ISO 527-1
Tensile Stress at Yield	35.2 ± 0.8	MPa	ISO 527-1
Tensile Stress at Break	30.0 ± 3.0	MPa	ISO 527-1
Elongation at yield	2.0 ± 0.0	%	ISO 527-1
Elongation at break	6.0 ± 2.0	%	ISO 527-1
Flexural Strength	68 ± 5	MPa	ISO 178
Flexural Modulus	2120 ± 480	MPa	ISO 178
Izod Impact Strength, notched	10 ± 3	kJ/m²	ISO 180

[a]Property measured using the filament. All remaining properties are measured using 3D test specimens.



Page 1/2

Figure C.1: FILKEMP PLA-N Filament Technical Sheet (page 1).

Filkemp
Working together for new solutions

Thermal Properties		Units	Test Method
Melt Mass-Flow Rate	13 ± 2	g/10min	ISO 1133
Heat Deflection (HDT) at 0.455 MPa	135 ± 36	°F	ISO 75
Heat Deflection (HDT) at 1.820 MPa	129 ± 37	°F	ISO 75
Glass Transition, 1Hz	151 – 153	°F	ISO 6721
Coefficient of Thermal Expansion	8 x 10^{-5}	m/m°C	-
Melting Temperature[a]	342 ± 41	°F	ISO 11357
VICAT Softening Temperature	135 ± 36	°F	ISO 306
Printer Settings[b]		**Units**	**Test Method**
Extruder Temperature	392 – 419	°F	-
Plate Temperature	140	°F	-
Ventilation	0 – 50	%	-

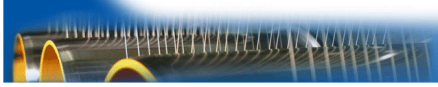
[b]Recommended settings. For the best results when printing with Filkemp filaments, carefully read the 3D printer manufacturer's instructions manual.

Additional Information
Regulatory Compliance: REACH / RoHs
Spool Weight: 1kg (2.2lbs)
All filaments are supplied in vacuum-sealed packaging containing a desiccant bag
Other sizes, spool weight and packaging are available upon request

Revision: 01/2022

Disclaimer:

This information is based on our current knowledge of raw materials and the manufacturing process and refers to the above mentioned products when leaving Filkemp. It is solely the customer's responsibility to determine if the product and information in this document are appropriate for the customer's end use. Responsibility for the use, storage, handling and disposal of the products herein is that of the purchaser or end user.



Page 2/2

Figure C.2: FILKEMP PLA-N Filament Technical Sheet (page 2).

Appendix D

Diffusion Coefficient Calculation Sheets

Dia	Hora/Amostra	1	2	3	4	5	6	7	
		3,2650	3,2700	3,2800	3,2900	3,2700	3,2750	3,2750	**Massa Inicial**
	12:00	3,5750	4,0250	4,2750	4,0500	3,4800	4,2950	4,4500	
04/jan	15:00	3,7000	4,2000	4,3400	4,1000	3,5500	4,3200	4,6700	
	18:00	4,7100	3,9200	4,3700	4,1000	3,8800	4,5700	4,4500	
	12:00	4,5750	4,4350	3,9350	4,2850	3,8850	4,8150	4,9050	
05/jan	15:00	4,4700	3,8200	4,6800	4,3100	4,4400	4,2200	4,7350	
19/jan	18:30	4,8000	4,8750	4,7550	4,6800	5,3050	5,1150	4,8650	**Massa imediatamente após retirar da água**
22-jan	19:00	3,2800	3,2900	3,3050	3,3250	3,3000	3,2800	3,3000	**Massa após descanso de 72h**

Msat (%)		0,4594	0,6116	0,7622	1,0638	0,9174	0,1527	0,7634	0,6758
h(m)		0,0030	0,0030	0,0031	0,0031	0,0031	0,0031	0,0031	
D		1,48E-10	8,79E-11	5,56E-11	2,74E-11	4,76E-11	1,58E-09	5,79E-11	2,87E-10
D1		0,0016	0,0012	0,0010	0,0007	0,0008	0,0050	0,0010	
D2		0,0014	0,0015	0,0014	0,0013	0,0019	0,0017	0,0015	

t (seconds) 1319400,0000

Average 1,26E-10

$$D = \pi \left(\frac{h}{4M_{sat}} \right)^2 \left(\frac{M_t}{\sqrt{t}} \right)^2$$

$$\text{Absorption (\%)} = \frac{(\text{Measured Mass} - \text{Initial Mass}) \times 100}{\text{Initial Mass}}$$

Figure D.1: Diffusion coefficient calculation sheet for group 2.

Dia	Hora/Amostra	1	2	3	4	5	6	7	
		3,27	3,275	3,29	3,275	3,275	3,255	3,25	**Massa Inicial**
	12:00	4,895	4,815	4,905	4,545	3,64	4,2	3,55	
04/jan	15:00	4,67	4,9	4,92	4,34	3,34	4,02	3,45	
	18:00	4,775	4,715	4,54	4,465	3,87	5,015	4,645	
	12:00	4,11	3,93	3,935	4,11	4,765	4,505	3,925	
05/jan	15:00	3,56	3,55	3,86	3,84	3,96	3,89	3,58	
19-jan	18:30	5,19	5,11	5,45	4,855	5,33	5,15	4,9	**Massa imediatamente após retirar da água**
22-jan	19:00	3,29	3,295	3,315	3,315	3,295	3,28	3,265	**Massa após descanso de 72h**

Msat (%)		0,6116	0,6107	0,7599	1,2214	0,6107	0,7680	0,4615	0,720547846
h(m)		0,0031	0,0031	0,0031	0,0031	0,0031	0,0031	0,0031	
D		4,15E-11	4,18E-11	2,73E-11	1,06E-11	4,18E-11	2,62E-11	7,18E-11	3,73E-11
D1		0,0013	0,0013	0,0010	0,0006	0,0013	0,0010	0,0017	
D2		0,0018	0,0017	0,0020	0,0015	0,0019	0,0018	0,0015	

t (seconds) 1319400

$$D = \pi \left(\frac{h}{4M_{sat}} \right)^2 \left(\frac{M_t}{\sqrt{t}} \right)^2$$

$$\text{Absorption (\%)} = \frac{(\text{Measured Mass} - \text{Initial Mass}) \times 100}{\text{Initial Mass}}$$

Figure D.2: Diffusion coefficient calculation sheet for group 5.

Dia	Hora/Amostra	1	2	3	4	5	6	7	
		3,26	3,26	3,27	3,27	3,29	3,27	3,26	**Massa Inicial**
	12:00	3,88	4,315	3,975	4,095	4,285	4,505	3,47	
04/jan	15:00	4,05	4,56	4,1	4,212	4,678	4,5	3,89	
	18:00	4,725	4,02	4,955	4,26	4,47	4,4	4,055	
	12:00	4,56	4,01	4,735	4,05	4,6	4,995	3,955	
05/jan	15:00	3,64	3,835	4,45	3,97	4,67	3,96	3,63	
19-jan	18:30	5,15	4,87	5,145	4,755	5	5,015	4,65	**Massa imediatamente após retirar da água**
22-jan	19:00	3,295	3,27	3,31	3,285	3,335	3,285	3,28	**Massa após descanso de 72h**

Msat (%)		1,0736	0,3067	1,2232	0,4587	1,3678	0,4587	0,6135	0,786045567
h(m)		0,0031	0,0031	0,0031	0,0031	0,0031	0,0031	0,0031	
D		1,35E-11	1,63E-10	1,05E-11	7,36E-11	8,54E-12	7,36E-11	4,10E-11	5,49E-11
D1		0,0007	0,0025	0,0006	0,0017	0,0006	0,0017	0,0013	
D2		0,0018	0,0015	0,0018	0,0014	0,0016	0,0016	0,0013	

t (seconds) 1319400

$$D = \pi \left(\frac{h}{4M_{sat}} \right)^2 \left(\frac{M_t}{\sqrt{t}} \right)^2$$

$$\text{Absorption (\%)} = \frac{\text{(Measured Mass} - \text{Initial Mass)} \times 100}{\text{Initial Mass}}$$

Figure D.3: Diffusion coefficient calculation sheet for group 6.

Dia	Hora/Amostra	1	2	3	4	5	6	7	Massa Inicial	
		6,775	6,805	6,775	6,78	6,77	6,805	6,82		
	12:00	6,77	6,82	6,775	6,8	6,78	6,805	6,83		
04/jan	18:00	6,79	6,82	6,78	6,81	6,79	6,815	6,835		
	12:00	6,795	6,82	6,81	6,81	6,79	6,82	6,86		
05/jan	15:00	6,8	6,82	6,79	6,81	6,79	6,82	6,84		
06/jan	15:00	6,795	6,825	6,79	6,81	6,79	6,82	6,84		
9-jan	19:00	6,8	6,83	6,79	6,815	6,795	6,823	6,845		
10-jan	16:00	6,8	6,83	6,79	6,82	6,79	6,825	6,84		
12-jan	19:00	6,8	6,835	6,8	6,825	6,8	6,835	6,845		
15-jan	16:00	6,81	6,845	6,8	6,825	6,8	6,83	6,855		
19-jan	18:30	6,81	6,84	6,8	6,83	6,805	6,835	6,85		
Msat (%)		0,5166	0,5143	0,3690	0,7375	0,5170	0,4409	0,4399		0,505017343
h(m)		0,0033	0,0033	0,0033	0,0033	0,0033	0,0033	0,0033		
D		2,83E-10	2,89E-10	5,45E-10	1,41E-10	2,82E-10	3,91E-10	3,94E-10	3,32E-10	
D1		0,0016	0,0016	0,0022	0,0011	0,0016	0,0019	0,0019		
D2		0,0064	0,0064	0,0064	0,0064	0,0064	0,0064	0,0064		

t (seconds) 1319400

average 2,83E-10

$$D = \pi \left(\frac{h}{4M_{sat}} \right)^2 \left(\frac{M_t}{\sqrt{t}} \right)^2$$

$$\text{Absorption (\%)} = \frac{(\text{Measured Mass} - \text{Initial Mass}) \times 100}{\text{Initial Mass}}$$

Figure D.4: Diffusion coefficient calculation sheet for group 8.

Dia	Hora/Amostra	1	2		3	4	5	6	7	
		6,85		6,895	6,87	6,85	6,84	6,85	6,865	Massa Inicial
17/mar	10:00	6,865		6,925	6,885	6,87	6,865	6,87	6,88	
18/mar	12:00	6,89		6,91	6,89	6,87	6,86	6,875	6,885	
	19:00	6,87		6,915	6,895	6,875	6,865	6,875	6,885	
19-marc	19:00	6,875		6,92	6,895	6,875	6,865	6,875	6,885	
20-mar	21:00	6,875		6,925	6,895	6,875	6,87	6,88	6,89	
21-mar	19:00	6,875		6,925	6,895	6,875	6,87	6,88	6,89	
22-mar	20:00	6,875		6,925	6,895	6,875	6,87	6,88	6,89	
23-mar	20:00	6,88		6,93	6,9	6,885	6,875	6,885	6,895	
24-mar	20:00	6,88		6,93	6,9	6,885	6,875	6,885	6,895	
01-abril.	15:00	6,88		6,93	6,905	6,885	6,875	6,885	6,905	
06-abril.	16:00	6,885		6,935	6,905	6,885	6,875	6,885	6,9	

Msat (%)		0,5109		0,5801	0,5095	0,5109	0,5117	0,5109	0,5098	0,520566723
h(m)		0,0034		0,0034	0,0034	0,0034	0,0034	0,0034	0,0034	
D		2,29E-10		1,80E-10	2,31E-10	2,29E-10	2,27E-10	2,29E-10	2,31E-10	2,22E-10
D1		0,0016		0,0014	0,0016	0,0016	0,0016	0,0016	0,0016	
D2		0,0052		0,0052	0,0052	0,0052	0,0052	0,0052	0,0052	

$$D = \pi \left(\frac{h}{4M_{sat}}\right)^2 \left(\frac{M_t}{\sqrt{t}}\right)^2$$

D1 D2

h is the specimen thickness (mm)

Msat is the percentage of absorbed water (%)

Mt is mass absorbed after time t (grams)

t is time (seconds)

time (s) 1749600

Figure D.5: Diffusion coefficient calculation sheet for group 13.

Dia	Hora/Amostra	1	2	3	4	5	6	7	
		6,92	6,94	6,945	6,925	6,92	6,94	6,93	**Massa Inicial**
17/mar	10:00	6,935	6,95	6,955	6,93	6,93	6,965	6,94	
	12:00	6,94	6,96	6,96	6,94	6,93	6,955	6,945	
18/mar	19:00	6,94	6,955	6,955	6,935	6,93	6,955	6,945	
	19:00	6,94	6,96	6,96	6,935	6,935	6,955	6,945	
19/mar	19:00	6,94	6,96	6,96	6,94	6,935	6,955	6,95	
20/mar	21:00	6,94	6,96	6,965	6,94	6,935	6,955	6,945	
21-mar	19:00	6,945	6,96	6,965	6,94	6,935	6,96	6,95	
22-mar	20:00	6,945	6,965	6,97	6,945	6,94	6,965	6,955	
23-mar	20:00	6,945	6,965	6,965	6,945	6,94	6,965	6,955	
24-mar	20:00	6,945	6,965	6,965	6,945	6,94	6,965	6,96	
01-abril	15:00	6,955	6,97	6,97	6,955	6,95	6,97	6,96	
06-abril.	16:00	6,96	6,975	6,975	6,955	6,95	6,97	6,96	

Msat (%)		0,5780	0,5043	0,4320	0,4332	0,4335	0,4323	0,4329	0,463748427
h(m)		0,0034	0,0034	0,0034	0,0034	0,0034	0,0034	0,0034	
D		1,83E-10	2,41E-10	3,29E-10	3,25E-10	3,24E-10	3,28E-10	3,26E-10	2,94E-10
D1		0,0015	0,0017	0,0019	0,0019	0,0019	0,0019	0,0019	
D2		0,0000	0,0000	0,0000	0,0000	0,0000	0,0000	0,0000	

time (s) 1749600

$$D = \pi \left(\frac{h}{4M_{sat}} \right)^2 \left(\frac{M_t}{\sqrt{t}} \right)^2$$

$$\text{Absorption (\%)} = \frac{\text{(Measured Mass} - \text{Initial Mass)} \times 100}{\text{Initial Mass}}$$

Figure D.6: Diffusion coefficient calculation sheet for group 15.